HELSINGIN YLIOPISTO
HELSINGFORS UNIVERSITET
UNIVERSITY OF HELSINKI

Master`s thesis
Department of Geosciences and Geography
Petrology and Economic Geology

PHANEROZOIC DIKES OF IBEX HILLS, SADDLEPEAK HILLS AND SALT SPRING HILLS, CALIFORNIA; PETROGRAPHY, GEOCHEMISTRY AND ORIGIN

Heini Hakala
May 2021

UNIVERSITY OF HELSINKI
FACULTY OF SCIENCE
DEPARTMENT OF GEOSCIENCES AND GEOGRAPHY
PL 64 (Gustaf Hällströmin katu 2)
00014 Helsingin yliopisto

HELSINGIN YLIOPISTO
HELSINGFORS UNIVERSITET
UNIVERSITY OF HELSINKI
MATEMAATTIS-LUONNONTIETEELLINEN TIEDEKUNTA
MATEMATISK-NATURVETENSKAPLIGA FAKULTETEN
FACULTY OF SCIENCE

Tiedekunta – Fakultet – Faculty Faculty of Science	Koulutusohjelma – Utbildningsprogram – Degree programme Master's programme in geology and geophysics	
Opintosuunta – Studieinrikting – Study track Petrology and Economic Geology		
Tekijä – Författare – Author Heini Hakala		
Työn nimi – Arbetets titel – Title Phanerozoic dikes of Ibex Hills, Saddlepeak Hills and Salt Spring Hills, California; petrography, geochemistry and origin		
Työn laji – Arbetets art – Level Master's thesis	Aika – Datum – Month and year May 2021	Sivumäärä – Sidoantal – Number of pages 114 + 3 appendices

Tiivistelmä – Referat – Abstract

A NW–SE trending dike swarm cuts Miocene volcanic rocks in the Ibex Hills and Precambrian to Cambrian cratonic rocks and sedimentary strata in the Saddlepeak Hills and Salt Spring Hills in southern Death Valley, California. These dikes are aligned with Jurassic and Cretaceous dike swarms of eastern California that are linked to the Mesozoic North American Cordilleran magmatism. The Ibex Hills dikes have been previously dated and yield K-Ar date of 12.7 Ma and are coeval with the early stage of the Miocene Basin and Range crustal extension in Death Valley. This Master's thesis examines in detail the geology, petrography and geochemistry of the previously unstudied dikes of Ibex Hills, Saddlepeak Hills and Salt Spring Hills of southern Death Valley and a ~90 Ma dike of Mojave Desert to discuss (1) their petrogenetic link to each other and (2) their geologic significance.

The samples and field observations were obtained in 2019. The Ibex Hills samples are relatively fresh compared to the dikes of Saddlepeak Hills and Salt Spring Hills which are pervasively altered by secondary minerals and have been subject to low-grade metamorphism. The sub-solidus processes that have modified the mineral assemblages of the metamorphic dikes are also reflected in various degrees of major element mobility and LOI. The whole-rock geochemical composition of the Ibex Hills and Mojave Desert samples is trachyandesite to trachyte, the Saddlepeak Hills and Salt Spring Hills samples are andesites. One Saddlepeak Hills sample is basaltic and, based on mineralogy, texture and composition, represents a 1.1 Ga diabase intrusion. All studied samples are enriched in LREEs and LILEs and have negative Ta-Nb anomaly, representing magmas with typical subduction zone characteristics with enriched lithospheric mantle component in source.

EPMA and in situ LA-MC-ICP-MS analysis of plagioclase phenocrysts of two Miocene samples of Ibex Hills shows variation in anorthite content and $^{87}Sr/^{86}Sr$ ratios across phenocryst profiles indicating open-system magma chamber evolution with episodes of recharge, hybridization and assimilation during the crystallization. Variation in anorthite content and $^{87}Sr/^{86}Sr$ ratios between samples suggest heterogeneities in the source magmas.

The studied dikes represent multiple episodes of dike emplacements in southern Death Valley. The Miocene dikes of Ibex Hills, coeval with the Basin and Range crustal extension, indicate an early period of southwest directed extension in the southern Death Valley. The metamorphosed dikes of Saddlepeak Hills and Salt Spring Hills represent one or more episodes of older dike emplacement and could be coeval with the Mesozoic magmatism of North American Cordilleran orogeny and the Cretaceous dike of Mojave Desert. However, geochronological analysis is needed to verify the exact ages of these dikes.

Avainsanat – Nyckelord – Keywords
Dike swarms, Death Valley, Basin and Range, post-solidus alteration, geochemistry, *in situ*, LA-MC-ICP-MS, Sr isotopes

Säilytyspaikka – Förvaringställe – Where deposited
HELDA – University of Helsinki Digital Repository

Muita tietoja – Övriga uppgifter – Additional information

HELSINGIN YLIOPISTO
HELSINGFORS UNIVERSITET
UNIVERSITY OF HELSINKI
MATEMAATTIS-LUONNONTIETEELLINEN TIEDEKUNTA
MATEMATISK-NATURVETENSKAPLIGA FAKULTETEN
FACULTY OF SCIENCE

Tiedekunta – Fakultet – Faculty	Koulutusohjelma – Utbildningsprogram – Degree programme
Matemaattis-luonnontieteellinen tiedekunta	Geologian ja geofysiikan maisteriohjelma

Opintosuunta – Studieinrikting – Study track
Petrologia ja taloudellinen geologia

Tekijä – Författare – Author
Heini Hakala

Työn nimi – Arbetets titel – Title
Kalifornian Ibex-, Saddlepeak- ja Salt Spring -vuorien fanerotsooiset juonet; petrologia, geokemia ja alkuperä

Työn laji – Arbetets art – Level	Aika – Datum – Month and year	Sivumäärä – Sidoantal – Number of pages
Pro gradu	Toukokuu 2021	114 + 3 liitettä

Tiivistelmä – Referat – Abstract

Luode–kaakko-suuntainen juoniparvi leikkaa mioseeninaikaisia vulkaanisia kiviä eteläisen Kuolemanlaakson Ibex-vuorilla ja prekambrista peruskalliota sekä prekambrisia ja kambrisia sedimenttikiviä Saddlepeak- ja Salt Spring -vuorilla Kaliforniassa. Nämä juonet ovat samansuuntaisia itäisen Kalifornian jura–liitukautisien juoniparvien kanssa, jotka liittyvät mesotsooiseen Pohjois-Amerikan Kordilleerivuoriston kehittymiseen. Ibex-vuoren juonten K-Ar-ikä on 12.7 Ma ja ne edustavat varhaista Basin ja Range -kuoren riftiymää eteläisessä Kuolemanlaaksossa. Tämä pro gradu -tutkielma tutkii Ibex-, Saddlepeak- ja Salt Spring -vuorien juonien sekä Mojaven aavikon liitukautisen juonen petrografiaa ja geokemiaa ja tulkitsee näiden juonien (1) ikäjakaumaa sekä (2) geologista merkitystä.

Näytteet ja kenttämittaukset työssä käsiteltävistä juonista kerättiin vuoden 2019 aikana. Ibexin näytteiden mineraalit ovat kiteytyneet pääosin kivisulasta. Saddlepeakin ja Salt Springin näytteiden mineraaliseurueet ovat kauttaaltaan sekundäärisiä ja matala-asteisen metamorfoosin tai hydrotermisen toiminnan muodostamia. Post-magmaattiset prosessit ovat muokanneet mineraaliseurueiden lisäksi näytteiden pääalkuainekoostumuksia ja volatiilipitoisuuksia. Ibexin ja Mojaven aavikon näytteet vaihtelevat koostumukseltaan trakyandesiiteista trakyytteihin, Saddlepeakin ja Salt Springin näytteet ovat andesiitteja. Yksi Saddlepeakin näytteistä edustaa mineraalien, tekstuurin ja koostumuksen perusteella Death Valleyn 1.1 Ga diabaasi-intruusiota. Kaikki työssä käsiteltävät näytteet ovat rikastuneet LILE- ja LREE-elementeistä, ja niillä on negatiivinen Ta-Nb-anomalia edustaen siten tyypillisiä merellisen litosfäärilaatan alityöntövyöhykkeiden sulia, joiden lähdekomponentteihin kuuluu rikastunut litosfäärivaippa.

Kahden mioseeninaikaisen Ibex-vuoren näytteiden plagioklaasihajarakeiden anortiittipitoisuutta analysoitiin elektronimikroanalysaattorilla (EPMA) sekä $^{87}Sr/^{86}Sr$-suhteita laserablaatio induktiivisesti kytketyllä massaspektrometrillä (LA-MC-ICP-MS). Tulokset osoittavat vaihtelua niin anortiittipitoisuuksissa kuin $^{87}Sr/^{86}Sr$-suhteissa sekä näytteiden välillä että yksittäisien hajarakeiden profiileissa ytimestä reunoille. Vaihtelu hajaraeprofiileissa osoittaa magmakammioihin tunkeutuneen uutta magmaa, magmojen sekoittuneen ja kontaminoituneen kiteytymisen aikana. Erot näytteiden välisissä pitoisuuksissa viittaavat paikallisiin heterogeenisyyksiin magmasulien lähteissä.

Tässä työssä tutkitut juonet edustavat useita intruusiotapahtumia. Ibexin mioseeninaikaiset juonet edustavat Basin ja Range -kuoren riftiytymistä ja osoittavat, että Kuolemanlaaksossa kuoren laajeneminen oli aluksi lounaan suuntainen. Saddlepeakin ja Salt Springin metamorfiset juonet edustavat yhtä tai useampaa vanhempaa juoni-intruusiojaksoa. Nämä juonet saattavat edustaa mesotsooista Kordilleerivuoriston kehittymisen aikaista magmatismia. Tämän todentamiseen vaaditaan kuitenkin isotooppi-iänmääritys.

Avainsanat – Nyckelord – Keywords
Juoniparvet, Kuolemanlaakso, Basin ja Range, post-magmaattiset prosessit, geokemia, *in situ*, LA-MC-ICP-MS, strontium isotoopit

Säilytyspaikka – Förvaringställe – Where deposited
HELDA – Helsingin yliopiston digitaalinen arkisto

Muita tietoja – Övriga uppgifter – Additional information

TABLE OF CONTENTS

1. INTRODUCTION

Dikes are shallow intrusive rocks that mark sheet-like magma-filled bodies in the crust. By definition, high-angle orientation of dikes separates them from horizontally orientated concordant sheet structures, sills. Typically dikes are emplaced in pre-existing fractures that act as conduits for pressurized magma that is generated in the mantle or crust. The ascending magma may widen the pre-existing cracks if the magma pressure exceeds the dike perpendicular stress field. Large mafic dike swarms were typically emplaced during the Proterozoic and are commonly found in Archean and Proterozoic crustal terrains, for example the 1.2 Ga Mackenzie dike swarm of the Canadian Shield or the ~1.8 Ga mafic dike swarm of the North China Craton (Hou 2012, Ernst et al. 2001).

Overall, dike swarms are beneficial in reconstructing paleostress fields and prior plate movement directions. The emplacement of dikes acts as a response to extensional stress and dikes are thus indicators of local stress field. Parallel dike swarms indicate extension such as crustal rifting whereas radiating dike swarms develop around igneous centers such as volcanoes or mantle plumes. Parallel dike swarm trends perpendicular to the minimum compressional stress direction ($\sigma 3$) or maximum extensional stress and parallel to the maximum compressional stress ($\sigma 1$) and, regionally, their orientation indicates the direction of extensional tectonic regime (Hou et al. 2010, Hou 2012). Near-vertical dike intrusion coeval with crustal extension indicates that the stress field perpendicular to dike trend ($\sigma 3$) is horizontal. Crustal rifting can be accompanied by dike emplacement, As in the Miocene Chambers Well dike swarm associated with Basin and Range crustal extension in southeastern California (Gans et al. 2016).

Although parallel dike swarms are usually conspicuous markers of extensional tectonic events such as rifting or break up of continents, dike swarms are also recorded in compressive tectonic settings. Dike swarms related to colliding plate margins provide evidence of local extension stress field at least at upper crustal level within the compressive stress field. Synconvergent extension is identified in orogenic settings from Alps to the Himalayas, yet the driving mechanism remain under discussion (Wells and Hoisch 2008). In the Cordilleran orogeny of the western USA synconvergent extension represents complex structural setting of compressional stress combined with local and temporal extension evident in, for example, extensional shear zones, exhumation of core

complexes and detachment and normal faults coeval with the orogenesis (Hodges and Walker 1992, Wells and Hoisch 2008). Dike swarms coeval with arc magmatism are recognized in the western USA and a number of Jurassic dike swarms has been linked to the Nevadan orogeny (Wolf and Saleeby 1992).

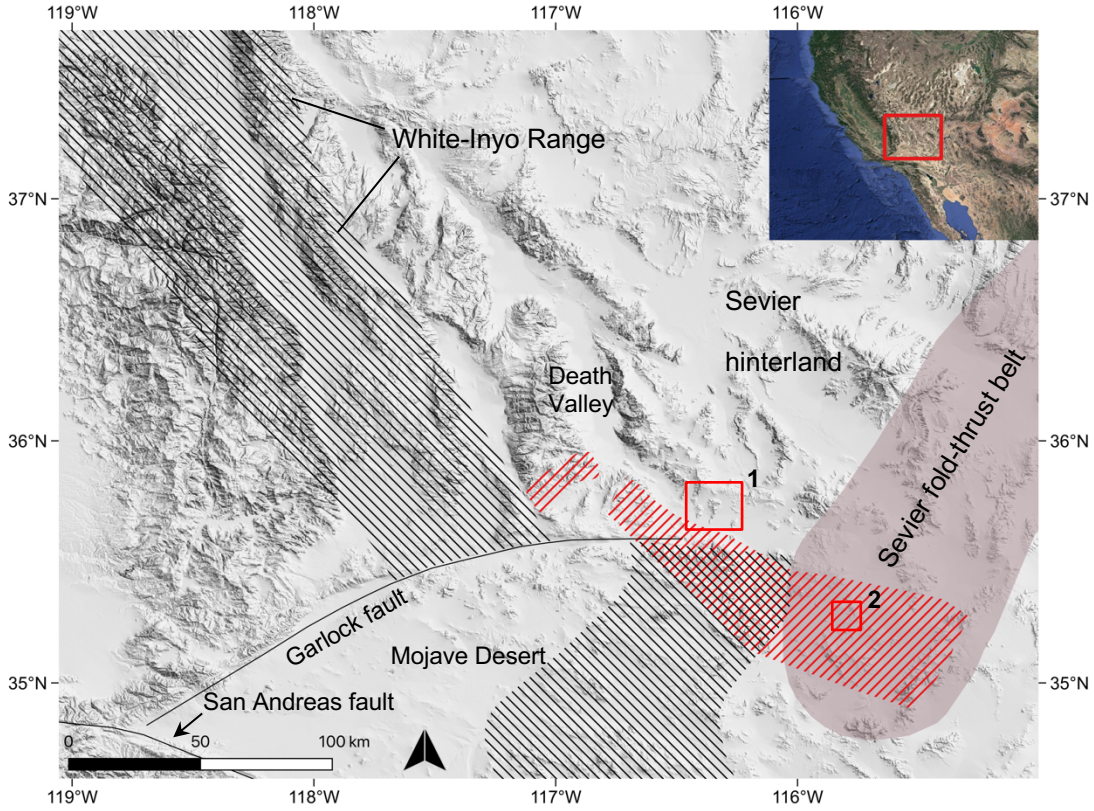

Figure 1. Map of southern California and environs. The black hatched shadowing represents the extension of Independence dike swarm after Carl and Glazner (2002). The red hatched shadowing represents the extent of Mesozoic plutons in southern Death Valley after Rämö et al. (2002). The location of Sevier fold-thrust belt and Sevier hinterland after DeCelles (2004). The squares represent the sample locations of this study, 1) southern Death Valley and 2) northeastern Mojave Desert. Insert shows location of study area relative to southwestern USA.

Perhaps the most studied and extensive example of the synconvergent Cordilleran dike swarms is the Independence dike swarm spanning from Sierra Nevada to the Mojave Desert (Figure 1). The Independence dike swarm was emplaced contemporaneously with the arc magmatism of Sevier orogeny, possibly reflecting temporal crustal extension or relaxation, or injection of dikes into oblique shear zones and representing dike emplacement contemporaneous with shear stress (Chen and Moore 1979, Hopson et al. 2008). Dikes of similar age have emplaced in the White-Inyo Range in eastern California

(Figure 1), and these dikes may be connected to the Independence dike swarm (Ernst 1997). The Independence dike swarm has originally been assigned an age of 148 Ma (Chen and Moore 1979) but has since been suggested to include dikes of Cretaceous or younger age (Coleman et al. 2000).

A NW-SE trending dike swarm was mapped by Bennie Troxel and James Calzia in southern Death Valley (Troxel, B. W. and Calzia, J. P., unpublished mapping, 2018). The dikes cut Proterozoic cratonic rocks and Cambrian sedimentary strata of Saddlepeak Hills and Salt Spring Hills, but no further analysis have been conducted on the dikes since their discovery. A NW-SE trending mafic dike on the eastern flank of the Ibex Hills mountain, located adjacent to the Saddlepeak Hills, has been analyzed with K-Ar method, yielding 12.7 Ma (Troxel and Calzia 1994), and is thus coeval with the Basin and Range crustal extension that commenced in Death Valley ca. 13 Ma (Fowler and Calzia 1999). Prior to this study, the unexamined dike swarm of Saddlepeak Hills and Salt Spring Hills has been considered cogenetic with the 12.7 Ma dike of Ibex Hills.

This thesis examines the hypothesis of the relationship of the dikes of Ibex Hills to the dike swarm of Saddlepeak Hills and Salt Spring Hills. The thesis work commenced by a field campaign in April 2019 with sampling of several dikes from Saddlepeak Hills, Salt Spring Hills and Ibex Hills, including the K-Ar dated 12.7 Ma dike. Preliminary field observations and petrographic inspection revealed a metamorphic overprint on the dikes of Saddlepeak Hills and Salt Spring Hills, compromising their temporal connection to the Miocene dike of Ibex Hills and augmenting the theme of the thesis. To enable comparison with a sample of different age, a sample from a subparallel Cretaceous dike from Mojave Desert is included.

The main objectives of this thesis are to (1) outline the mineralogical and textural features using petrography, (2) provide a whole-rock geochemical characterization of the samples and (3) evaluate changes in Miocene crystallizing magma source compositions through mineral chemistry and *in situ* Sr isotope profiles of plagioclase phenocrysts. In light of these results the study focuses on testing the petrogenetic similarity of the samples, evaluating the effects of post-solidus processes on their mineralogical and geochemical nature and assessing magma chamber dynamics during crustal extension in southern Death Valley. Finally, relative age constraints on the dikes are proposed. Overall, the

thesis brings new information about these previously unstudied dikes and their connection to the extensional tectonics of southern Death Valley.

2. GEOLOGIC SETTING

2.1 Proterozoic basement of Mojavia

The southwestern United States is part of the North American Cordillera, recording some 600 million years of tectonic evolution from rifting and generation of passive continental margin to subduction driven compression and crustal thickening, and finally to transform deformation and crustal extension (Dickinson 2004). The crystalline Proterozoic basement rocks of the study area and vicinity are representative of the Mojave crustal province that stretches across eastern California and western Nevada (Bennet and DePaolo 1987, Condie 1992) This area is now exposed in response to Cenozoic extension tectonics and exhumation.

The Mojave crustal province was assembled by accretion of arc material onto the southwestern margin of Laurentia during an early Paleoproterozoic orogeny; the specifics of the evolution and tectonic significance of Mojave crustal province in relation to the North American craton have remained unclear (Bennet and DePaolo 1987, Wooden and Miller 1990, Condie 1992, Anderson et al. 1993, Rämö and Calzia 1998). The lithological assemblage of the Mojave crustal province comprises ortho- and paragneisses with minor metapelite and amphibolite (Bennet and DePaolo 1987, Condie 1992, Anderson et al. 1993) and metamorphic grade ranging from amphibolite to granulite facies (Anderson et al. 1993). Nd isotopic composition (Bennet and DePaolo 1987, Rämö and Calzia 1998) and U-Pb ages (Wooden et al. 2012) suggest a mantle derived component mixed with Archean to Paleoproterozoic recycled metasedimentary crust. Paleoproterozoic ~1.7 to ~1.6 Ga and Mesoproterozoic ~1.4 Ga intrusive suites have stitched the Mojave crustal province assemblage. These cratonic rocks are intruded by ca. 1.1 Ga diabase sills and dikes (Heaman and Grotzinger 1992).

The Nd isotopic composition of the Proterozoic rocks from the Mojave crustal province represent unique values in relation to samples elsewhere in the southwestern United States, and the Mojave crustal province is distinct from the neighboring Yavapai and Mazatzal Proterozoic crustal provinces in its metamorphic grade, old Nd-depleted mantle model ages, geochemical character and origin (Bennet and DePaolo 1987, Anderson 1993, Rämö and Calzia 1998). The Paleoproterozoic metamorphic basement is locally overlain by angular unconformity of Meso- to Neoproterozoic sedimentary deposits that record a period of stable continental crust, and Neoproterozoic to Cambrian miogeocline representative of late Proterozoic rifting, initiation of the Cordilleran orogeny and formation of passive continental margin at the southwest/west of the North American craton (Barth et al. 2009, Wooden et al. 2012). Re-Os isotope composition of mantle xenoliths shows enriched lithospheric mantle underneath the cratonic Mojave, preserving its Archaean mantle component despite extensive deformation throughout the Cordilleran orogenesis (Lee et al. 2001).

2.2 Death Valley

The Death Valley extensional basin in southeastern California is a significant and complex example of Cenozoic Basin and Range crustal extension (Snow and Wernicke 2000). Located south of the Walker Lane dextral shear zone and at the eastern margin of the Eastern California Shear Zone (Dokka and Travis 1990, Bidgoli et al. 2015), the Death Valley region has been subject to both extensional and dextral transtension during the Cenozoic (Serpa and Pavlis 1996, Bidgoli et al. 2015). Following its position in a compound of active Basin and Range deformation, Death Valley incorporates a series of fault zones (Figure 2). These include the right lateral Northern Death Valley fault zone, the Furnace Creek fault zone (FCFZ) (now inactive), the normal Black Mountains fault zone (BMFZ), the right lateral Southern Death Valley fault zone (SDVFZ) and the left-lateral Garlock fault zone (Knott et al. 2005).

The Paleoproterozoic crystalline basement rocks in Death Valley are locally exposed and are overlain by angular unconformity by Meso- to Neoproterozoic Pahrump Group (Crystal Spring Formation, Beck Spring Dolomite, Kingston Peak Formation). These sedimentary strata reflect the breakup of Rodinia and the forming of a passive continental

margin at the southwestern margin of Laurentia (Stewart 1970). The Pahrump Group is unconformably overlain by Neoproterozoic miogeocline sequence which comprise of Noonday Dolomite, Johnnie Formation and Stirling Quartzite (Stewart 1970, Corsetti and Kaufman 2005).

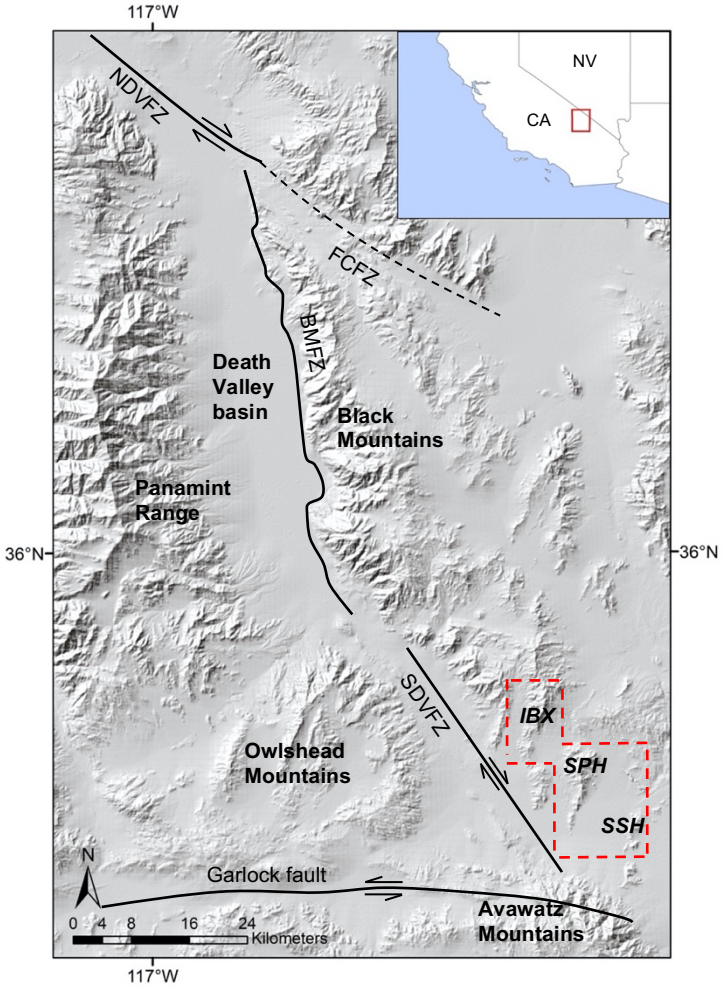

Figure 2. Map of Death Valley showing locations of major mountain ranges. The black lines represent major fault zones. The study area is located in the south-eastern corner. IBX = Ibex Hills; SPH = Saddlepeak Hills; SSH = Salt Spring Hills; Black Mountains fault zone; FCFZ = Furnace Creek fault zone; NDVFZ = Northern Death Valley fault zone; SDVFZ = Southern Death Valley fault zone. Insert shows location of area relative to California (CA) and Nevada (NV).

In response to subduction of oceanic plate underneath the western margin of the North American plate, compression and crustal thickening of the Mesozoic Sevier orogeny modified the Death Valley landscape from the Late Jurassic to Cretaceous (DeCelles 2004). The signs of this Mesozoic Cordilleran compressional tectonics in Death Valley have since been overprinted by Cenozoic extensional deformation and coeval igneous processes. Nevertheless, Mesozoic compressional system remains evident in southeast

verging fold-thrust structures in the Neoproterozoic to Cambrian North American craton passive margin miogeocline deposits (DeCelles 2004, Pavlis et al. 2014) and in northeast verging fold-thrust structures in southeastern California, which Pavlis et al. (2014) recognized as being related to a younger (Late Mesozoic to Paleogene) northwest trending thrust event.

The present-day Death Valley topography is shaped by Miocene crustal extension. Miocene deformation in central Death Valley is characterized by low-angle detachment and strike-slip faults. The relationship between detachment and strike-slip faults is not apparent and has been explained by the rolling hinge model, which explains the low-angle detachment faults as governing and the strike-slip faults as edges to the detachment faults (e.g. Snow and Wernicke 2000). In contrast, the pull-apart model describes the strike-slip faults as the dominating factor in creating extension, followed by detachment faults, such as extension between two Death Valley strike-slip faults, the Garlock and Furnace Creek faults (Serpa and Pavlis 1996). Based on the structural and stratigraphic relationships between Death Valley mountain ranges and basins, the prevailing interpretation of Death Valley extension supports the pull-apart model with deeply rooted faults directing the extension (Miller and Prave 2002, Miller and Pavlis 2005). Northwest migrating crustal extension in Death Valley commenced ~13 Ma ago and ceased 5–3 Ma ago. The 13.4 to 12.4 Ma southwest dipping Kingston Range detachment fault indicates earlier, southwest directed extension in the southern Death Valley region (Fowler and Calzia 1999). The crustal extension in Death Valley region has been south-west to west-northwest directed and the total extension has been estimated from 30 to 100%. Extension related listric and planar normal faults and both right-lateral and left-lateral strike-slip faults are common (Calzia and Rämö 2000).

2.2.1 Southern Death Valley

The area of interest of this study considers three adjacent mountain ranges: Ibex Hills, Saddlepeak Hills and Salt Spring Hills, located in the southern Death Valley (Figure 2). They are bounded by Black Mountains to the north, Avawatz Mountains to the south and Kingston Range to the east. The sinistral Garlock Fault intersects with the dextral Southern Death Valley Fault Zone southwest of Salt Spring Hills.

Ibex Hills exhibit a compound structure of a Proterozoic to Cambrian stratigraphic sequence from Proterozoic Pahrump Group to Noonday and Johnnie Formations, followed by Stirling Quartzite, Wood Canyon Formation and finally by Zabriskie Quartzite (Figure 3). A number of fault structures with various orientations transect the sedimentary strata. Both contractional and extensional deformation have been mapped at Ibex Hills, extension direction both southwest (earlier, fault displacement and dip direction) and northwest (Fleming 2018).

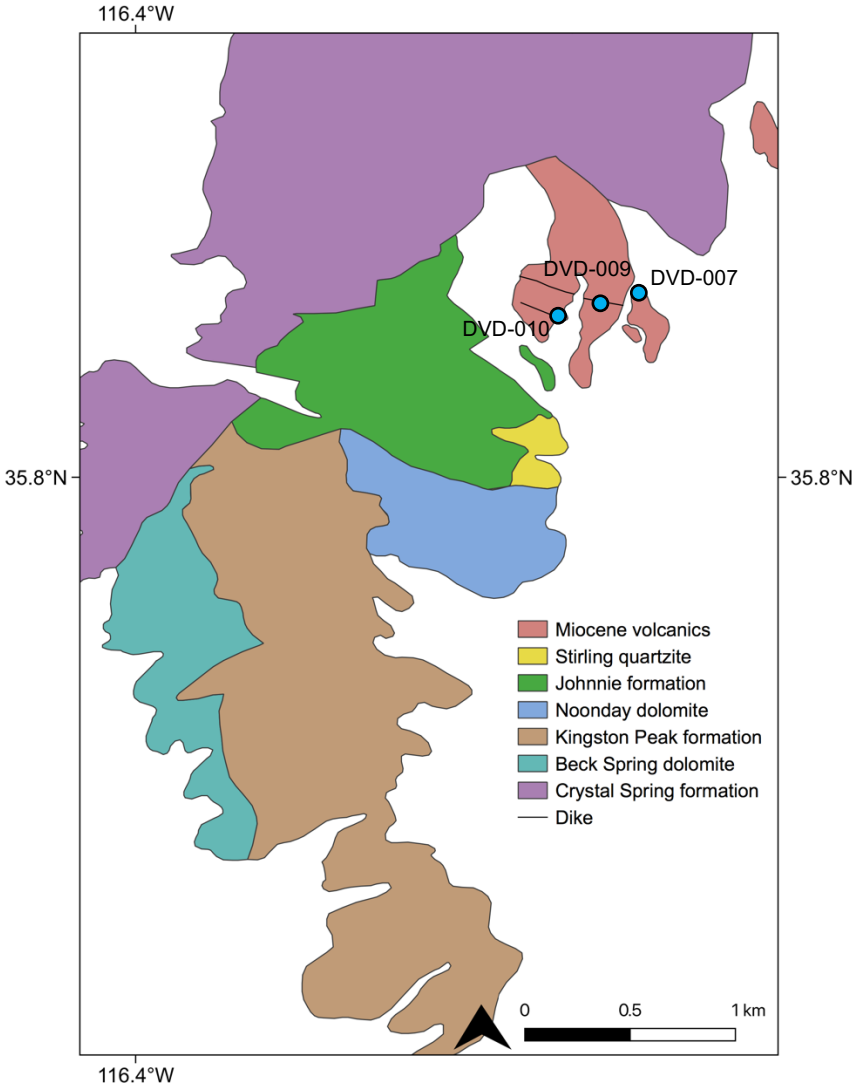

Figure 3. Simplified geologic map of southern Ibex Hills. Modified after Fleming (2018). Locations for samples DVD-007, DVD-009 and DVD-010 are indicated by blue dots. Cf. Figure 2 for the location of the map relative to Death Valley.

To the east of Ibex Hills, the stratigraphy of Saddlepeak Hills is dominated by the Proterozoic Kingston Peak Formation (Figure 4). The stratigraphically lower Crystal Spring Formation and Beck Spring Dolomite (Pahrump Group) are found on the western side of Saddlepeak Hills. Proterozoic Noonday Dolomite and Johnnie Formation are scattered in the northern, eastern and southern flanks of the mountain. The Crystal Spring Formation is cut by 1.1 Ga diabase that runs along the bottom of the western hillside. The Noonday Dolomite and Johnnie Formation are unconformably overlain by Miocene dacite to basalt lava flows and tuffs. In the northern Saddlepeak Hills, compositionally similar Miocene intrusions cut the Kingston Peak Formation (Troxel and Calzia 1994, Troxel and Calzia, unpublished mapping, 2018).

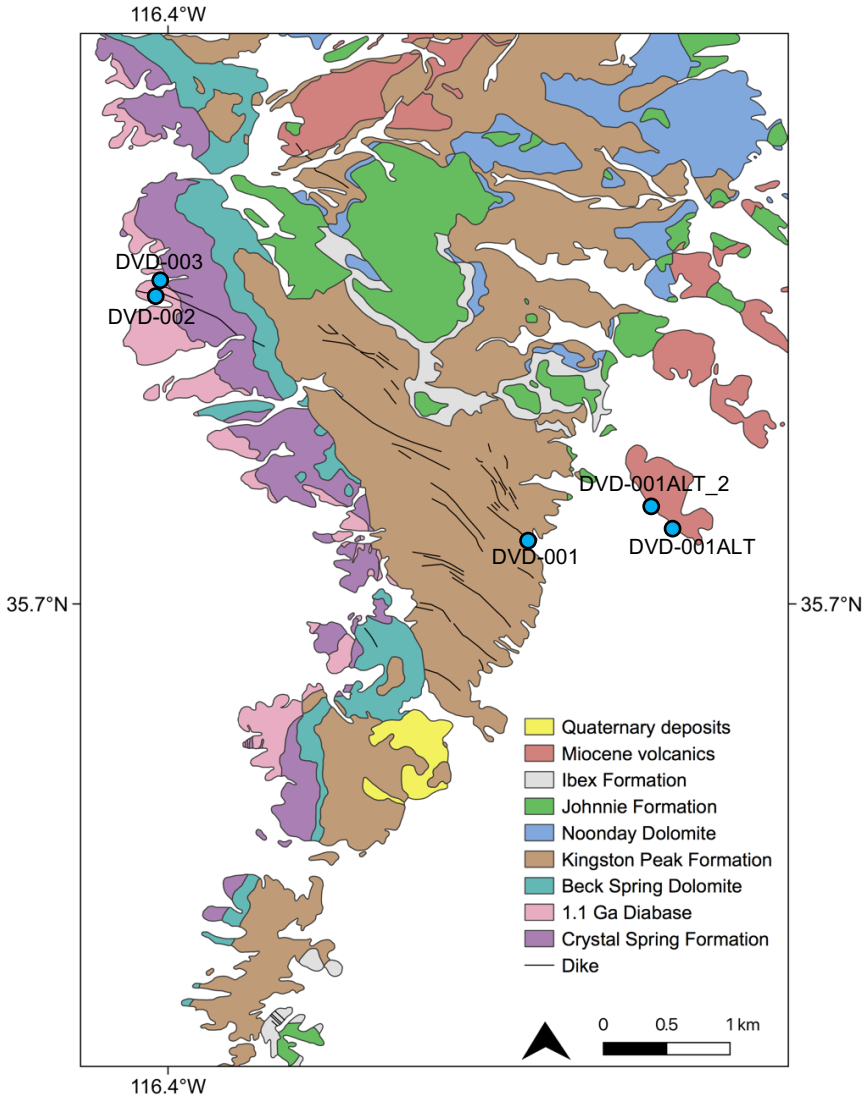

Figure 4. Simplified geologic map of Saddlepeak Hills. Modified after Troxel and Calzia (unpublished mapping, 2018). Sample locations for DVD-001, DVD-001ALT, DVD-001ALT_2, DVD-002 and DVD-003 are indicated by blue dots. Cf. Figure 2 for the location of the map relative to Death Valley.

Southeast of Saddlepeak Hills Mesozoic intrusive rocks and Miocene megabreccia are exposed on the southern flank of Salt Spring Hills (Figure 5). The stratigraphic sequence of Salt Spring Hills evolves from the west to the east from Neoproterozoic Johnnie Formation and Stirling Quartzite to Cambrian Wood Canyon Formation (Troxel and Calzia, unpublished mapping, 2018).

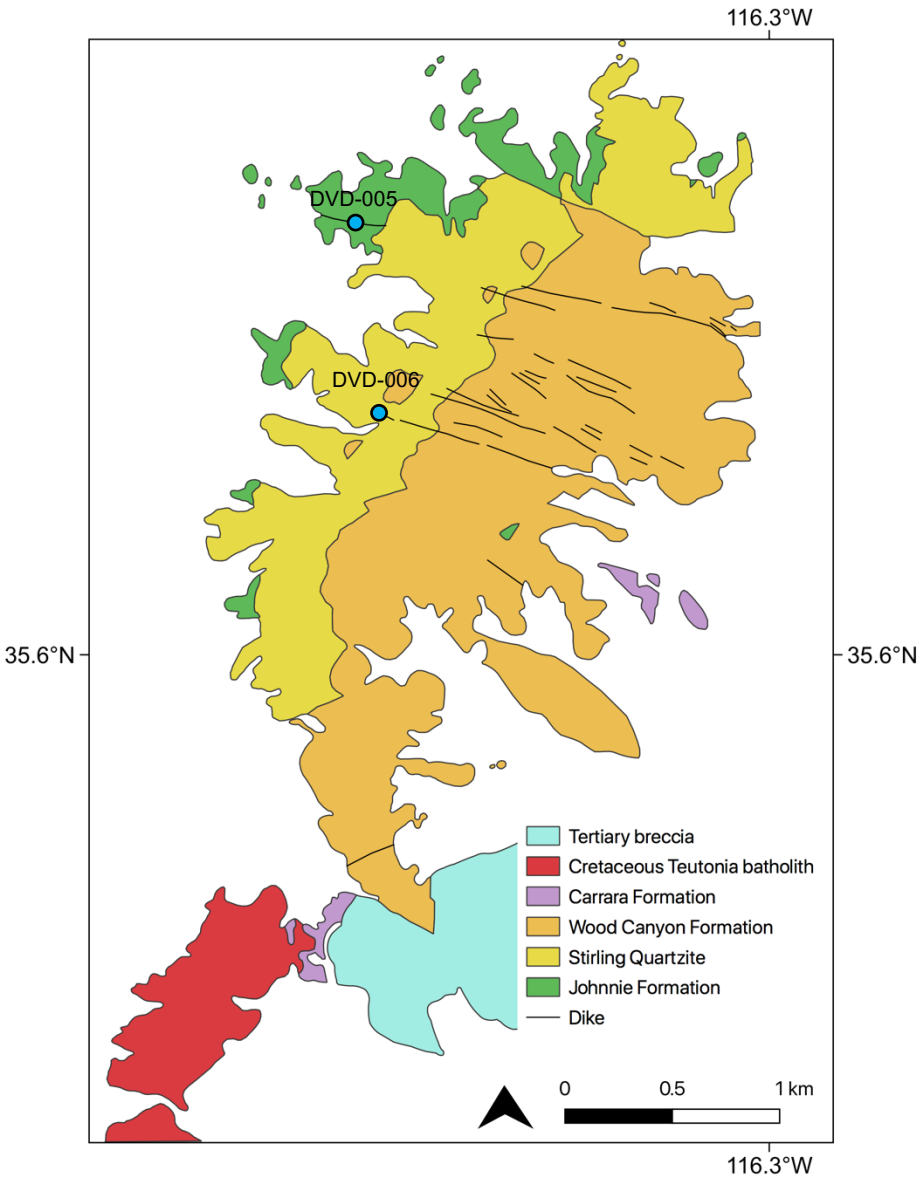

Figure 5. Simplified geologic map of Salt Spring Hills. Modified after Troxel and Calzia (unpublished mapping, 2018). Blue dots indicate location for samples DVD-005 and DVD-006. Cf. Figure 2 for the location of the map relative to Death Valley.

Southern Death Valley provides challenges to the common characteristics of Death Valley extension structures and kinematics. Fault and detachment structures in the southern Death Valley area indicate a period of southwest directed extension pre-dating the northwest directed extension. Northwest trending faults and dikes in the Saddlepeak Hills and Salt Spring Hills suggest initial southwest directed extension (Troxel et al. 1992, Troxel and Calzia, unpublished mapping, 2018). Fleming (2018) mapped southwest dipping low-angle faults in Ibex Hills that support argument for the initial extension direction to the southwest. Northwest dipping low-angle and younger high-angle normal faults record a change in direction of the extension. By analyzing extension related Miocene sedimentary basins Amargosa Chaos and Sperry Hills, rock-avalanche deposits and their source areas, Topping (1993) suggested that this change from southwest directed extension to northwest occurred at ~7.8 Ma. Further evidence for southwest directed extension is found in the Kingston Range ca. 35 km to the west of the northern margin of Saddlepeak Hills. The southwest dipping Kingston Range detachment fault displaces the Proterozoic Pahrump Group, Proterozoic to Cambrian miogeoclinal deposits and Miocene Resting Spring Formation estimated 6 km to the southwest of their source. The detachment fault cuts a 13.4 Ma hypabyssal sill and is cut by 12.4 Ma Kingston Peak granite and may thus have been formed between 13.4 and 12.4 Ma (Fowler and Calzia 1999).

To the south, the north-eastern Mojave block has undergone significant vertical-axis clockwise rotation during the late Cenozoic. The implications of the rotation of the adjacent northeastern Mojave block to the geology of Death Valley has not been extensively studied. It has, however, been suggested that, for example, extension in the Owlshead Mountains, located west of the study area, was triggered by clockwise rotation of the Mojave block (Guest et al. 2003).

2.3 Northeastern Mojave Desert

Mojave Desert is located south of Death Valley, with the Garlock Fault serving as a boundary between these two regions (Figure 1). The area of interest for this study is located in northeastern Mojave Desert, on the western side of Cima Dome between Halloran Hills and New York Mountains. Proterozoic metamorphic and igneous rocks

(Wooden and Miller 1990), Proterozoic to early Paleozoic metasedimentary rocks (Stewart 1970), and Middle Jurassic to Late Cretaceous plutonism (Beckerman 1982, DeWitt et al. 1984, Walker et al. 2002) are overlain by Miocene to recent volcanic rocks of Cima volcanic field (Figure 6).

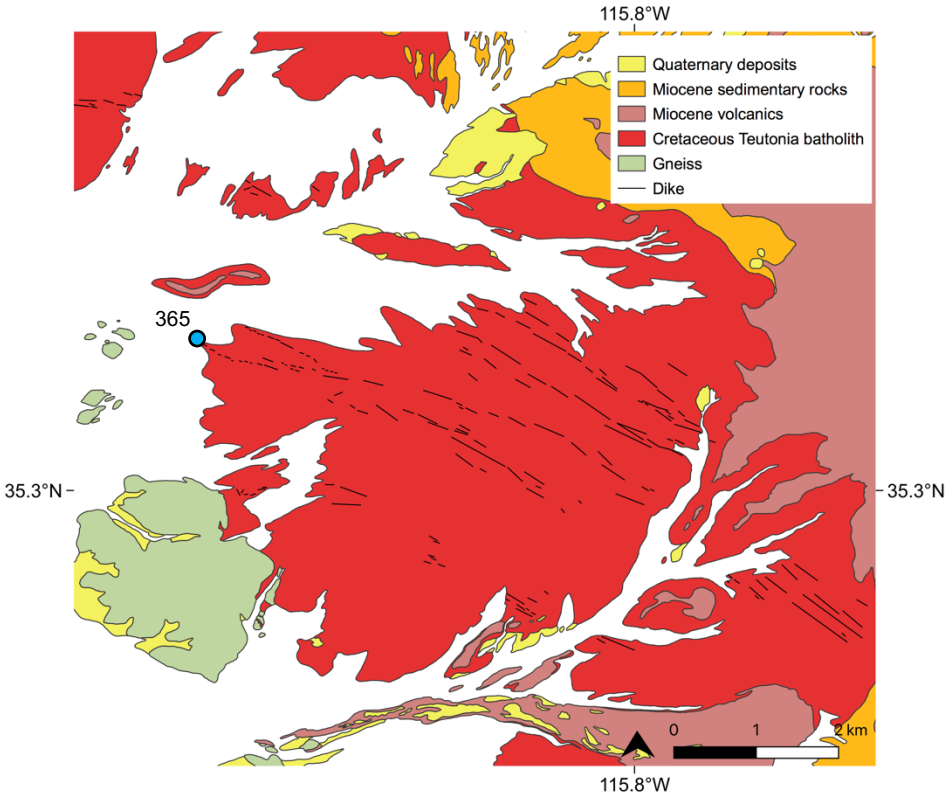

Figure 6. Simplified geologic map of western Cima volcanic field, northeastern Mojave Desert. Modified after Wilshire et al. (2002). Sample 365 location is indicated by blue dot. Cf. Figure 1 for the location of the map in reference to southern California.

The Cretaceous (97 to 90 Ma) Teutonia batholith represents arc magmatism of the Cordilleran orogeny. This large intrusive complex is formed mainly of quartz monzonite and with less abundant granodiorite, diorite and granite (Beckerman 1982, DeWitt et al. 1984) and is cut by felsic to mafic dikes. Mafic-intermediate Cretaceous dikes are well exposed west of Cima dome and are emplaced in the felsic member of the Teutonia batholith (biotite monzogranite). The dike swarm is northwest trending, yields a K-Ar age ~90 Ma and is representative of the later stages of Mesozoic arc magmatism (Wilshire et al. 2002).

3. SAMPLES

The samples considered in this study comprise one metamorphic dike and one altered dike from the Salt Spring Hills, two metamorphic dikes (of which one is Proterozoic metadiabase), one altered dike, one Miocene basalt, and one Miocene rhyolite porphyry from the Saddlepeak Hills, two Miocene dikes and one Miocene stock from the Ibex Hills, and one Cretaceous dike from the northeastern Mojave Desert. The locations of the samples are shown in Figures 3-6. Thin sections for petrographic study were prepared from all these samples. Whole-rock geochemical analysis was performed on all samples except the basalt and rhyolite samples of Saddlepeak Hills. Miocene stock and one Miocene dike of Ibex Hills were studied in greater detail using electron microprobe (EPMA) analysis of plagioclase and *in situ* plagioclase strontium isotope geochemistry (LA-MC-ICP-MS). The samples are summarized in Table 1. The sample categories are distributed based on their age (Cretaceous, unknown, Miocene), the age unknown samples are separated by their secondary mineralogy (metamorphic, altered).

Table 1. Summary of samples from Saddlepeak Hills, Salt Spring Hills, Ibex Hills and Mojave Desert.

Sample ID	Location	Rock type	Thin section	Whole-rock	EPMA	LA-MC-ICP-MS
Cretaceous						
365	Mojave Desert	Trachyandesite	X	X[1]		
Metamorphic						
DVD-003*	Saddlepeak Hills	Metadiabase	X	X[2]		
DVD-002	Saddlepeak Hills	Meta-andesite	X	X[2]		
DVD-005	Salt Spring Hills	Meta-andesite	X	X[1]		
Altered						
DVD-001	Saddlepeak Hills	Meta-andesite	X	X[1]		
DVD-006	Salt Spring Hills	Meta-andesite	X	X[2]		
Miocene						
DVD-007	Ibex Hills	Trachyte	X	X[1]	X	X
DVD-009	Ibex Hills	Trachyandesite	X	X[2]	X	X
DVD-010	Ibex Hills	Trachyandesite	X	X[2]		
DVD-001ALT	Saddlepeak Hills	Basalt	X			
DVD-001ALT_2	Saddlepeak Hills	Rhyolite	X			

1 = Whole-rock geochemical analysis at Agat Laboratories.
2 = Whole-rock geochemical analysis at Peter Hooper GeoAnalytical Lab.
* = 1.1 Ga diabase.

4. METHODS

4.1 Field studies

Six days of field observations and sampling was carried out in Ibex Hills, Saddlepeak Hills and Salt Spring Hills in southern Death Valley, California in April 2019 (cf. Figures 2-5). Located between the Black Mountains in the north and the left-lateral Garlock Fault in the south, the three mountain ranges cover approximately ~300 km^2 area in the southwestern corner of the Death Valley extensional terrane. The author was accompanied by Dr. James Calzia (USGS) in the field. Field work was based on the unpublished mapping data by Bennie Troxel and James Calzia and on the previously dated dike of Ibex Hills (Troxel and Calzia 1994), assumed to be related to the rest of the dike swarm. A total of five dikes and one volcanic stock were sampled for petrographic and whole-rock chemistry analysis. Sample GPS location as well as dike trend, dip and width were recorded. Additional samples considered in this study include two Miocene dikes in Ibex Hills, Miocene basaltic lava flow and rhyolite porphyry in Saddlepeak Hills and a Cretaceous dike in northeastern Mojave Desert, collected by Dr. James Calzia and Dr. Tapani Rämö (University of Helsinki).

4.2 Petrography

A total of 25 thin sections were prepared at the Department of Geosciences and Geography, University of Helsinki for petrographic study. Petrographic examination of the eight dikes, stock, basaltic lava flow and felsic porphyry was performed by optical microscope at the University of Helsinki.

4.3 Whole-rock geochemistry

Four samples (two dikes of Saddlepeak Hills and Salt Spring Hills, a Miocene volcanic stock of Ibex Hills and a Cretaceous dike of Mojave Desert) were analyzed for whole-rock geochemical composition at AGAT Laboratories, Canada. The samples were

crushed and pulverized to <200 mesh for geochemical analysis. Major element oxides were determined by wavelength dispersive X-ray fluorescence spectrometry (WD-XRF). The analysis was performed on glass beads prepared by fusing each pulverized sample with lithium metaborate/lithium tetraborate flux. Trace elements were analyzed by inductively coupled plasma optical emission spectrometry (ICP-OES; 20 elements) and inductively coupled plasma mass spectrometry (ICP-MS; 40 elements) from samples that were fused with sodium peroxide at 750°C and dissolved in a dilute nitric acid. Detection limits for the analysis methods and each element are listed in USGS Contract Chemistry Method Summaries (site visited 01.06.2020).

Five additional dike samples (three dikes of Saddlepeak Hills and Salt Spring Hills and two Miocene dikes of Ibex Hills) were analyzed for ten major and minor elements and 19 trace elements by X-ray fluorescence spectrometry at Peter Hooper GeoAnalytical Lab at Washington State University. Samples analyzed at GeoAnalytical Lab were pulverized to <200 mesh, fused with di-lithium tetraborate in 1000°C to form beads which were then reground and polished. The analysis was performed with ThermoARL Advant´XP+ X-ray fluorescence spectrometer. The full outline of sample preparation, analytical procedure and standards used is available at the Peter Hooper GeoAnalytical Lab Technical notes (site visited 03.08.2020).

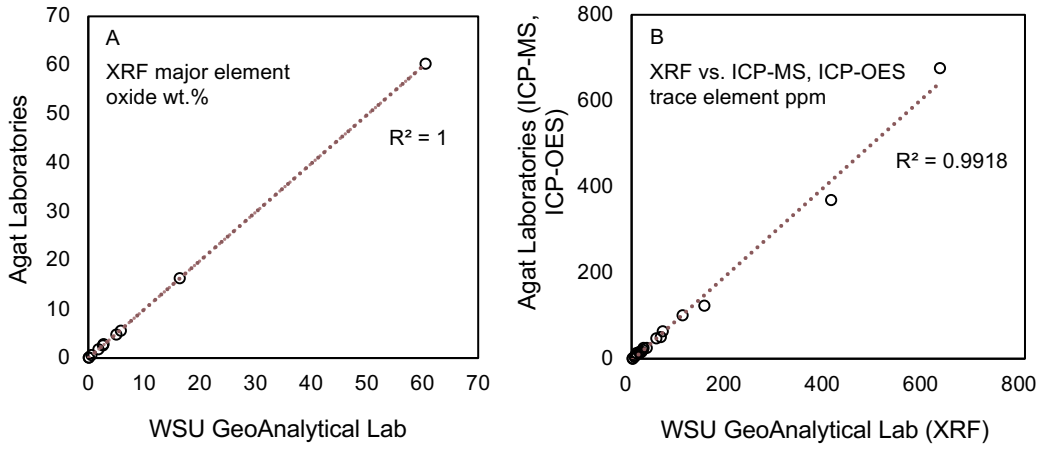

Figure 7. Correlation of analysis methods between Agat Laboratories and WSU GeoAnalytical Lab for A) major element oxides wt.% and B) trace elements ppm.

One sample was analyzed at both laboratories to monitor method comparability. Figure 7 shows correlation between the two laboratories for major element oxides wt.% (XRF) and trace elements ppm (XRF, ICP-MS/-OES).

4.4 Mineral chemistry

Composition of plagioclase from two Miocene samples of Ibex Hills (trachyte stock and trachyandesite dike) were analyzed at the Department of Geosciences and Geography at University of Helsinki. Two carbon coated thick sections (~300 μm), prepared at the University of Helsinki, were analyzed using JEOL JXA 8600 electron probe microanalyzer (EPMA) equipped with four wavelength-dispersive (WDS) spectrometers. Due to a faulty signal cable, only three out of four spectrometers were functioning, and Fe was not detected during the analysis. However, as the aim was to measure the amounts of the end member compositions in plagioclase, the effect of omitting Fe from the analysis has a nominal effect for the purpose of this study. The microprobe was set to 15 kV acceleration voltage and 15 nA beam current. Focused beam was used for all measurements. The matrix was corrected using the PAP-method (Pouchou and Pichoir 1984) with PointElectronic SAMx hardware and the SAMx analytical software package. The following standards were used for determining the accuracy of the EPMA analysis: Plagioclase (An_{30}) for Ca and Al, Albite for Na and Si, Sanidine for K, Periclase for Mg and Barite for Ba.

During the analysis, the beam current drifted from 15 nA to 15.3 nA, causing the analysis element oxide total to drop as low as 93.27 for some of the measurements (the measurement totals range from 93.27 to 100.31). However, the stoichiometric calculations (Na+K+Ca=1; Si+Al=4) were not affected by the drifting measurement total, thus the chemical formula remains valid for all measurements regardless of the total. For the purpose of this study, i.e. analyzing the plagioclase An (mol.%) content, no measurements were omitted from the analysis due to low total. The plagioclase mineral formulae were calculated based on (O=8) atoms per formula unit.

4.5 Strontium isotope geochemistry

As heavy radiogenic isotopes do not measurably fractionate during partial melting or fractional crystallization, they are valuable in the recording of source isotopic composition of magmas. *In situ* laser ablation multi-collector inductively coupled plasma mass spectrometry (LA-MC-ICP-MS) method can accurately identify details of changes in crystallizing magma Sr isotopic composition, recorded in the mineral growth zones (Ramos et al. 2004). In order to identify source composition, highlight possible source heterogeneities between samples and investigate magma chamber conditions during the Miocene Basin and Range extension magmatism underneath Ibex Hills, core to rim $^{87}Sr/^{86}Sr$ ratios were measured from selected plagioclase phenocrysts from two Miocene samples of Ibex Hills.

In situ $^{87}Sr/^{86}Sr$ analyses of plagioclase phenocrysts (n = 17) were performed on two thick sections (~300 μm) from trachyte stock (DVD-007) and trachyandesite dike (DVD-009) of Ibex Hills with LA-MC-ICP-MS at the Finnish Geosciences Research Laboratory (SGL, Suomen geotieteiden tutkimuslaboratorio) in two analysis sessions. The analyses were conducted with a Photon Machine Analyte G2 laser microprobe and Nu Plasma HR MC-ICP-MS with nine Faraday detectors and amplifiers with 10^{11} Ω resistors. The thick sections were ablated in HelEx ablation cell with He gas (gas flows 0.4 and 0.1 l/min) (Muller et al. 2009). All analyses were conducted in static ablation mode with beam diameter of 110 μm, beam energy density of 3 J/cm^2 and pulse frequency of 20 Hz. The data were collected in static mode with five collectors (^{84}Sr-Kr, ^{85}Rb, ^{86}Sr-Kr, ^{87}Rb-Sr, and ^{88}Sr).

The effect of instrumental fractionation on measured Sr isotope ratios were corrected with exponential law and $^{86}Sr/^{88}Sr$ value of 0.1194. Throughout the analysis, the isobaric interference of ^{87}Rb on ^{87}Sr was monitored and the ^{85}Rb ion signal and a value of 0.38571 for the $^{87}Rb/^{85}Rb$ ratio was used for correcting the interference. The isobaric interference of ^{86}Kr on ^{86}Sr was corrected using a 30s background measurement prior to every ablation. Each ablation was run for 120s to obtain an internal precision of $\leq \pm 0.000020$ (2σ). To verify the accuracy of the laser ablation protocol, repeated measurements were performed on two standards throughout both of the analysis sessions. For the in-house plagioclase megacryst standard from the Cameroon volcanic chain, Mir a (Rankenburg

et al. 2004), the average $^{87}Sr/^{86}Sr$ ratio was 0.70299728 ± 0.000082 (2σ, n = 13). This is comparable with the solution reference value 0.703057 ± 0.000007 (2σ, average duplicated analysis by MC-ICP-MS on two separate grains). The average $^{84}Sr/^{86}Sr$ ratio 0.05630 ± 0.00018 (2σ, n =8) for the standard was obtained. The value is comparable with the accepted value 0.056 ± 0.0001 (Thirlwall 1991). The second standard BHVO-2G gave an average $^{87}Sr/^{86}Sr$ value 0.703414 ± 0.000084 (1σ, n = 6) and it is within the error of the GEOREM database preferred value 0.703476 ± 0.000007.

The analytical precision (1σ) is between 0.000007 and 0.000022 for all accepted analysis spots which is adequate for isotope ratio range in 0.0001 units (Davidson et al. 2007). The data are presented as measured values as the data back-calculated to initial values of 12.4 Ma lie within the analytical error of the measured values.

5. FIELD OBSERVATIONS

Original map (Troxel and Calzia, unpublished mapping, 2018) data show a swarm of northwest trending dikes in both Saddlepeak Hills and Salt Spring Hills. Due to time restrictions regarding field work, only outcrops exposed at the bottom of hillsides were examined and sampled. Based on petrographic study, all sampled dikes from Saddlepeak Hills and Salt Spring Hills have secondary mineral overprint, whereas samples from Ibex Hills are relatively fresh (see Chapter 6). Overall, the dikes considered in this study trend NW–SE, are mostly nearly vertical and 1.4 to 4 m wide.

5.1 Metamorphic and altered dikes of southern Death Valley

An exposed dike (sample DVD-001) on the eastern side of Saddlepeak Hills (~ 2.9 km west from Highway 127) cuts Neoproterozoic Kingston Peak diamictite and runs parallel to a northwest trending fault zone (Figure 8). The dike is northwest trending (N35°W), drips 50° to the south and is pinching and swelling along its length with maximum thickness of 1.4 m at the sampling location. The hand sample is fine- to medium-grained, purple colored inequigranular rock with dark to rust colored oxidized, originally mafic

phenocrysts of up to 5 mm long. The groundmass is composed of fine-grained mafic mineral and white feldspar.

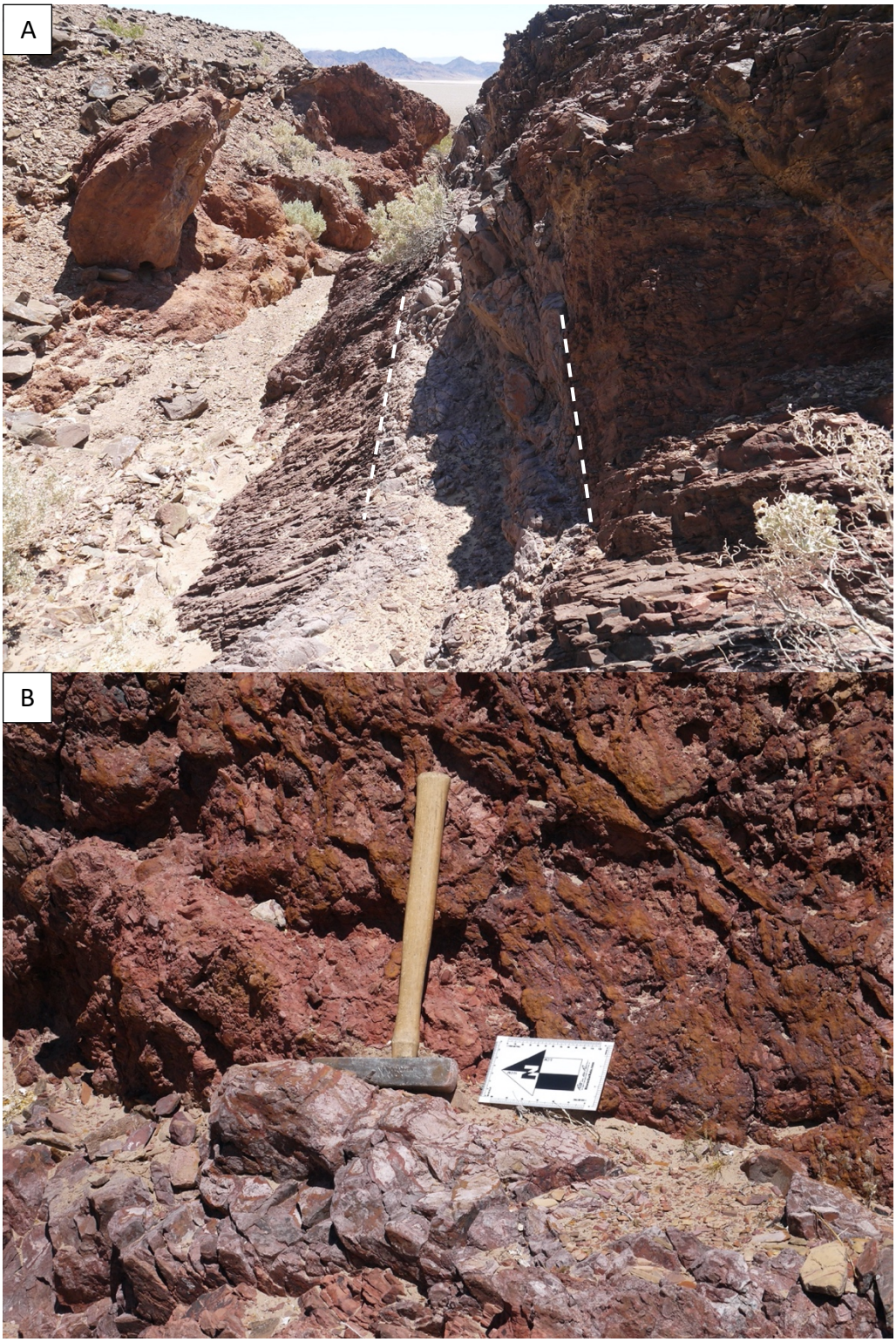

Figure 8. A) Fine- to medium-grained metamorphic dike DVD-001 with oxidized phenocrysts (not visible in photo) from eastern side of Saddlepeak Hills. Dike width is ~1.4 m and the image is facing southeast. B) Dike contact with Kingston Peak diamicton. Photos by the author.

Two parallel dikes on the western side of Saddlepeak Hills cut green, coarse grained 1.1 Ga diabase sill (cf. Heaman and Grotzinger 1992), ~1.5 km east from Saratoga Springs Road. Locally the exposed dikes can be distinguished from the diabase sill by grain size or color. Fine-grained light green meta-andesite dike (sample DVD-002, Figure 9) trends 60° to the northwest and dips 70° to the south. Due to weathering the contact of the dike with diabase is difficult to determine but the approximate width of the dike is 4 m. The dike has a roughly equigranular texture with generally ~1 mm large grains of white feldspar and small mafic mineral grains in light green fine-grained groundmass. A separate darker green dike (sample DVD-003, Figure 10) trends 45° to the northwest. There are no definite boundaries exposed, but the dike appears to be widening towards the downside of the hill. The average grain size is ~1-2 mm, although some feldspar laths are slightly larger. The texture is roughly equigranular. In comparison with sample DVD-002, this sample has slightly larger grain size, darker green color and abundant mafic minerals.

Figure 9. Meta-andesite dike DVD-002 on the western side of Saddlepeak Hills in contact with 1.1 Ga diabase. Dike is to the right and diabase host rock is to the left. Photo by the author.

Figure 10. Metabasaltic dike DVD-003 on the western side of Saddlepeak Hills in contact with 1.1 Ga diabase. Photo by the author.

Two dikes were sampled on the western side of Salt Spring Hills (accessible via Highway 127 and over Little Dumont Dunes). A locally porphyritic dike with altered long laths up to 4-5 mm in size and 1-2 mm white feldspar in sage green fine-grained (<1 mm) groundmass cuts the Neoproterozoic Johnnie Formation (sample DVD-005, Figure 11). The altered minerals are light colored with green tint. Some small mafic and brown oxidized minerals are also observed. Lineated veins are visible on a cut surface. The dike is vertical, runs 60° to the northwest with maximum width of 1.5 m. The outcrop shows intense weathering and no clear contact with the surrounding rocks is exposed. The dike leaves a topographically lower trail in the host rock with a cover of weathered sediment from the dike and host rock. The dike is locally exposed through the sediment. Approximately 1.2 km to the south, nearly vertical (80°S) northwest trending (N40°W) 3 m wide dike cuts Neoproterozoic Stirling Quartzite (sample DVD-006, Figure 12). The dike is recognizably hydrothermally altered, deep red in color with leached pale batches towards the margin. The dike margins show yellow colored alteration that continues to the host quartzite at the contact. The general texture is vesicular and fine-grained with a small number of ~1 mm long white feldspar grains.

Figure 11. Porphyritic meta-andesite dike DVD-007 located on the western side of Salt Spring Hills. The 1.5 m dike cuts Neoproterozoic Johnnie Formation. Photo by the author.

Figure 12 continues…

Figure 12. A) Pervasively altered meta-andesite on the western side of Salt Spring Hills. B) Contact with Neoproterozoic Sterling Quartzite. Leached patches in the dike are visible towards the contact (right) with conversion into rusty discoloration that continues into the quartzite (left). Vesicles are visible in the leached part below camera lens. Photos by the author.

5.2 Miocene dikes and related rocks of southern Death Valley

Miocene samples considered in this study include porphyritic stock with volcanic texture and two porphyritic dikes emplaced in the stock. This igneous body lies on the eastern side of Ibex Hills, south of Moorhouse talc mine and ca. 300 m west of Ibex Spring and covers approximately 1 km^2. The stock is purple colored porphyritic trachyte with ~5 mm long white plagioclase and slightly smaller altered rusty amphibole phenocrysts in light grey-purple fine-grained groundmass (sample DVD-007, Figure 13). Two northwest trending porphyritic trachyandesite dikes cut the porphyritic stock. Sample DVD-009 is a 4-m-wide dike, with relatively fresh ~5 mm plagioclase and altered amphibole phenocrysts in in a medium grey microcrystalline groundmass (Figure 14). Vesicles with secondary fill cover approximately 5% of the rock mass. The dike shows chilled margins against the igneous stock. DVD-010 has white plagioclase and fresh mafic phenocrysts

in aphanitic groundmass with less abundant vesicles compared to DVD-009 (Figure 14). Overall, the dikes are northwest trending and nearly vertical.

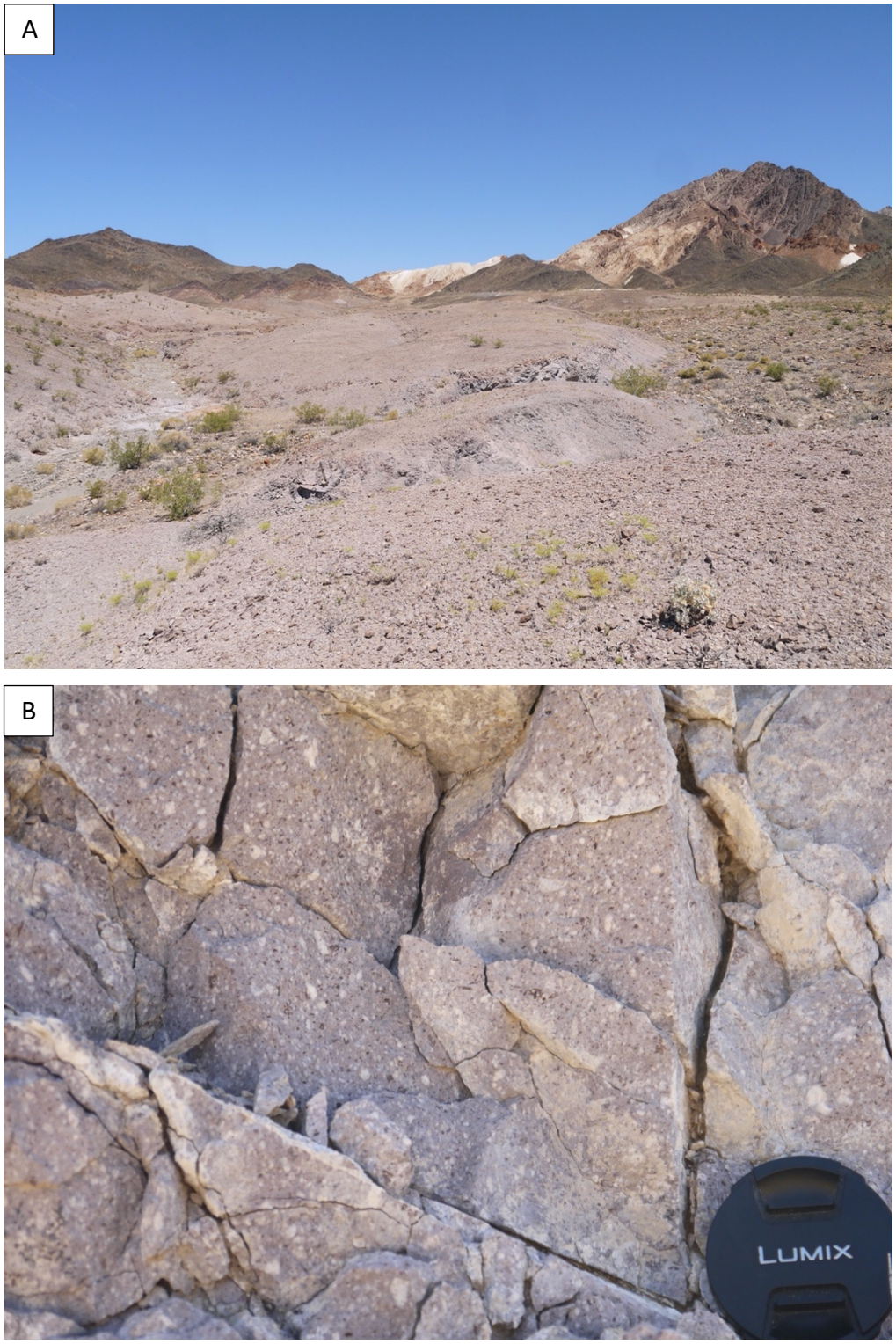

Figure 13. A) Purple colored trachyte stock DVD-007. Image facing north and Moorhouse talc mine can be seen in the back. B) Close-up image of DVD-007 with white feldspar and mafic phenocryst in purple groundmass. Photos by the author.

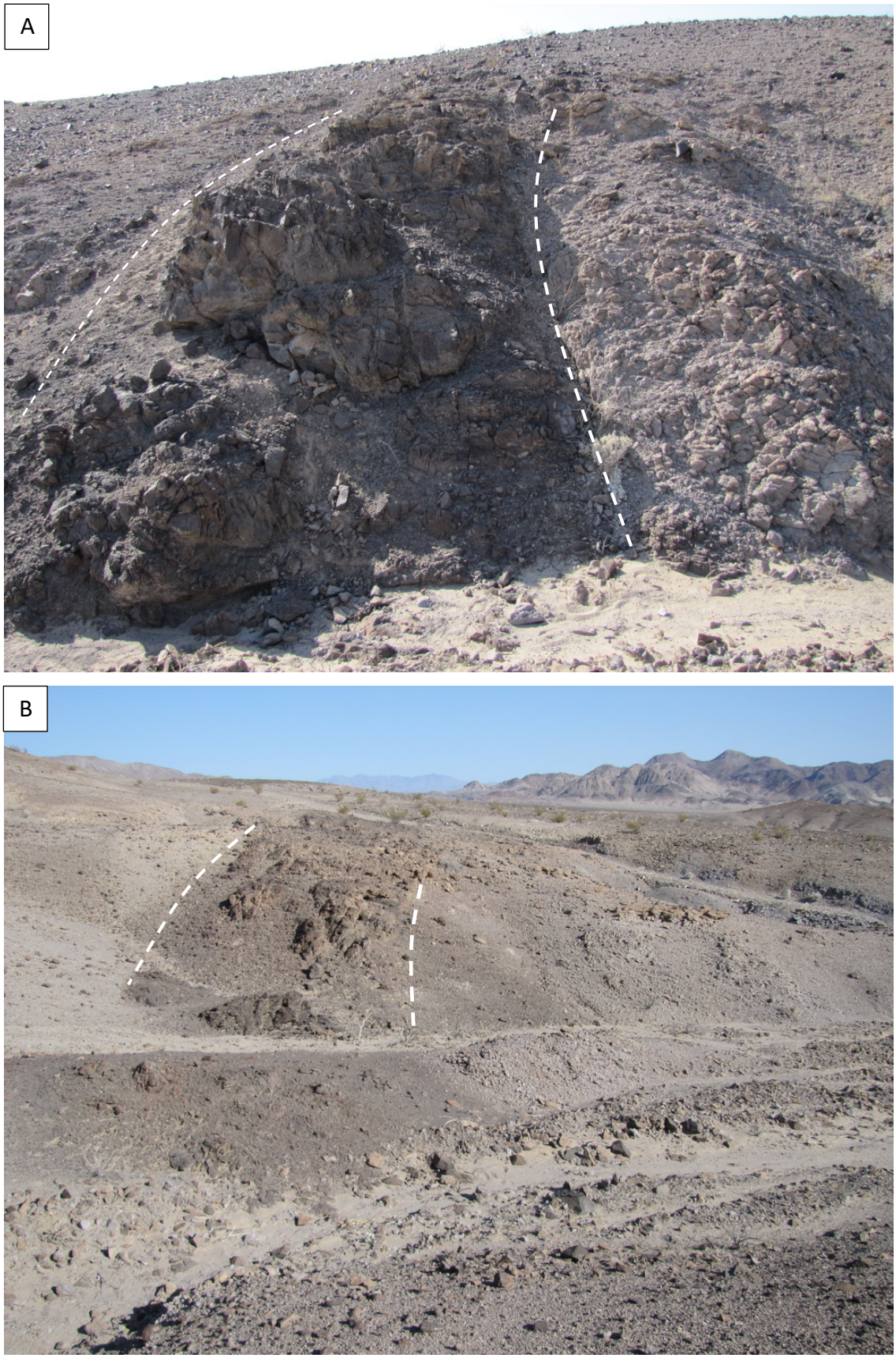

Figure 14 continues…

Figure 14. Miocene trachyandesite dikes A) DVD-009 and B) DVD-010 of Ibex Hills cutting Miocene trachyte stock of Ibex Hills (DVD-007). C) Trachyandesite enclave in trachyte stock. D) Trachyandesite dike with plagioclase feldspar phenocrysts in dark purple groundmass. Photos: Tapani Rämö.

Basalt and felsic porphyry samples were collected adjacent to the western Saddlepeak Hills and ~950 m east of sample DVD-001 location. This igneous body comprises Miocene basaltic lava with plagioclase and amygdules with secondary fill in aphanitic groundmass (DVD-001ALT, Figure 15). The basalt is topped by Miocene felsic porphyry (DVD-001ALT_2). These rocks continue northward and unconformably overlie the Kingston Peak Formation intruded by the metamorphosed dikes. Contact relations between the basalt and felsic flows are not exposed.

Figure 15. Miocene basaltic lava flow (DVD-001ALT) adjacent to the eastern flank of Saddlepeak Hills and location of the metamorphic sample DVD-001. Photo: Tapani Rämö.

5.3 Cretaceous dike of Mojave Desert

An inequigranular dike cuts Cretaceous Teutonia batholith in the northeastern Mojave Desert (sample 365, Figure 16). The dike is 2.5 m wide, northwest striking (N55°W) and dipping 61° to the north and is part of a swarm of northwest trending mafic dikes. The dike has amphibole phenocrysts in green fine-grained groundmass. Small plagioclase

feldspar grains are abundant, and the sample contains few ~1 mm quartz xenocrysts with dark reaction rim.

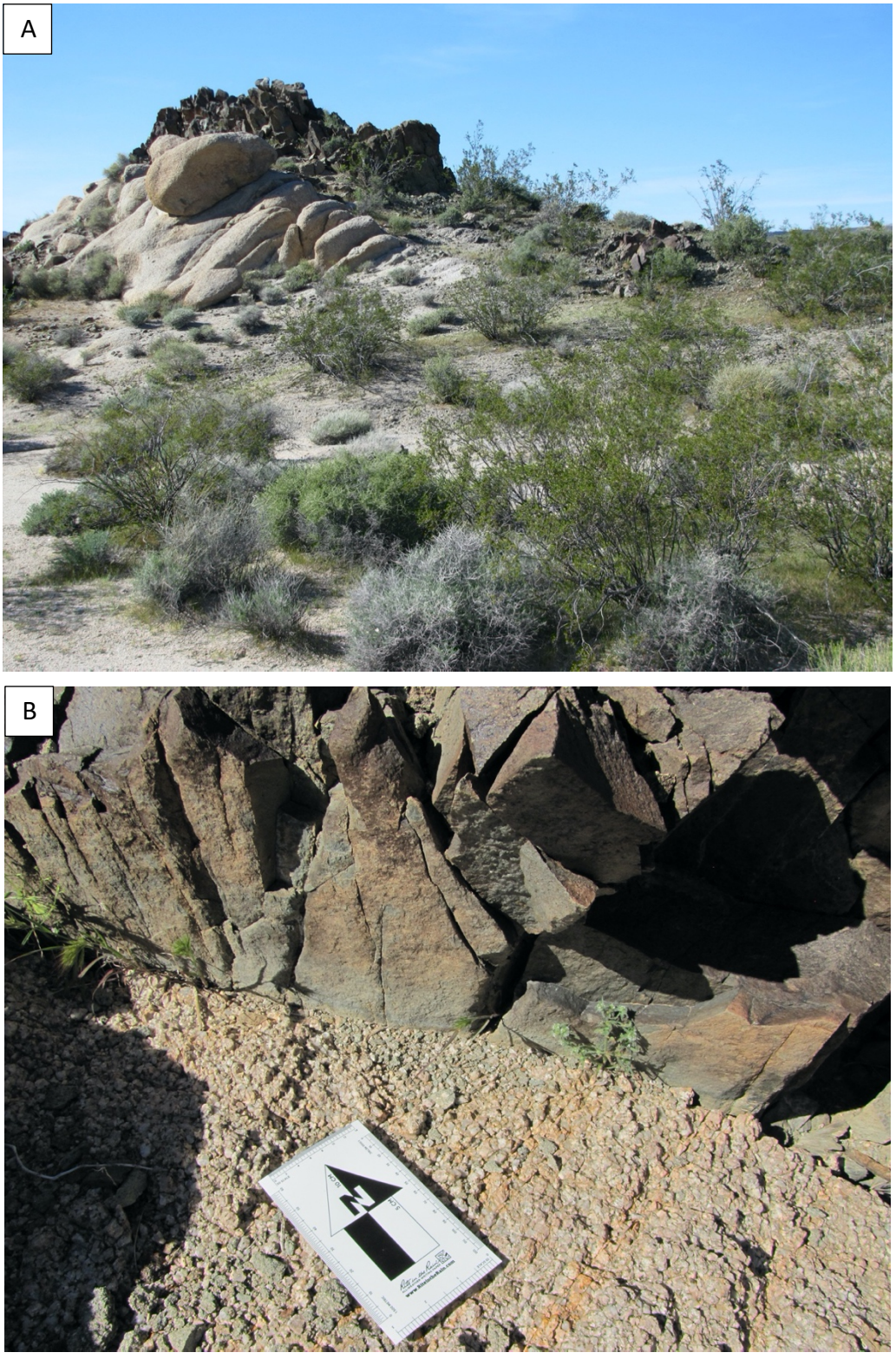

Figure 16. A) and B) Cretaceous trachyandesite dike of northeastern Mojave Desert (darker rock) cutting Cretaceous Teutonia batholith (lighter rock). Photos: Tapani Rämö.

6. PETROGRAPHY

The petrography of the studied samples is described below by adopted lithological division. The Miocene samples are relatively fresh with abundant felspar, amphibole and biotite. The Cretaceous dike is altered but has retained some magmatic features. The dikes of Saddlepeak Hills and Salt Spring Hills have a pervasive secondary mineral overprint. However, based on their secondary mineralogy, these dikes are distinguished into two groups. The metamorphic sample group is characterized by chlorite, epidote and albite whereas the altered sample group has abundant sericite, secondary quartz and feldspar and oxides. Pervasive post-magmatic alteration complicates the examination of the metamorphic and altered samples. Preserved primary minerals and original textures are sparse but pseudomorphs are utilized in interpreting the original petrography.

6.1 Metamorphic samples of Saddlepeak Hills and Salt Spring Hills

6.1.1 Proterozoic metadiabase DVD-003

The petrography of DVD-003 is almost completely marked by secondary features (Figure 17). Pervasively altered plagioclase feldspar with microsaussurite composed of epidote and chlorite dominates the mineral assemblage. The plagioclase laths are on average up to 1 mm long and lack preferred orientation. The visibility of the grain boundaries is somewhat unclear due to the level of alteration but concentration of chlorite at mineral edge outlining the boundaries is indicative of the primary texture. Chlorite smears the grain at the boundaries whereas epidote forms cloudy and small anhedral grain aggregates similar to the epidote alteration seen in sample DVD-002, except in this sample the epidote pseudomorphs the entire grain. The emplacement of chlorite is not restricted to plagioclase and is found as flaky or massive patches across the section. Epidote found between plagioclase pseudomorphs forms clear and coarse euhedral to subhedral grains. Opaque Ti-Fe-oxide minerals are abundant and are associated with interstitial chlorite. Large, ~2-4 mm in diameter opaque mineral, possibly ilmenite, are often skeletal or embayed and have a thin corona of titanite. Smaller opaque mineral is found in polymineral aggregates and they lack the titanite corona. These could be magnetite and of a separate crystallization phase to the ilmenite. Primary apatite and secondary biotite,

amphibole and rutile form accessory phases. Apatite is an abundant accessory mineral and forms prismatic euhedral crystals. Anhedral biotite with pale brown to dark green pleochroism show alteration to chlorite at grain boundaries and has opaque minerals at cleavage cracks. Dark green anhedral secondary amphibole is often associated with biotite. Brown oxidation product stains the sample and sometimes resembles prismatic mineral habit and is thus possibly an alteration product of an originally mafic mineral.

Much cannot be said about the primary features of the sample, but the randomly orientated plagioclase pseudomorphs often partially enclosed in opaque minerals indicate original subophitic to ophitic texture. The abundance of this pseudomorph suggests plagioclase to be most abundant primary mineral; chlorite, amphibole, biotite and Fe-oxide alteration between feldspar pseudomorphs imply primary interstitial mineral assemblage was predominantly mafic.

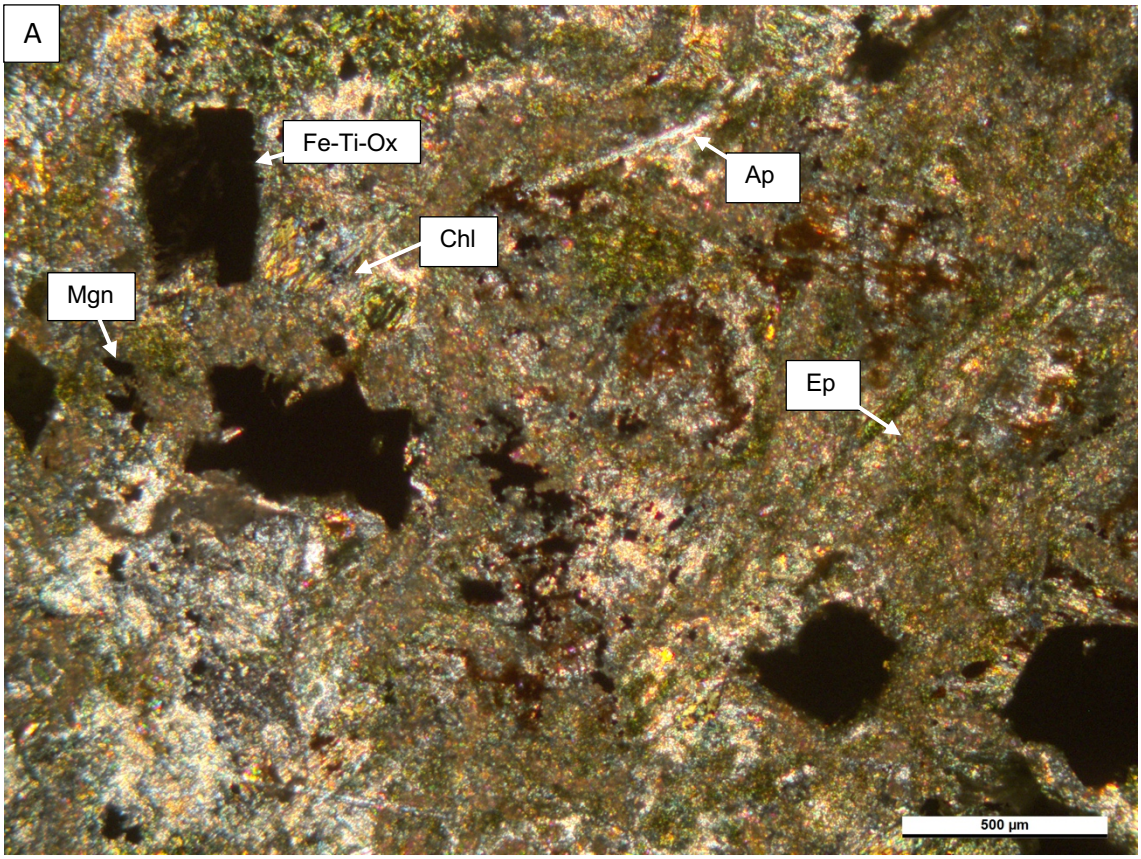

Figure 17 continues…

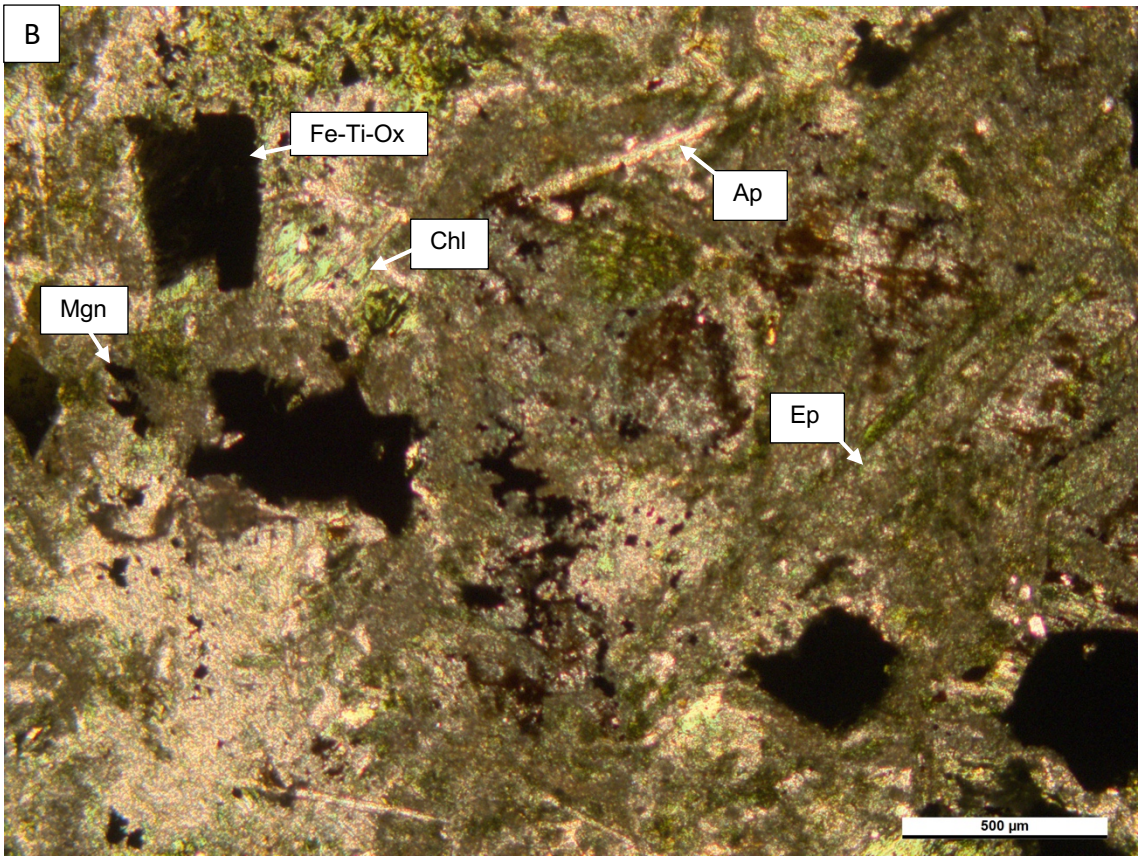

Figure 17. Basaltic sample DVD-003 of Saddlepeak Hills displaying plagioclase strongly altered with chlorite and epidote. Large opaque minerals are Fe-Ti oxides and smaller diamond shaped are possibly magnetite. Chlorite and brown oxidation stain cover the sample. Abundant apatite is visible especially in plain polarized light (B). A) XPL and B) PPL. Ap = apatite; Chl = chlorite; Ep = epidote; Fe-Ti-ox = Fe-Ti oxide; Mgn = magnetite.

6.1.2 Fine-grained meta-andesite DVD-002

Sample DVD-002 has been moderately altered with saussuritized/sericitized plagioclase feldspar, epidote and chlorite as main minerals and apatite, muscovite and opaque mineral accessory phases (Figure 18). Plagioclase is the most abundant mineral and can be found as ~0.5 mm long subhedral to anhedral grains with often irregular grain boundaries in contact with epidote, chlorite and other plagioclase grains. Myrmekite-like intergrowths can be found at grain boundaries. Late- or post-magmatic albitization of the primary Ca-rich plagioclase is common, and most plagioclase grains have been altered by epidote. Epidote forms cloudy aggregates of small irregular microcrystals that most commonly occupy the plagioclase core. Sericite alteration is common in plagioclase grains where epidote alteration has not taken place or has been minimal. Except as a co-product of albitization of Ca-rich plagioclase, epidote can also be found as larger and clear euhedral grains commonly in bundles with secondary feldspar, chlorite and muscovite,

representing crystallization after circulating fluid. Interstitial space between plagioclase contains chlorite and secondary silicate. Chlorite with anomalous blue and purple interference colors can be found as irregular massive patches across the sample. Accessory apatite forms small needle-like inclusions in feldspar.

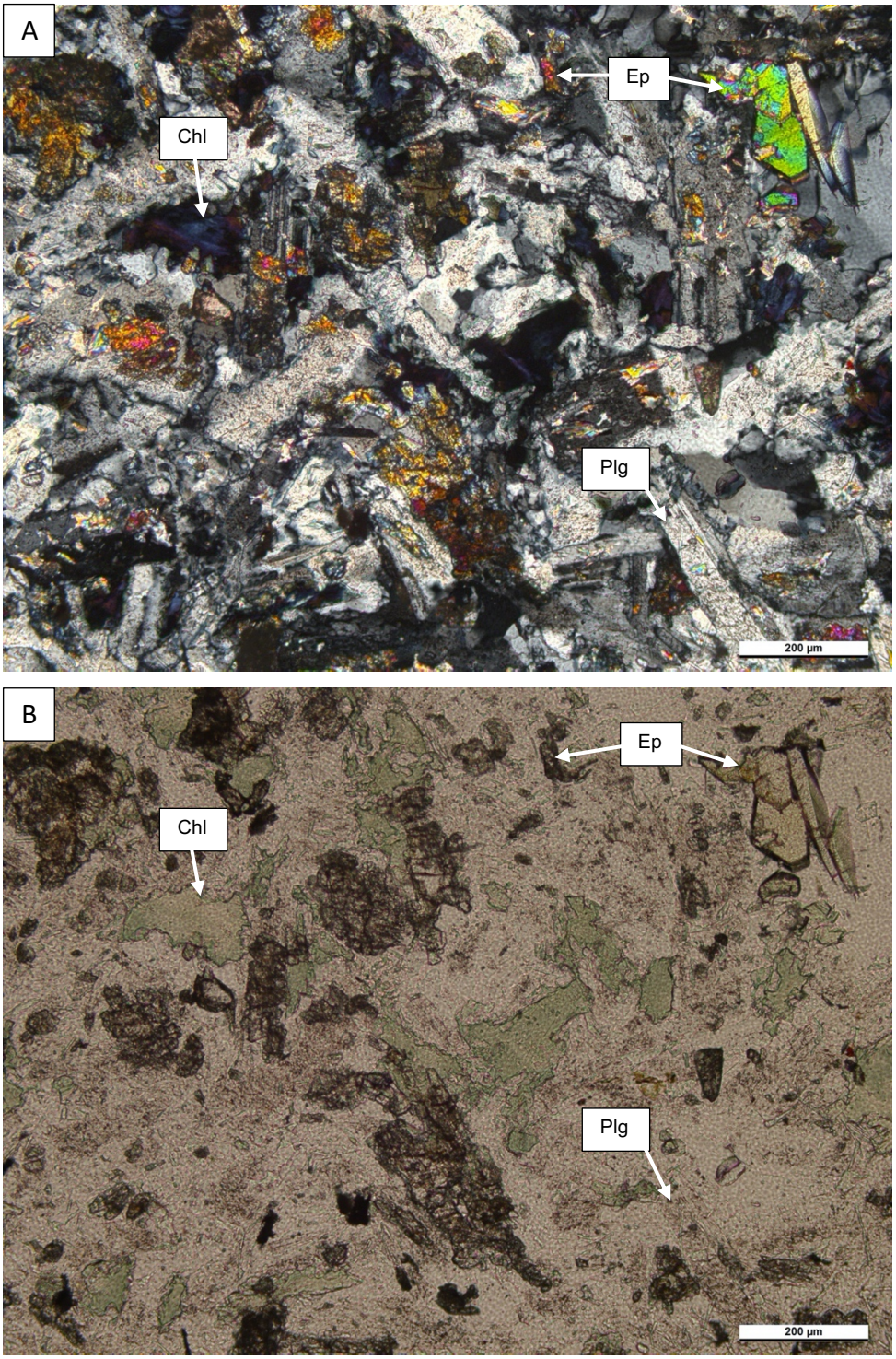

Figure 18. Plagioclase feldspar with sericite and microcrystalline epidote alteration (co-product of plagioclase albitization) is the most abundant mineral in sample DVD-002 of Saddlepeak Hills. Twin lamellae are visible

in some of the grains. Chlorite patches are common across the sample. Euhedral epidote grains are on the top right corner. A) XPL and B) PPL. Chl = chlorite; Ep = epidote; Plg = plagioclase.

6.1.3 Porphyritic meta-andesite DVD-005

Sample DVD-005 shows pervasive post-crystallization alteration with no primary mineral phases preserved (Figure 19). The sample is, however, rich in two pseudomorphs. Plagioclase feldspar pseudomorphed by sericite has retained its relict euhedral mineral shape. A thin albitic (determined optically) feldspar rim is sometimes preserved from pervasive sericitic alteration and on a rare occasion a hint of twin lamellae can be observed. Cloudy fine-grained anhedral epidote is spread across the sericitic feldspar but epidote alteration witnessed here is not as abundant as in samples DVD-002 and DVD-003. Less abundant phenocryst with long prismatic grains and hexagonal cross sections suggests monoclinic, possibly a mafic origin. These phenocrysts have been completely pseudomorphed by epidote, chlorite and carbonate and they often occur as mineral bundles of several grains. Epidote alteration commonly dominates these phenocrysts although occasionally carbonate and/or chlorite form the principal alteration phases. Opaque minerals form discontinuous rim around these pseudomorphs, and they can also be found in the mid-section of the grain, especially in association with chlorite. Epidote is usually clear and subhedral, sometimes the grains appear stained. Chlorite displays anomalous blue to purple interference colors. Chlorite is also found as irregular patches in the interstitial space between the phenocrysts with altering anomalous brown and blue interference colors that cover approximately 30% of the mineral fabric. Opaque minerals and magmatic apatite are found as accessory phases. Some opaque minerals have leucoxene rim. The groundmass is composed of secondary silicate, chlorite and small anhedral epidote. Numerous cracks and veins with brown oxidation stain run parallel to each other throughout the sample, possibly representing the flow of hydrothermal fluids. Larger veins are filled with fibrous carbonate organized perpendicular to the vein wall.

Again, the post-crystallization alteration makes assessing the original petrography of this sample only indicative at best. The two pseudomorphs suggest that plagioclase feldspar and a less abundant mafic mineral formed the main mineral phases. The plagioclase pseudomorphs are ~ 1 mm in size and some of the mafic pseudomorphs are as long as 5 mm. This suggest fine to medium phaneritic or porphyritic-phaneritic texture, depending on the igneous interstitial texture.

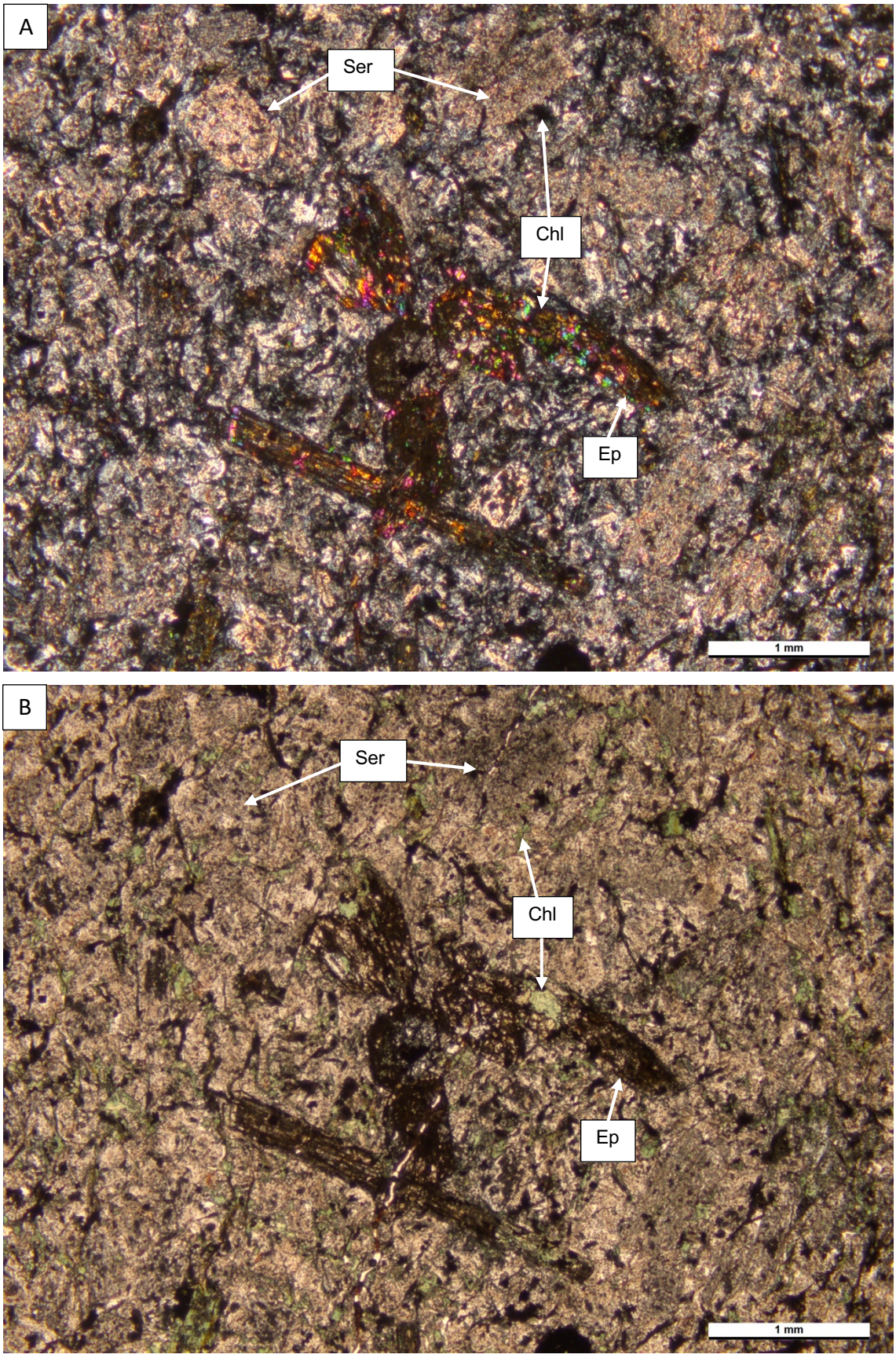

Figure 19. Andesite dike DVD-005 of Salt Spring Hills showing grain aggregate of originally mafic minerals altered to epidote, chlorite and carbonate. The hexagonal and prismatic crystal habits are still visible.

Feldspar with pervasive sericite and epidote alteration is abundant and small patches of chlorite is scattered around the sample. A) XPL and B) PPL. Chl = chlorite; Ep = epidote; Ser = sericite.

6.2 Altered dikes of Saddlepeak Hills and Salt Spring Hills

6.2.1 Meta-andesite DVD-001

DVD-001 shows blastoporphyritic texture with oxidized, possibly originally mafic, and less abundant sericitic pseudomorphs after plagioclase phenocrysts (Figure 20). Apart from magmatic accessory apatite, no original mineral phases are present. The prevailing altered fabric with phenocrysts suggests that the texture prior to alteration may have been porphyritic. The oxidized phenocrysts have, on occasion, preserved their relict crystal habit that of stubby prismatic grains and hexagonal cross sections characteristic of monoclinic minerals. This is especially true close to the dike margin where the crystal boundaries are clear and well preserved – towards the middle of the dike the oxidized mineral grain boundaries are not as sharp and contain inclusions of sericitic plagioclase laths. Less commonly, patches of calcite alteration and microcrystalline secondary quartz with undulatory extinction can also be observed in the oxidized phenocrysts. Sericite after feldspar phenocrysts are rare. The sericitization of the feldspar is pervasive and the grains are completely altered to muscovite. The grain boundaries are still clear, and the altered feldspar grains are commonly up to 1 mm long. The groundmass is dominated by sericitized plagioclase microlites, quartz, possibly deuteric feldspar and opaque minerals. Low Na_2O in the sample suggests that albitic feldspar is not abundant (see Section 7.1). Apatite forms an accessory phase. Vein filled with secondary granular calcite cuts the section.

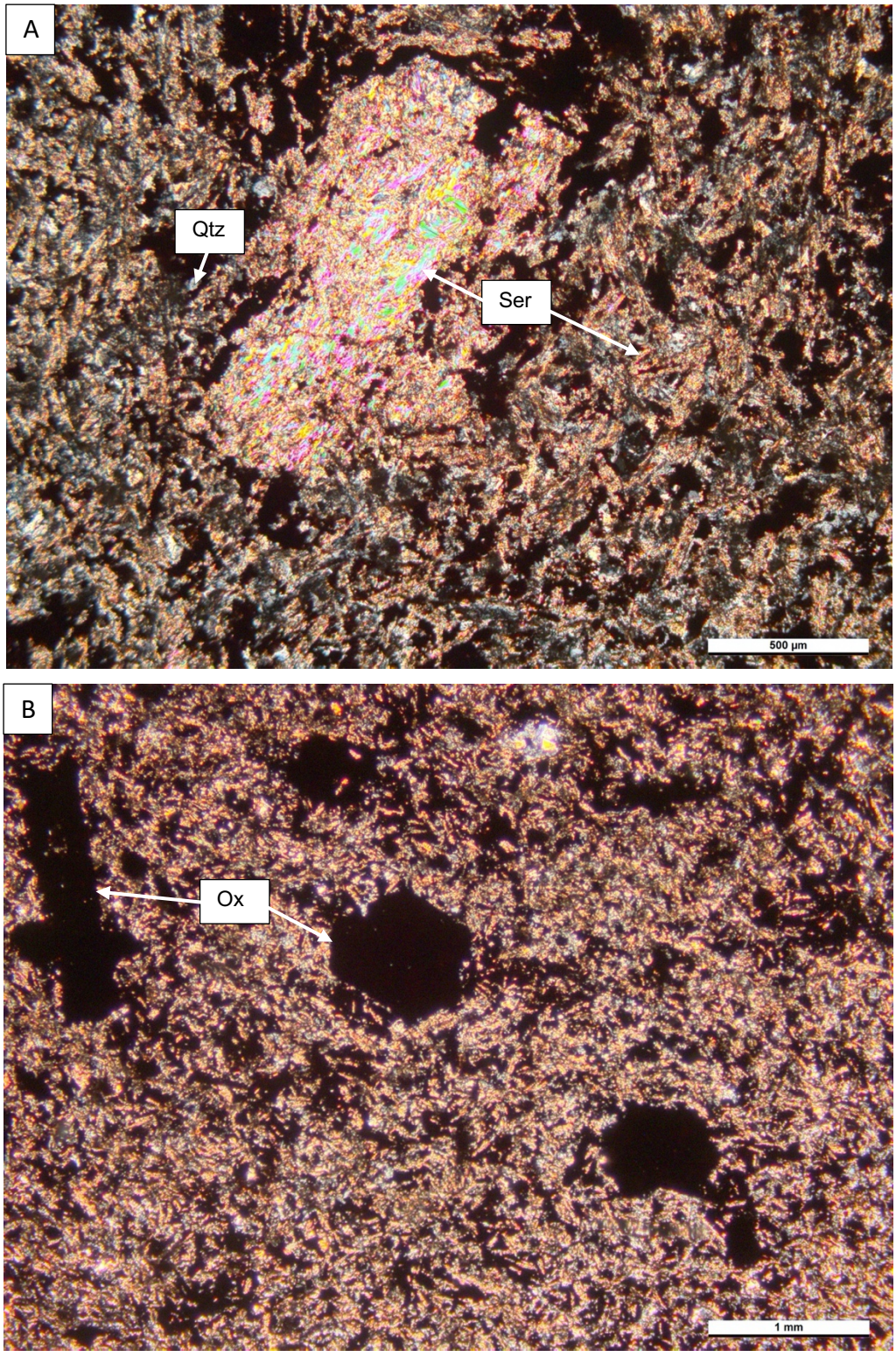

Figure 20. A) Feldspar phenocryst completely altered by sericite with clear prismatic grain boundaries in fine-grained groundmass of altered feldspar and opaque minerals in sample DVD-001 of Saddlepeak Hills. B) Common oxidized phenocrysts with hexagonal and prismatic crystal habit, suggesting an altered monoclinic primary mineral (DVD-001). Ox = oxidized minerals; Ser = sericite; Qtz = quartz.

6.2.2 Strongly altered meta-andesite DVD-006

This sample has been subject to the most intensive post-crystallization alteration out of the studied samples and little can be said about the mineral assemblage or texture prior to the alteration (Figure 21). There are, however, stubby phenocrysts showing pervasive muscovite-sericite alteration, a possible pseudomorph after feldspar. Smaller grains with similar sericite alteration and secondary silicate are found in the groundmass. Opaque minerals are abundant, and they are randomly scattered over the sample. There are rare oxidized patches with clear boundaries resembling either prismatic grains or hexagonal cross sections – these could be oxidized mafic minerals. Irregular oxidized patches are distributed across the section indicating circulation of fluids and filling vesicles. Coarse-grained aggregates of carbonate often fill these oxidized patches. Small-grained aggregates of rutile are common. The sample has a single fresh apatite grain, which could be of magmatic origin or a xenocryst.

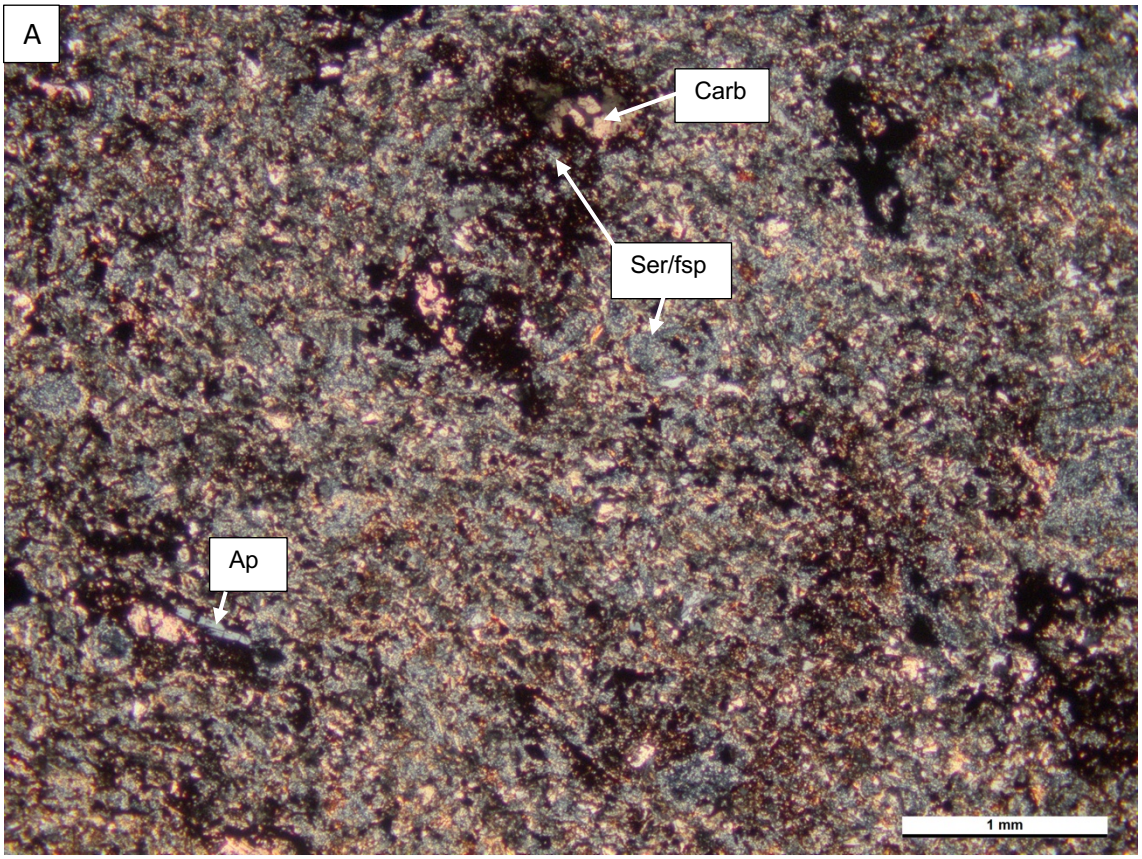

Figure 21 continues…

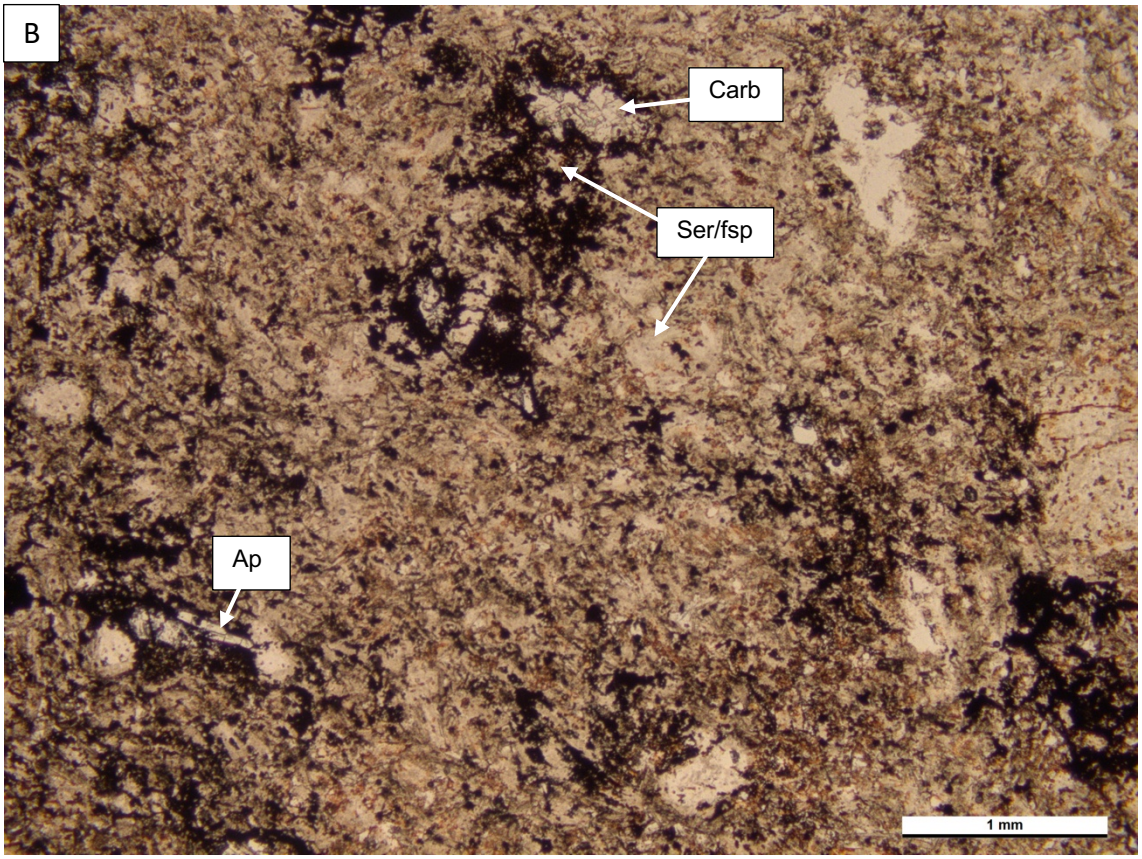

Figure 21. Strongly altered andesite dike DVD-006 of Salt Spring Hills with irregular oxidised patches. A prismatic oxidized grain with numerous, possibly originally feldspar, mineral inclusions and coarse-grained carbonate is located towards the top of the image and could be remains of an originally mafic mineral. Smaller grains, possibly feldspar with pervasive sericite/secondary silicate alteration are abundant. Apatite grain is visible towards the bottom-left corner of the image. A) XPL and b) PPL. Ap = apatite; Carb = carbonate; Fsp = feldspar; Ser = sericite.

6.3 Miocene stock and dikes of Ibex Hills

The Miocene rocks considered in this study differ from the altered dikes of Saddlepeak Hill and Salt Spring Hill in their texture and degree of post-crystallization alteration. The Miocene samples have porphyritic texture and, apart from minor sericitization of plagioclase, alteration of mafic minerals and secondary calcite, the mineral phases are pristine.

6.3.1 Trachyte stock DVD-007

DVD-007 is a porphyritic stock with plagioclase, amphibole and biotite phenocrysts (Figure 22). The plagioclase phenocrysts are euhedral to subhedral and up to ~4 mm long. Apart from minor sericite alteration, the plagioclase is fresh. Some plagioclase show

compositional zoning and fluid inclusions and cracks are common. The cracks are sometimes filled with brown oxidized fluid product. Most plagioclase phenocrysts have sieve and other disequilibrium textures, especially towards the grain boundaries. The mafic phenocrysts have been exposed to strong post-magmatic alteration. Amphibole forms the most abundant mafic phenocryst phase. The amphibole has a thick opaque rim and, although mostly euhedral or subhedral, often has evidence of embayed texture at grain boundaries. Brown biotite phenocrysts are slightly smaller, euhedral to subhedral and displays strongly mottled texture with a thin opaque rim and abundant opaque mineral inclusions. Both amphibole and biotite interlock plagioclase grains. The groundmass is composed of plagioclase microlites, amphibole, biotite and opaque minerals. Apatite and zircon form the accessory phases. Apatite is mostly found as inclusions in the amphibole opaque rim. There are few fractures filled with calcite and clay minerals.

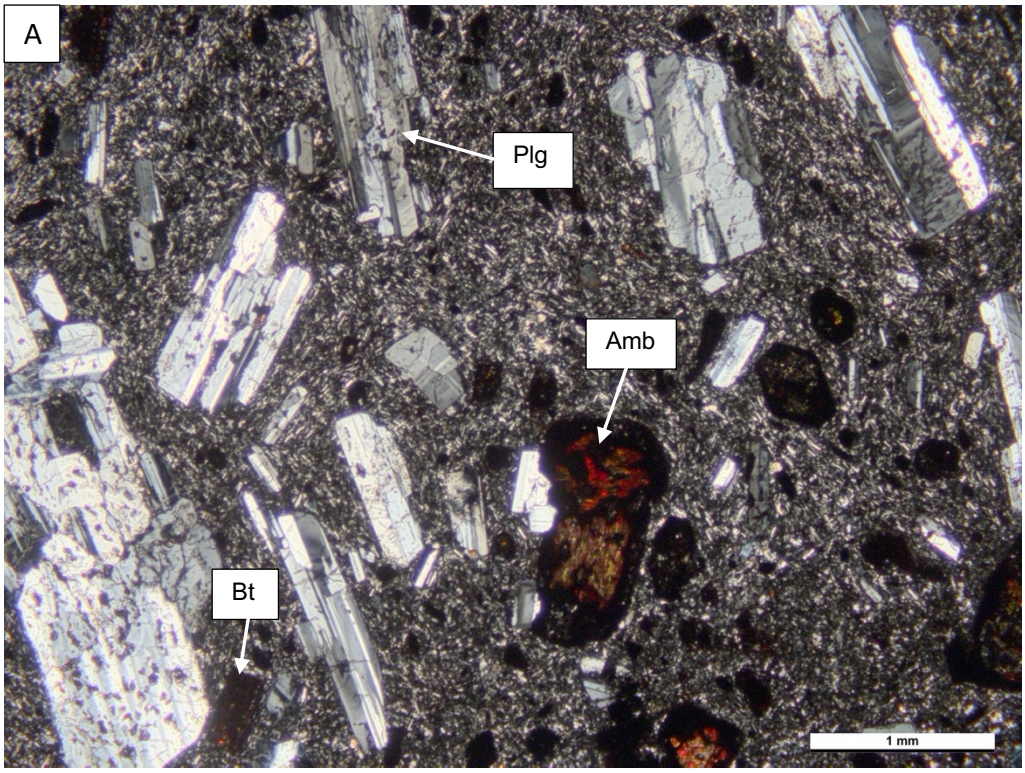

Figure 22 continues…

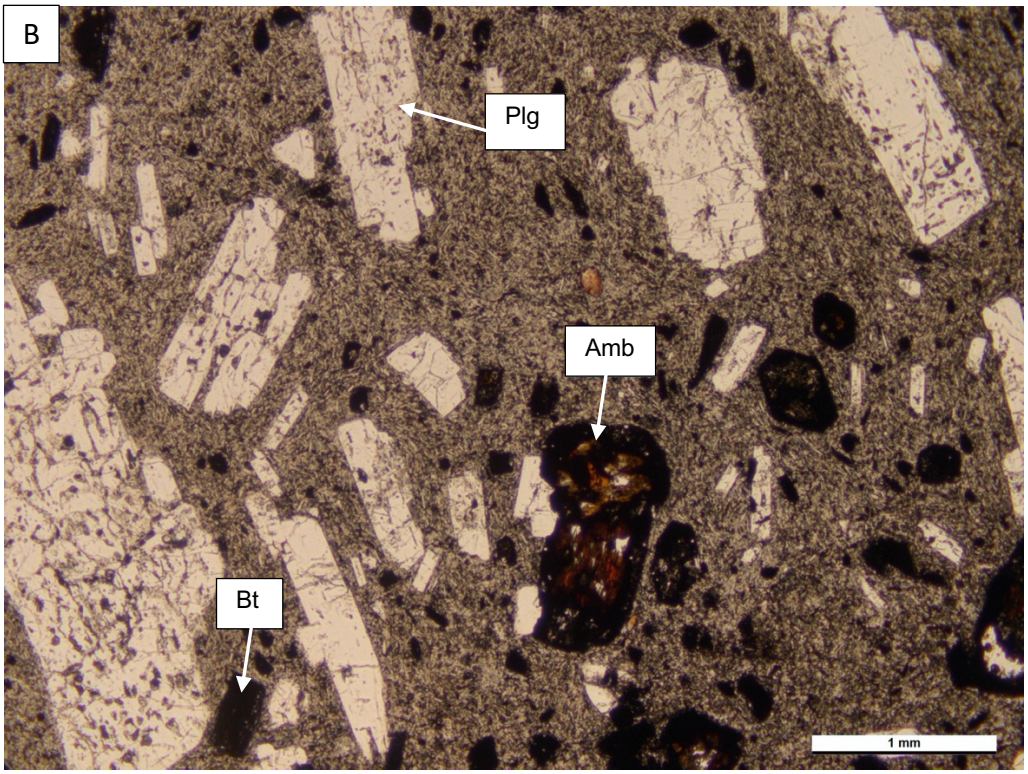

Figure 22. Trachyte stock DVD-007 of Ibex Hills with euhedral plagioclase, amphibole and biotite phenocrysts. Both amphibole and biotite have strong post-magmatic alteration. Amphibole forms slightly larger grains with thick opaque rim (two grains in the center) and biotite is smaller with thinner opaque rim (e.g. bottom left corner). Dissolution textures in plagioclase are common (e.g. coarse sieve texture in the large phenocryst on the left). Groundmass is composed of fine-grained plagioclase and mafic minerals. A) XPL and B) PPL. Amb = amphibole; Bt = biotite; Plg = plagioclase.

6.3.2 Trachyandesite dike DVD-009

DVD-009 has porphyritic texture with plagioclase, amphibole and biotite phenocrysts (Figure 23). Laths and stubby crystals of euhedral plagioclase with maximum ~5 mm long grains form the most abundant phenocryst phase. The plagioclase grains are rarely clear and numerous cracks, fluid inclusions and dissolution textures cover the grain. Coarse-sieve dissolution texture can often be found at the core. Fine-sieve texture with fluid inclusion chains are found towards the edge of some of the plagioclase. Amphibole (hornblende) with strong green color forms the second phenocrysts phase after plagioclase. The hornblende is euhedral to subhedral with opaque rim at the grain boundaries. Alteration is sometimes extensive, leaving only patches of magmatic amphibole inside the mineral boundaries. Fine secondary mosaic silica alteration is visible in some of the amphiboles, but oxide stain often masks the altered spots. Smaller amphibole phenocrysts show either partial or complete alteration into calcite. Plagioclase microlites and opaque minerals form the groundmass. The sample has abundant irregular amygdules filled with secondary epidote, chalcedony, calcite and brown oxidation stain.

Biotite, apatite and zircon are present as accessory minerals. Apatite can be found in groundmass and as inclusions in amygdules and amphibole.

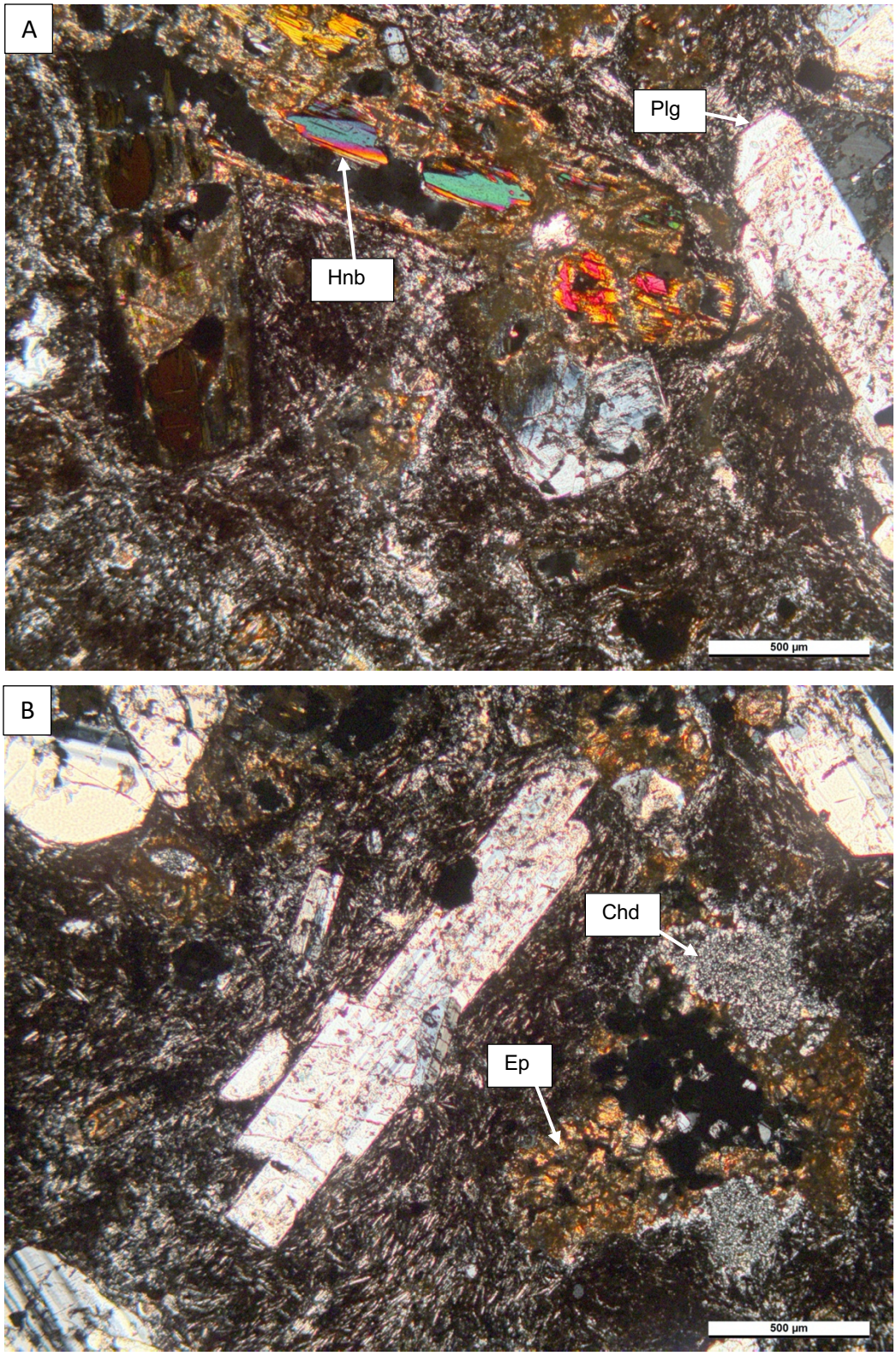

Figure 23. Trachyandesite dike DVD-009 of Ibex Hills. A) Euhedral to subhedral plagioclase and hornblende phenocrysts in groundmass of plagioclase microlites and mafic minerals. Hornblende has been strongly altered. B) Amygdules filled with secondary epidote, chalcedony and calcite are common. Hnb = hornblende; Chd = chalcedony; Ep = epidote; Plg = plagioclase.

6.3.3 Trachyandesite dike DVD-010

This sample has porphyritic texture with plagioclase, clinopyroxene, amphibole and biotite phenocrysts (Figure 24). The plagioclase phenocrysts are euhedral to subhedral with maximum diameter approximately 4 mm. Cracks and inclusions are typical and sericite alteration is common. The phenocrysts show dissolution textures. Coarse sieve texture is abundant in larger phenocrysts. A thin layer of sericite alteration is sometimes found towards the grain boundary. Zoning is present is some plagioclase but generally not to the similar degree as in samples DVD-007 and DVD-009. Clinopyroxene forms euhedral phenocryst that often form glomerocrysts. All clinopyroxene phenocrysts have been affected by post-magmatic processes and the magmatic phase has for the most part been replaced by calcite. Some grains have been completely pseudomorphed by calcite. Hornblende phenocrysts are subhedral and often found in mineral clusters with plagioclase. The grain boundaries between hornblende and plagioclase are distorted but the hornblende has opaque rims. Carbonate alteration is observed towards the edges of the grains and along cleavages and cracks. Smaller oxidized grains of anhedral amphibole is present in smaller quantities than hornblende. Biotite has opaque rims. Amygdules do occur but in smaller quantity than in DVD-009. They are irregular in shape and commonly filled with carbonate and chalcedony. Apatite and opaque minerals form accessory phases and can be found among the groundmass of plagioclase microlites and as inclusions in the phenocryst phases. Groundmass has plagioclase microlaths, opaque oxide grains and glass.

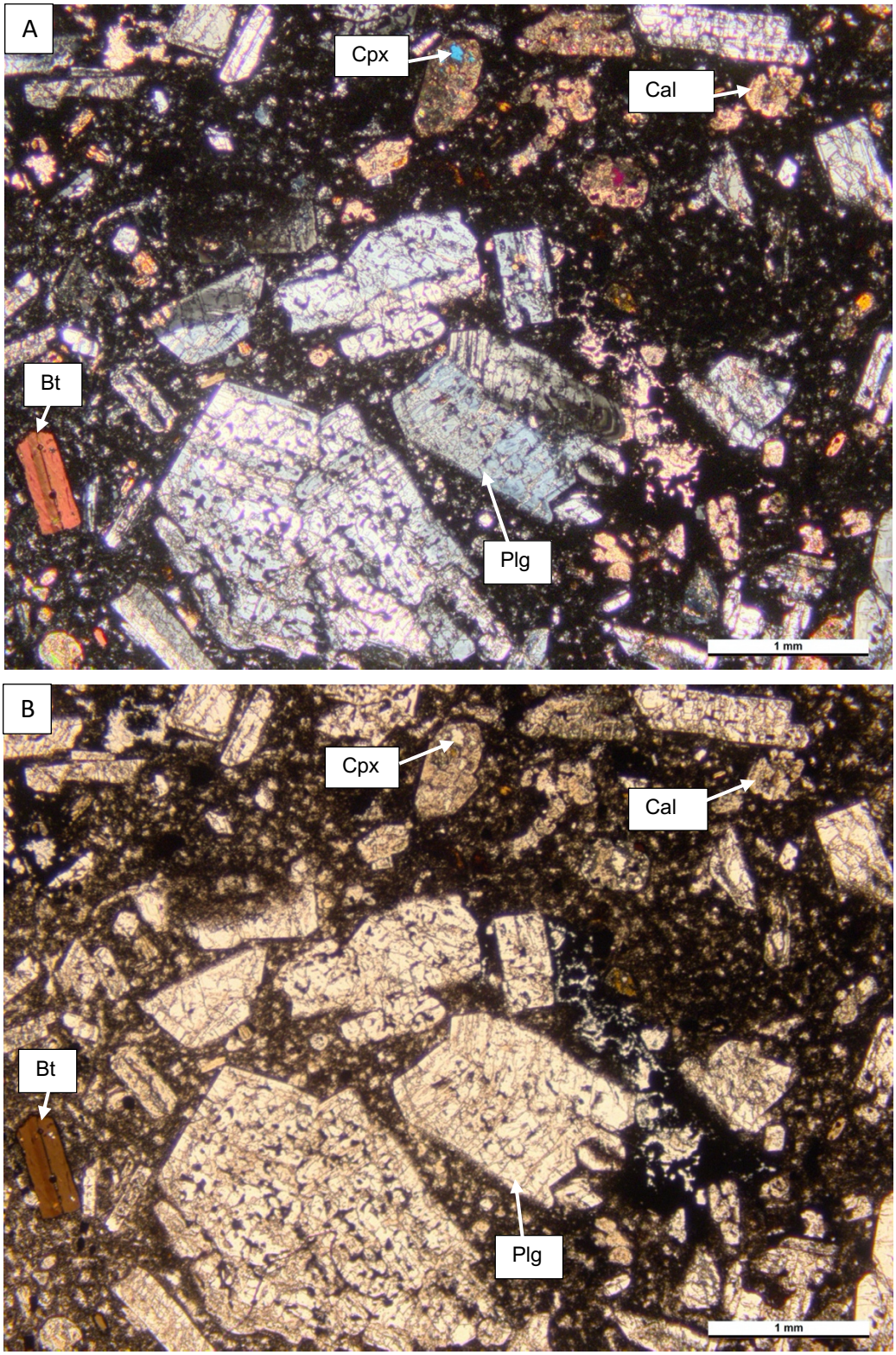

Figure 24. Trachyandesite dike DVD-010 of Ibex Hills showing abundant sub- to euhedral plagioclase phenocrysts, often with sieve textures, and biotite and clinopyroxene phenocryst in groundmass composed of plagioclase microlites, opaque minerals and volcanic glass. Clinopyroxene grains have been mostly pseudomorphed by calcite, but some magmatic pyroxene is visible in the grains towards the top of the image. A) XPL and B) PPL. Bt = biotite; Cal = calcite; Cpx = clinopyroxene; Plg = plagioclase.

6.4 Miocene volcanic rocks of Saddlepeak Hills

6.4.1 Saddlepeak Hills basalt flow DVD-001ALT

DVD-001ALT is a porphyritic volcanic rock with plagioclase and pervasively oxidized olivine phenocrysts (Figure 25). Plagioclase forms up to ~5 mm long euhedral to subhedral grains. The plagioclase is relatively fresh, although sericite alteration is present in minor amounts typically close to mineral edge, resembling a reaction corona. Dissolution sieve textures are occupying some of the grains and occasionally Fe-oxidation product runs along cracks. Olivine has been completely pseudomorphed to iddingsite. Amygdules are abundant and often elongated or otherwise irregular in shape with chalcedony and Fe-oxide rim and calcite and ±zeolite core. The groundmass is composed of plagioclase, iddingsite after olivine pseudomorphs and opaque minerals.

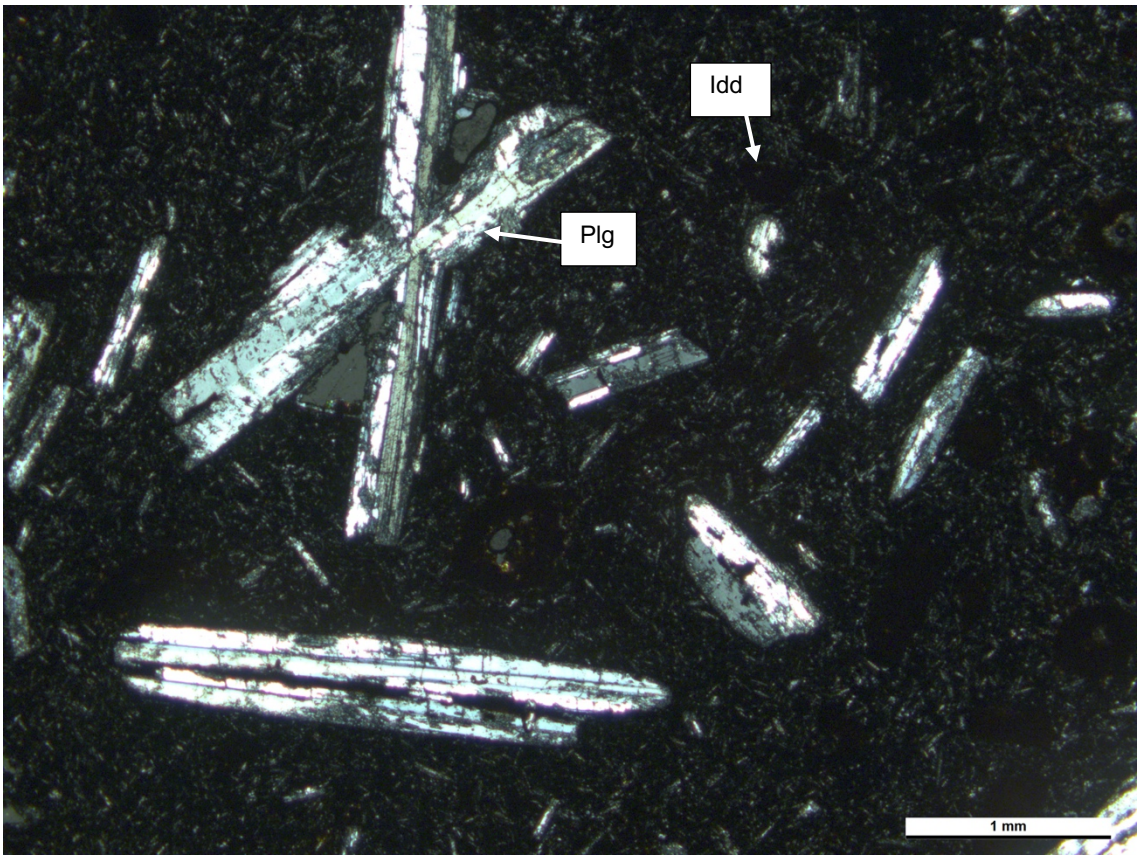

Figure 25. Miocene basalt sample DVD-001ALT of Saddlepeak Hills with plagioclase phenocrysts in groundmass composed of fine-grained feldspar and mafic minerals and volcanic glass. The smaller dark minerals are olivine phenocrysts completely pseudomorphed by iddingsite. Idd = iddingsite; Plg = plagioclase.

6.4.2 Saddlepeak Hills rhyolite porphyry DVD-001ALT_2

DVD-001ALT_2 is a porphyritic rhyolite with compositionally and texturally different fragments (microlites, tuff, glass) with sanidine and biotite phenocrysts. Sanidine phenocrysts are subhedral to euhedral (Figure 26). They often display zoning or simple twinning. Sericitic alteration is common but only minor along cracks. Granular calcite alteration in feldspar can form larger alteration patches. Magmatic biotite is generally euhedral with opaque rim. Some biotite has been oxidized and when this is the case, the grains are subhedral or display embayed texture.

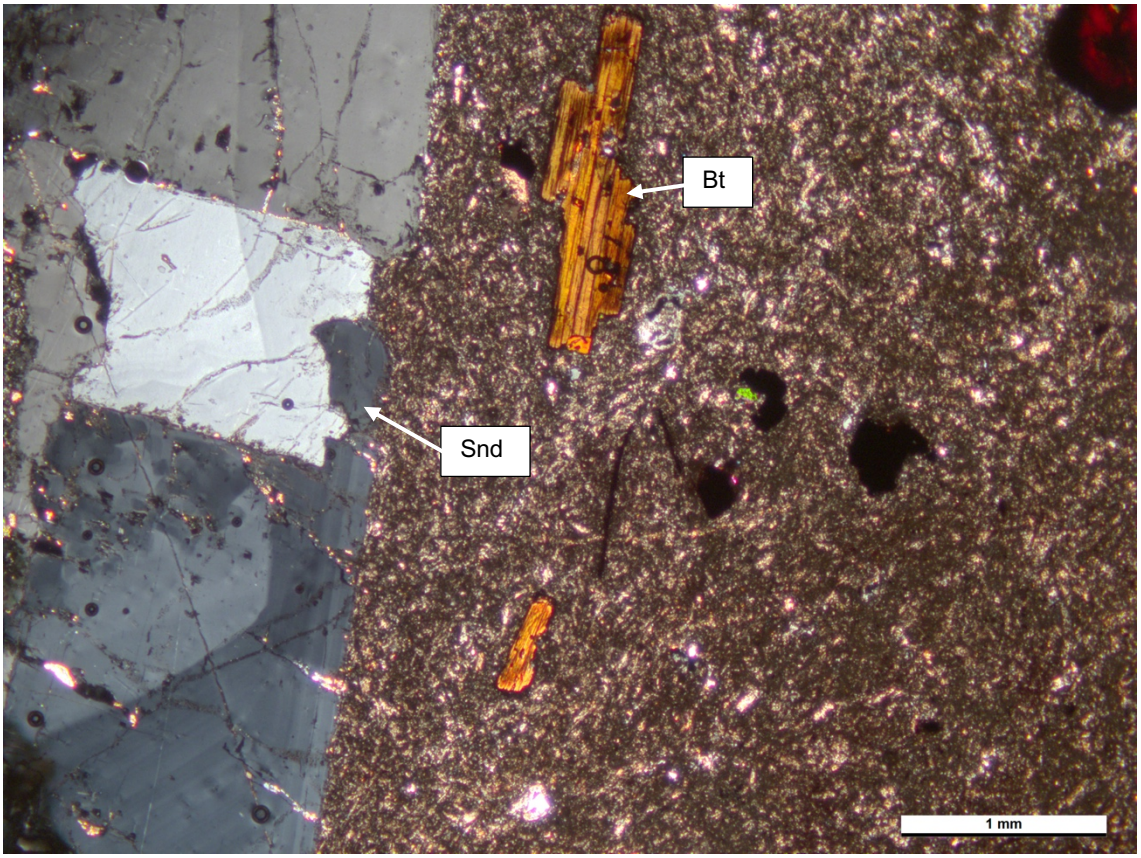

Figure 26. Large euhedral sanidine and smaller euhedral biotite phenocrysts in fine-grained groundmass in Miocene rhyolite sample DVD-001ALT_2 of Saddlepeak Hills. Bt = biotite; Snd = sanidine.

6.5 Cretaceous dike of Mojave Desert

6.5.1 Trachyandesite dike 365

Sample 365 is characterized by hornblende, strongly sericitic plagioclase feldspar, quartz, chlorite, epidote and carbonate (Figure 27). Hornblende forms euhedral to subhedral columnar and acicular crystals and hexagonal cross-sections. Zoning and simple twinning

are common features. Apart from some chlorite alteration at grain boundaries and rare chlorite and calcite alteration at cracks, amphibole appears to be magmatic. Plagioclase has been pervasively altered to sericite and into aggregates of microcrystalline epidote creating a cloudy appearance on the mineral grain. Irregular albite rims often surround the sericite cores, but more commonly the effect of alteration distorts the grain boundaries, making the assessment of the crystal form difficult. The sample is featured with subrounded ~1 mm large quartz xenocryst with chlorite/calcite or microcrystalline silica rim. Chlorite is found as alteration product of amphibole and filling interstitial spaces between amphibole and feldspar phenocrysts. Epidote is found in plagioclase and as larger subhedral to anhedral grains in association with chlorite, carbonate, secondary feldspar and minor secondary quartz, probably representing crystallization after circulating fluids. Veins, when present, are filled with carbonate and epidote. Apatite and opaque minerals form accessory phases.

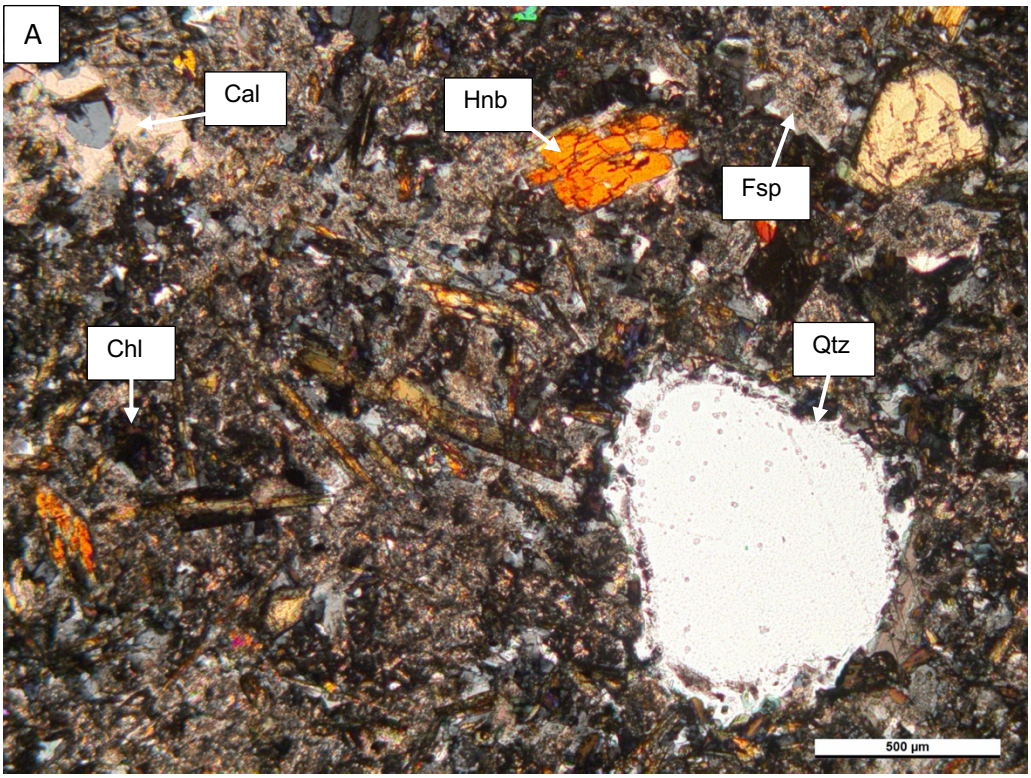

Figure 27 continues…

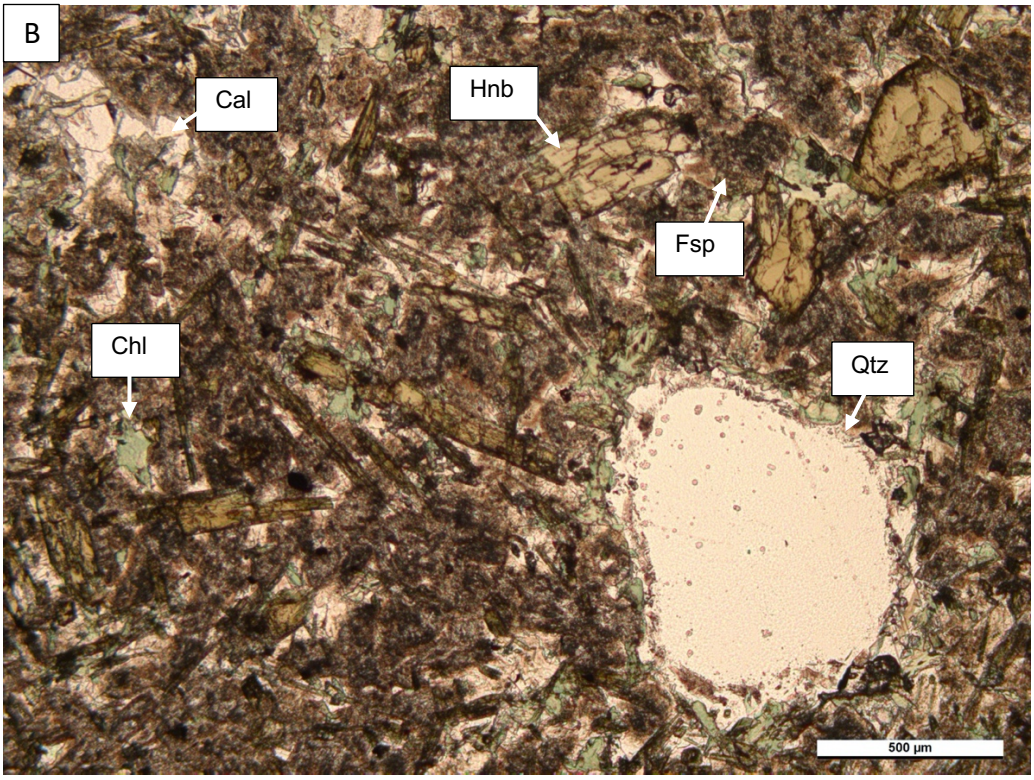

Figure 27. Cretaceous dike 365 of Mojave Desert displaying hornblende, feldspar (strongly altered with sericite), chlorite, calcite and a large quartz xenocryst. A) XPL and B) PPL. Cal = calcite; Chl = chlorite; Fsp = feldspar; Hnb = hornblende; Qtz = quartz.

7. WHOLE-ROCK GEOCHEMISTRY

The three Miocene samples of Ibex Hills, five dikes of Saddlepeak Hills and Salt Spring Hills and a Cretaceous dike of Mojave Desert were analyzed for whole-rock major oxide and trace element composition. The samples are characterized with a varying amount of LOI (1.46-8.89 %) implying that post-solidus processes have modified the chemical composition of at least some of the samples. The geochemical analysis results discussed below are normalized to 100 wt.% anhydrous. The full list of analysis results is presented in Appendix 1.

7.1 Major elements

Figure 28 shows classification of the studied samples on a total alkali vs. silica (TAS) diagram after Le Bas et al. (1986). The Miocene samples of Ibex Hills are characterized by intermediate composition straddling the alkaline-subalkaline boundary defined by Irvine and Baragar (1971) and these samples classify as trachyandesites (DVD-009 and DVD-010) to trachyte (DVD-007). The Cretaceous dike plots in the trachyandesite field and on the alkaline-subalkaline boundary together with the Miocene samples. The major element compositions of the metamorphosed and altered dikes are unlikely to represent the original magmatic composition. However, these samples are characterized as subalkalic and most of the dikes plot into the andesite field. The metadiabase sample of Saddlepeak Hills (DVD-003) has a considerably more mafic composition and plots as basaltic showing comparable composition to the 1.1 Ga Crystal Spring Diabase of Death Valley region (Hammond 1983, Vandyk et al. 2018).

The classification diagram (Figure 29) based on the immobile trace element ratios Zr/Ti and Nb/Y (modified by Pearce 1996 after Winchester and Floyd 1977) classifies all Miocene samples of Ibex Hills as trachyandesites. The Cretaceous dike plots into the subalkaline andesite/trachyandesite field together with the majority of the dikes of Saddlepeak Hills and Salt Spring Hills. Sample DVD-003 is basaltic.

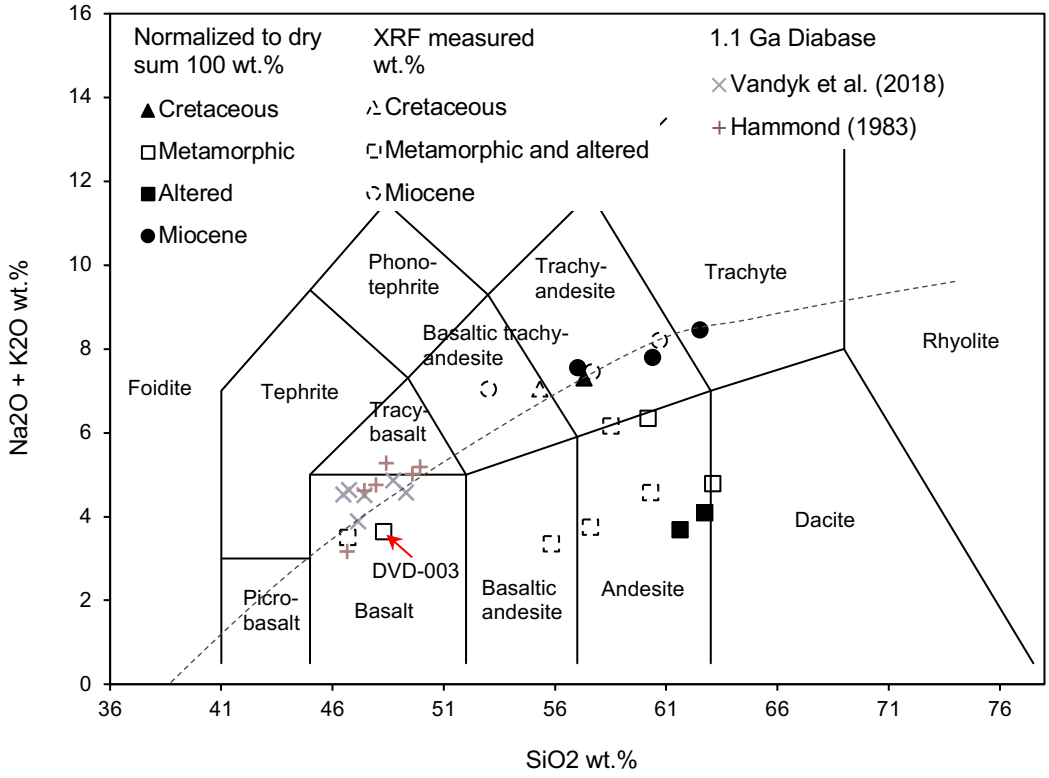

Figure 28. Total alkali vs. silica (TAS) diagram after Le Bas et al. (1986). The dashed line represents alkaline-subalkaline boundary after Irvine and Baragar (1971). Symbols with dashed edges represent measured element oxide wt.% (unnormalized). Comparison with 1.1 Ga Diabase of previous studies shows compositional affinity with sample DVD-003 (this study). The Cretaceous sample plots as trachyandesite, the metamorphic and altered samples as andesites (DVD-003 as basaltic) and the Miocene samples as trachyandesites and trachyte.

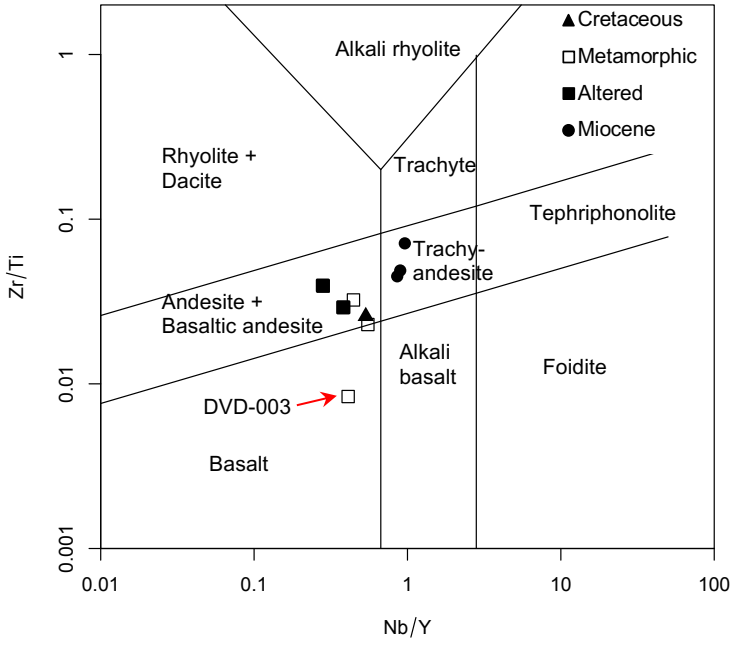

Figure 29. Immobile trace element discrimination diagram Zr/Ti vs. Nb/Y after Winchester and Floyd (1977) modified by Pearce (1996) for the analyzed samples. The Cretaceous, metamorphic and altered samples plot as andesites + basaltic andesites (DVD-003 as basaltic) and the Miocene samples as trachyandesites.

The major element oxides of the Miocene samples mostly correlate with the SiO_2 (Figure 30). TiO_2 (0.69-0.90 wt.%), FeO_T (4.47-5.86 wt.%), MnO (0.08-0.13 wt.%), CaO (3.94-9.63 wt.%) and P_2O_5 (0.47-0.59 wt.%) all decrease with increasing silica content whereas Al_2O_3 (16.83-17.41 wt.%), Na_2O (4.27-4.67) and K_2O (3.20-3.77 wt.%) show weak increase with the silica. CaO and P_2O_5 have the most pronounced decrease with increasing silica.

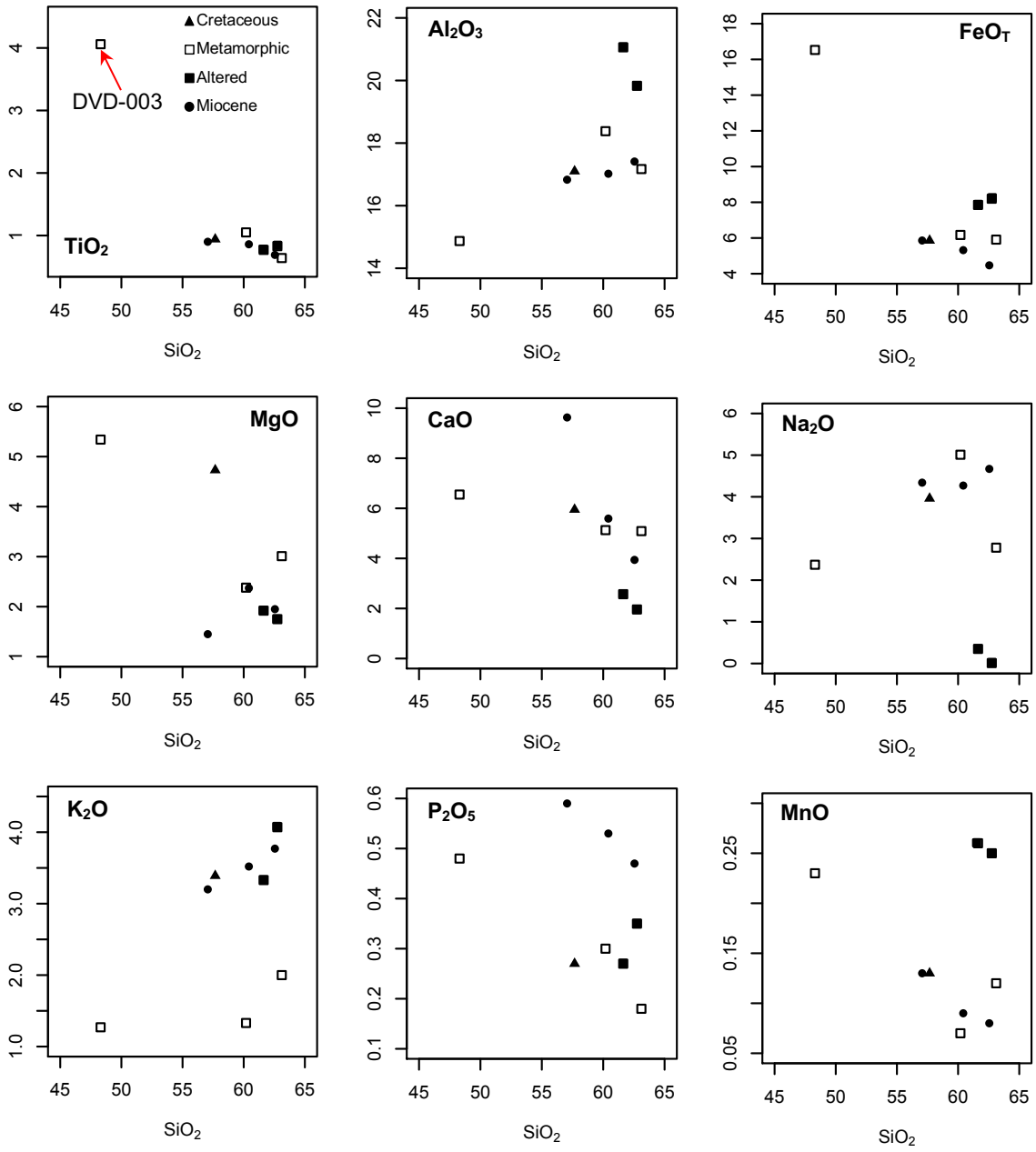

Figure 30. Major element wt.% oxides vs. SiO_2 wt.% diagrams for Miocene, metamorphic, altered and Cretaceous samples.

MgO varies between 1.45 and 2.37 wt.% and does not correlate with SiO_2. The Mg# ($Mg^{2+}/(Mg^{2+}+Fe^{2+})*100$) varies between 34 and 48. All Miocene samples are metaluminous with molar A/CNK <1.

The basaltic sample DVD-003 is distinguished from the rest of the Saddlepeak and Salt Spring Hills samples by high TiO_2 (4.06 vs. 0.64-1.05 wt.%), FeO_T (16.53 vs. 5.91-8.20 wt.%), MgO (5.34 vs. 1.75-3.01 wt.%) and P_2O_5 (0.48 vs. 0.18-0.35 wt.%) and low SiO_2 (48.30 vs. 60.19-63.11 wt.%) Al_2O_3 (14.87 vs. 17.7-21.06 wt.%). No correlation is detected between SiO_2 and major elements composition of the Saddlepeak and Salt Spring Hills dikes, except for the immobile TiO_2 which shows overall decrease with increasing SiO_2. The altered samples DVD-001 and DVD-006, which have the highest LOI (7.01 and 8.89 %), are set apart from the metamorphic samples DVD-002 and DVD-005 by elevated Al_2O_3, FeO_T and K_2O and lower MgO, CaO and Na_2O wt.%. All metamorphic dikes are metaluminous with molar A/CNK <1. The altered dikes are peraluminous and have the highest LOI % out of all analyzed samples. The Mg# varies from 31 to 52.

The Cretaceous dike (LOI: 3.12 %) plots very close to the Miocene dikes on most of the major element vs. silica diagrams (TiO_2: 0.94, Al_2O_3: 17.10, FeO_T: 5.86, MnO: 0.13, CaO: 5.95, Na_2O: 3.96, K_2O: 3.39 wt.%) apart from the lower P_2O_5 (0.27 wt.%) which is similar to the meta-andesite dikes and higher MgO (4.73 wt.%) which is close to the basalt magnesium composition. The Cretaceous dike Mg# = 63 is the highest of all studied samples. Like the Miocene samples and metamorphic dikes, the Cretaceous dike is metaluminous.

7.2 Trace elements

One Miocene sample, the Cretaceous dike, one metamorphic dike and one altered dike that were analyzed for all rare-earth elements by ICP-MS are represented on a chondrite normalized REE diagram in Figure 31. All REE-analyzed samples show smooth downward slope with a clear LREE enrichment. The Miocene sample has the most pronounced degree of LREE/HREE fractionation with $(La/Yb)_N = 31.45$, followed by the Cretaceous dike with $(La/Yb)_N = 15.27$ and finally the metamorphic and altered dikes

with $(La/Yb)_N$ = 9.30-10.58. The light REE enrichment is largest in the Miocene sample with $(La/Sm)_N$ = 6.24 while the Cretaceous dike and the metadikes have slightly smaller but fairly uniform LREE enrichment ($(La/Sm)_N$ = 4.07 and 4.06-4.58, respectively). The enrichment of heavy REEs is lower with $(Gd/Yb)_N$ = 2.83 in the Miocene sample, followed by the Cretaceous dike with $(Gd/Yb)_N$ = 2.42 and the metamorphic and altered dikes with $(Gd/Yb)_N$ = 1.40-1.66. None of the REE-analyzed samples have a clear Eu anomaly (Eu/Eu* = 0.89-0.94).

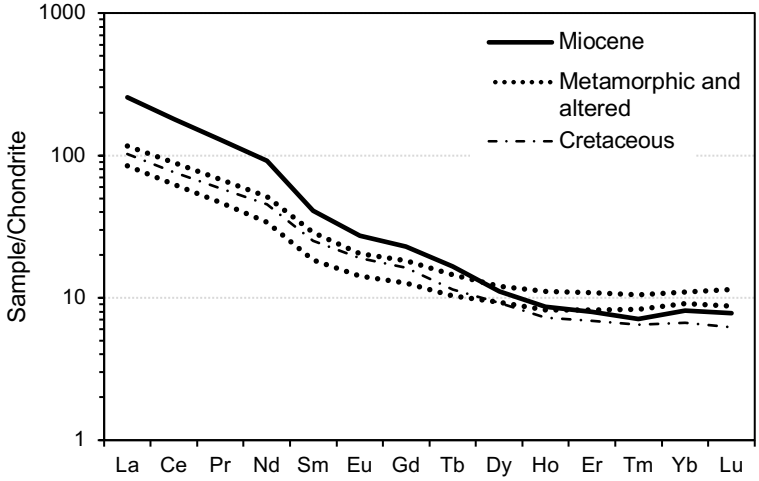

Figure 31. Chondrite normalized REE diagram for selected Miocene, metamorphic and altered, and Cretaceous samples. Normalization values after Boynton (1984).

The MORB-normalized multi-element diagrams (Pearce 1983) for all analyzed samples are shown in Figure 32. Elements Th, Hf, Sm and Yb were analyzed from samples 365, DVD-001, DVD-005, DVD-007 only. Most of the samples are characterized by overall enrichments in LILEs and Th, marked Ta–Nb depletion (Ta below detection limit) and Ce enrichment relative to the surrounding elements, and depleted Ti, Y and Yb (the most compatible elements) relative to MORB. The Miocene samples form a uniform pattern with each other with modest disparities in Sr and Th. The metamorphosed and altered dikes have scattered LILE (mobile element) profiles. The two altered dikes (samples DVD-001 and DVD-006) form a similar curve from depleted Sr to enriched Rb. Sample DVD-002 has anomalously positive Ba-peak. The meta-andesite samples are more comparable in the immobile HFSE elements (Nb to Yb). However, the basalt and meta-andesite DVD-002 (both from 1.1 Ga diabase) have uncommonly enrichment of Ti over

Y. The metamorphosed basalt is the only analyzed sample with enriched Ti and Y relative to MORB.

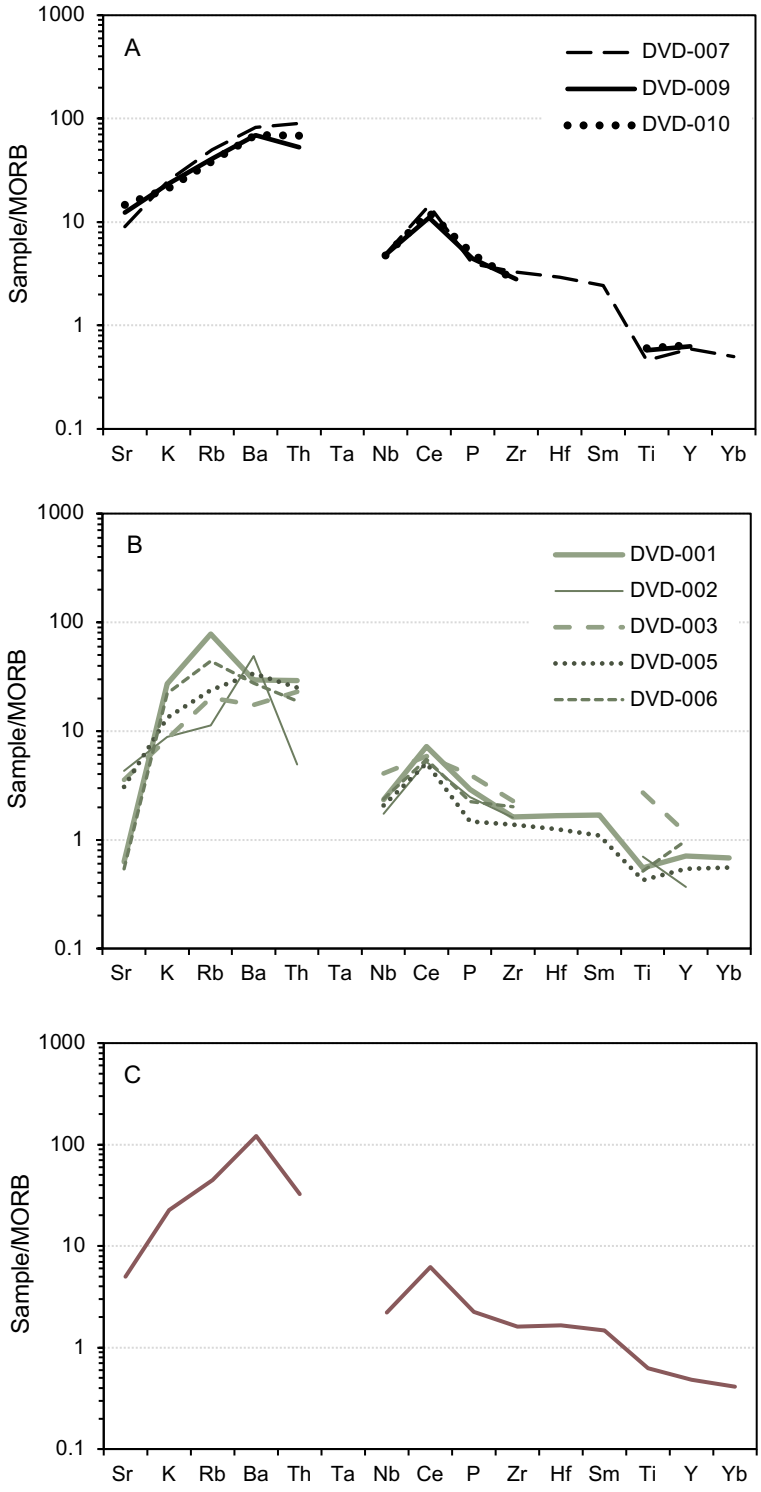

Figure 32. MORB-normalized (Pearce 1983) multi-element diagrams for A) Miocene, B) metamorphic and altered C) Cretaceous samples.

8. PLAGIOCLASE MAJOR ELEMENT COMPOSITION

Major element composition profiles of plagioclase phenocrysts from Miocene trachyte stock (sample DVD-007) and trachyandesite dike (sample DVD-009) were analyzed by EPMA in search of elemental variables for the Sr isotope study (Section 9) of the Miocene samples. The major element composition of 16 plagioclase phenocrysts were analyzed for this study, twelve from the trachyte stock and seven from the trachyandesite dike of Ibex Hills. All analyzed plagioclase phenocrysts have multiple EPMA analysis and total of 146 analysis spots were measured. Although clean mineral surfaces were selected for analysis, seven spots show measurement values that clearly indicate composition of inclusions or intergrowths (such as antiperthite). These data are omitted from the data analysis below, reducing the analysis data to 139 measurements. Figure 33 shows the chemical variability of the analyzed plagioclase on an Ab-An-Or ternary diagram. The analyzed plagioclase phenocrysts classify from oligoclase to labradorite and a clear distinction can be observed in the plagioclase composition between the trachyte stock and trachyandesite dike. A complete list of measured plagioclase major element compositions can be found in Appendix 2.

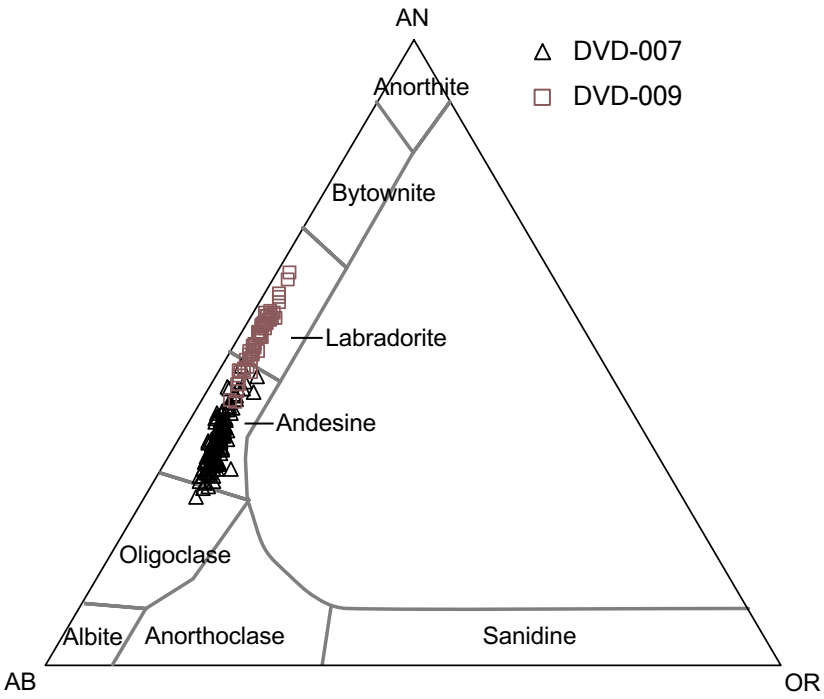

Figure 33. Plagioclase composition of Miocene trachyte stock (DVD-007) and trachyandesite dike (DVD-009) on an Ab-An-Or ternary diagram. The trachyandesite dike is generally more anorthite-rich although the samples partly overlap.

8.1 Trachyte stock of Ibex Hills (DVD-007)

The analyzed plagioclase phenocrysts (n = 9; 89 accepted analysis spots) from the Ibex Hills trachyte stock show the following major element content: SiO_2 52.90–62.20 wt.%, Al_2O_3 19.68–27.13 wt.%, MgO <0.08–0.33 wt.%, CaO 5.20–9.42 wt.%, Na_2O 4.41–7.44 wt.% and K_2O 0.42–1.62 wt.%. The trachyte plagioclase composition ranges from oligoclase to andesine (An_{27-48}) (Figure 34). The maximum variation in An content within a single phenocryst ranges from 4.73 to 20.82 mol.% units.

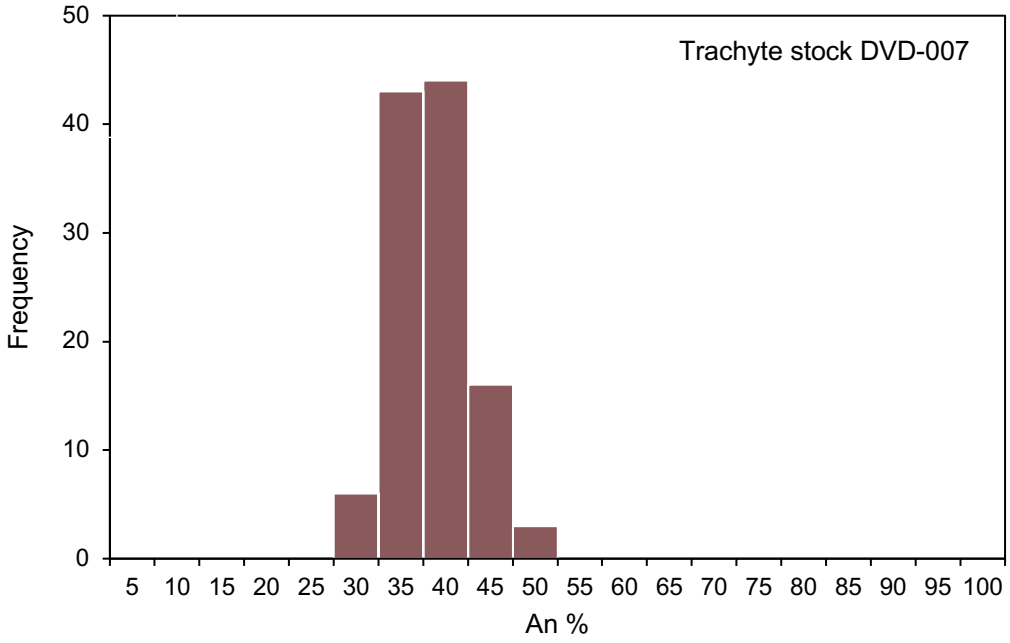

Figure 34. Variation of anorthite (mol.%) in plagioclase phenocrysts in Miocene trachyte stock of Ibex Hills (sample DVD-007).

8.2 Trachyandesite dike of Ibex Hills (DVD-009)

The plagioclase phenocrysts (n = 7; 52 accepted analysis spots) of the trachyandesite dike of Ibex Hills show the following major element composition: SiO_2 51.98–58.16 wt.%, Al_2O_3 23.43–29.03 wt.%, MgO <0.08–0.89 wt.% (<0.08: below detection limit), CaO 8.37–12.65 wt.%, Na_2O 3.89–6.28 wt.% and K_2O 0.32–0.83 wt.%. The anorthite content in the trachyandesite dike is predominantly higher than in the trachyte stock (An_{42-63}) with the plagioclase composition ranging from andesine to labradorite (Figure 35). The

maximum variation in An content within a phenocryst varies between 5.99 and 13.87 mol.% units.

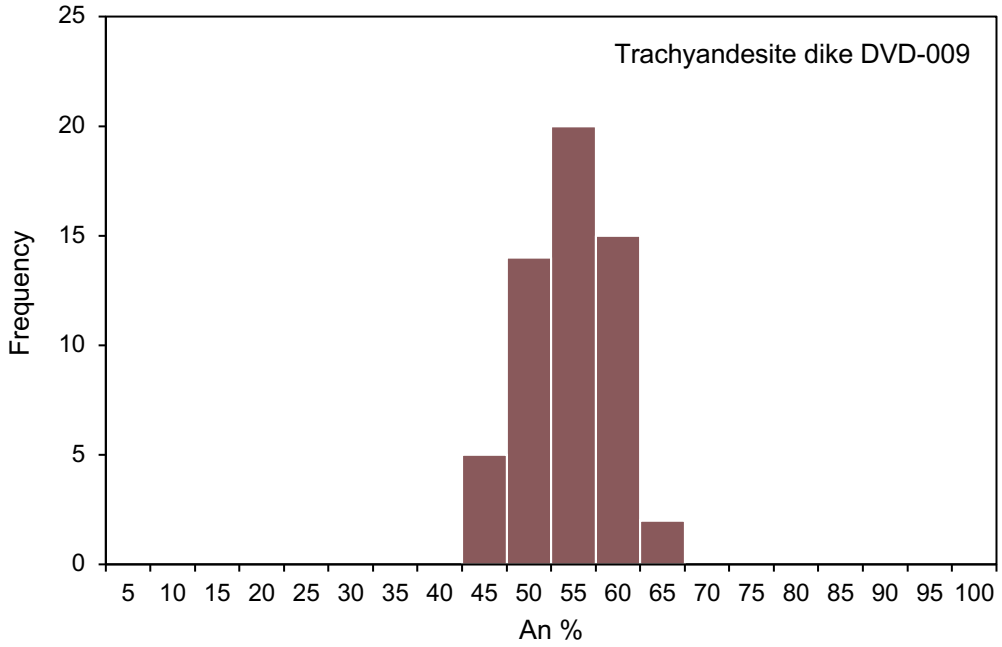

Figure 35. Variation of anorthite (mol.%) in plagioclase phenocrysts in Miocene trachyandesite dike of Ibex Hills (sample DVD-009).

9. PLAGIOCLASE STRONTIUM ISOTOPE COMPOSITION

All *in situ* laser ablation analyses were made on one thick section from the Miocene trachyte stock and another one from the trachyandesite dike. The Rb concentration within the plagioclase is considered as evidence of cracks, inclusions and overall contamination, thus analysis spots with $^{87}Rb/^{86}Sr$ ratio over 0.03 (n = 5) are omitted from the analysis to maintain the quality of data. The accepted spot mode analyses (n = 59) of 15 phenocrysts from the trachyte stock yielded measured $^{87}Sr/^{86}Sr$ values of 0.70719 to 0.70983 (Figure 36). The laser ablation measurements of the trachyandesite dike (21 phenocrysts; 48 accepted spots) resulted in overall slightly more uniform $^{87}Sr/^{86}Sr$ ratios ranging from 0.70737 to 0.70884 (Figure 36). The average of spot mode analysis is 0.70756 ± 0.00048 (1σ) for the stock, the dike has more radiogenic average with mean value of 0.70792 ±0.00035 (1σ), although the highest $^{87}Sr/^{86}Sr$ ratio was measured from the stock.

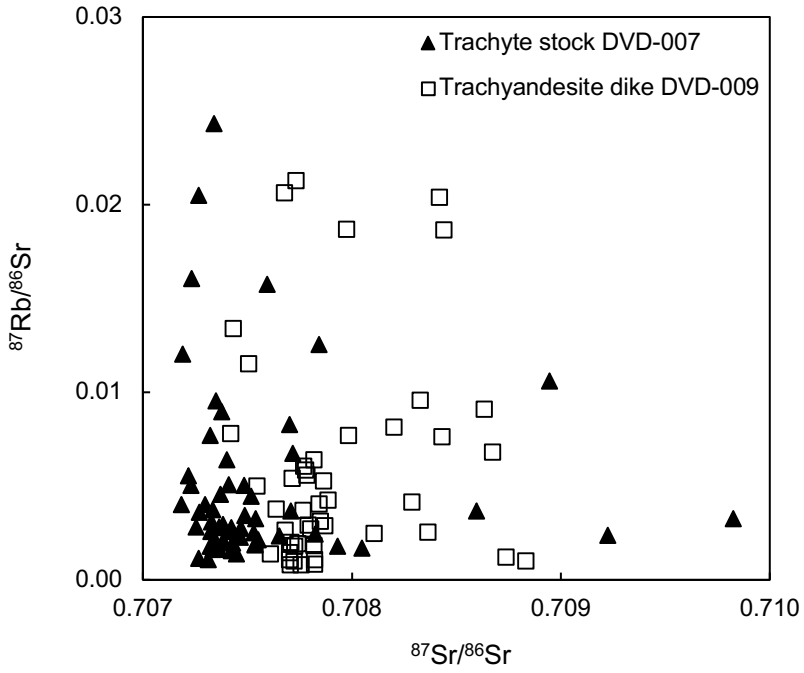

Figure 36. *In situ* laser ablation results from trachyte stock DVD-007 and trachyandesite dike DVD-009 of Ibex Hills represented on a $^{87}Sr/^{86}Sr$ versus $^{87}Rb/^{86}Sr$ diagram.

From the trachyte stock and trachyandesite dike the Sr isotope data from selected phenocrysts are coupled with plagioclase An mol percent for each analysis spot. The plagioclase anorthite composition data are presented as an average of two analysis spots for each LA-MC-ICP-MS measurement sites, except for spots where EPMA measurements provided unacceptable data. In these cases, the An mol percent is based on one measurement only (see Appendix 2). Figure 37 shows the locations of the analyzed phenocryst in the two thick sections (trachyte stock DVD-007 and trachyandesite dike DVD-009) and the approximate laser ablation analysis site (spot and line traverse mode) for the selected phenocrysts considered in this chapter.

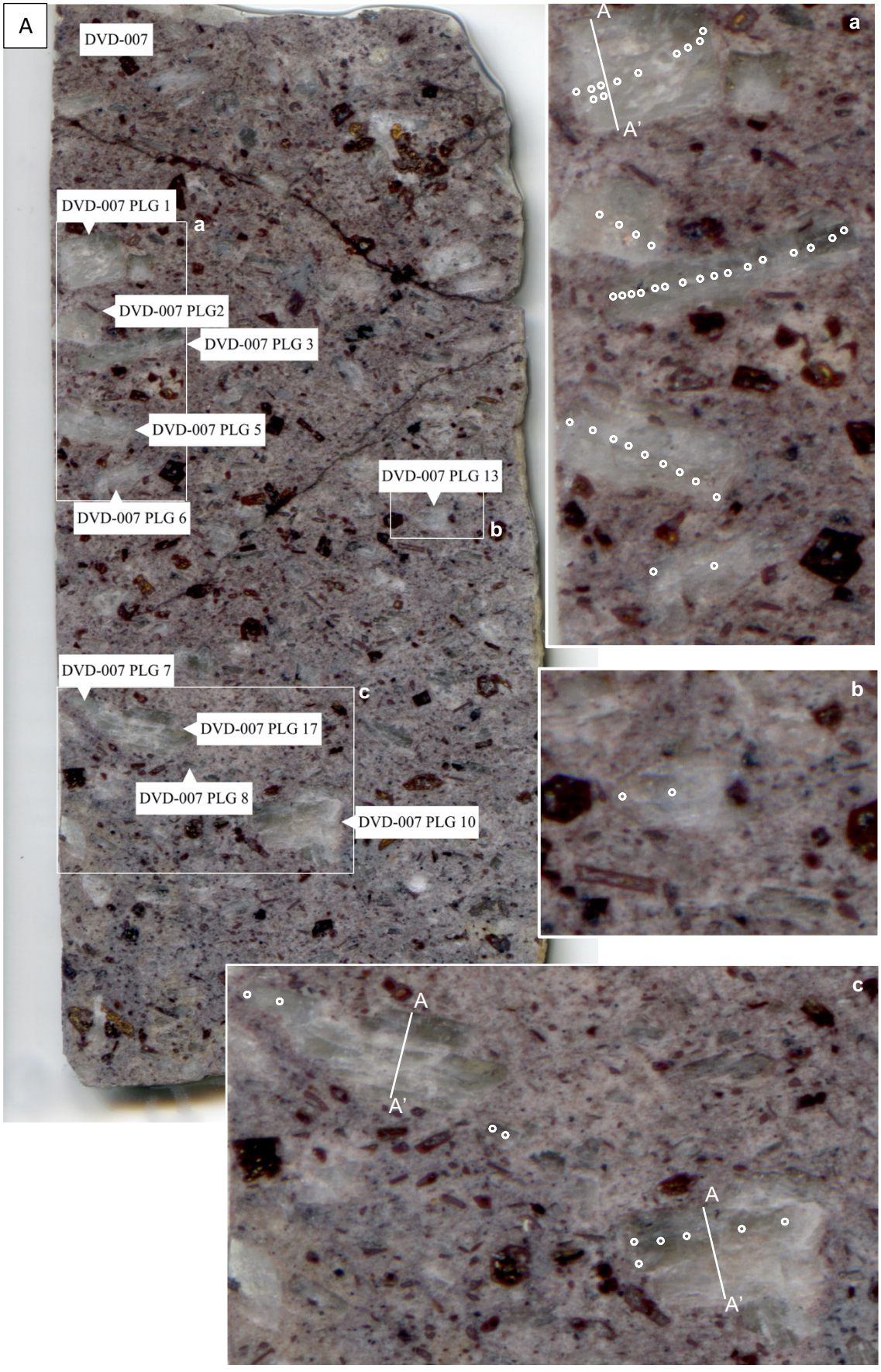

Figure 37 continues…

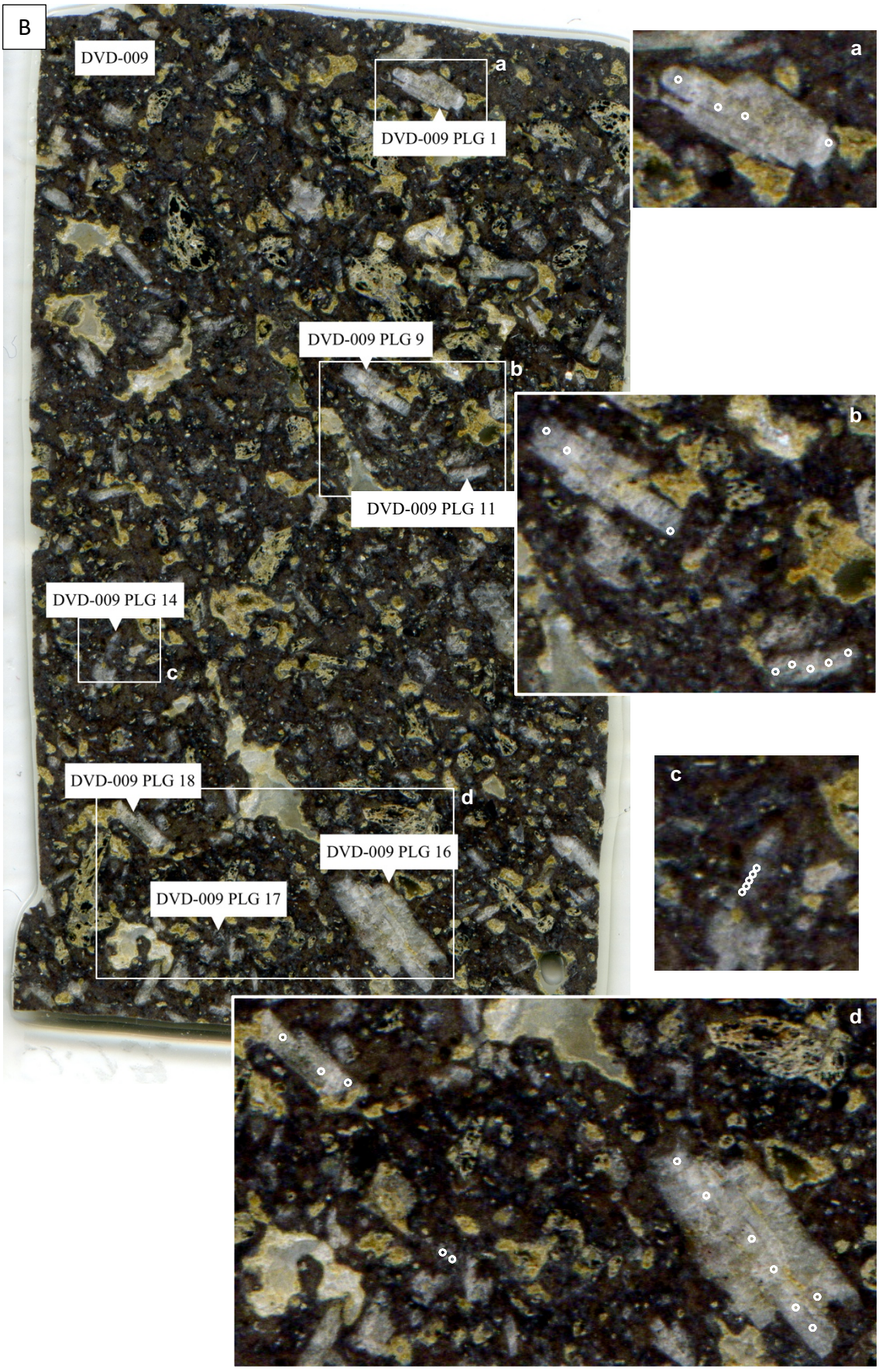

Figure 37. Thick section photographs of A) trachyte stock DVD-007 and B) trachyandesite dike DVD-009 of Ibex Hills showing locations (with blow-ups a-c (in A) and a-d (in B) of specified phenocrysts) of the selected

phenocrysts analysed for plagioclase major element and Sr isotope composition and laser ablation analysis spots and line traverse (A-A') sites within phenocrysts. Spot marker (white circle) not to scale.

The overall plagioclase characteristics of the selected phenocrysts from the analyzed samples are compared in Figure 38. Compositionally, the trachyte stock (DVD-007) is more evolved than the trachyandesite dike (DVD-009). The Sr isotopic compositions largely overlap; however, the least radiogenic $^{87}Sr/^{86}Sr$ ratios are measured in the trachyte stock, while the trachyandesite dike holds most of the more radiogenic $^{87}Sr/^{86}Sr$ ratios. It should be noted that all $^{87}Sr/^{86}Sr$ ratios exceeding the value of 0.708 in the trachyte stock are measured from a single phenocryst (see Chapter 9.1.1). The complete list of laser ablation measurements can be found in Appendix 3.

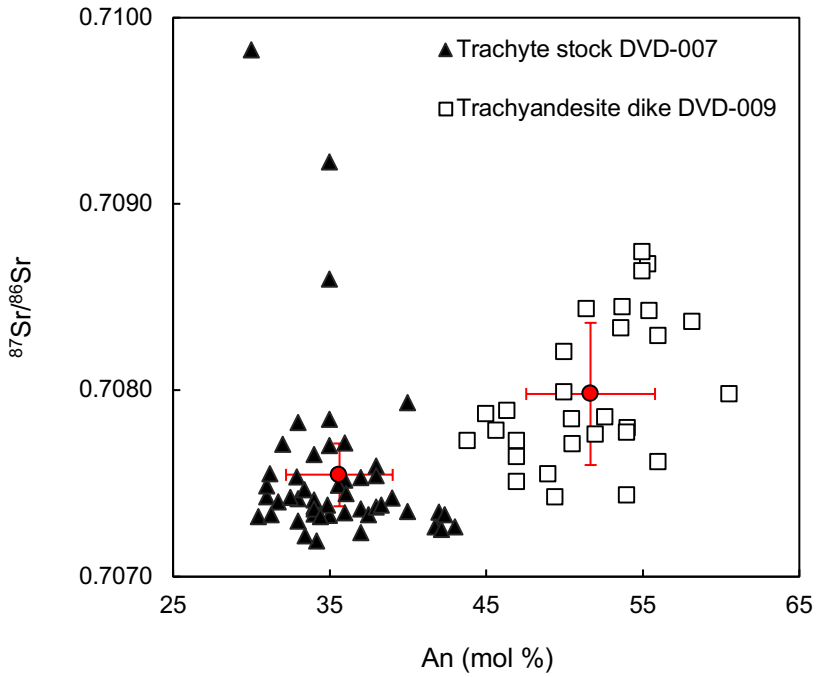

Figure 38. *In situ* laser ablation results from trachyte stock DVD-007 and trachyandesite dike DVD-009 of Ibex Hills represented on a $^{87}Sr/^{86}Sr$ versus An (mol.%) diagram highlighting the more anorthite rich and more radiogenic composition of the trachyandesite dike DVD-009. Red circles show average $^{87}Sr/^{86}Sr$ and An mol.% for both samples with 1σ error bars.

9.1 Trachyte stock of Ibex Hills (DVD-007)

Overall, the $^{87}Sr/^{86}Sr$ ratios measured in the trachyte stock phenocryst rims show slightly less radiogenic values than the ratios measured in the phenocryst mid sections, although there is overlap in the values (Figure 39). The three measurements with $^{87}Sr/^{86}Sr$ ratio exceeding 0.7080 are all analyzed in crystal DVD-007 PLG 1. No major differences can be observed in phenocryst An content between core and rim.

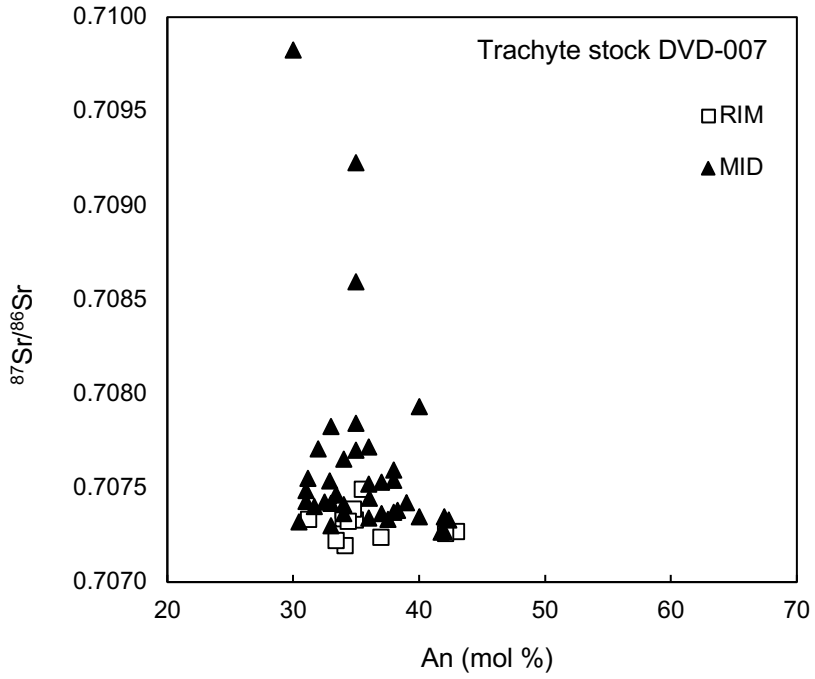

Figure 39. Phenocryst rim and mid-section values of representative phenocrysts in dacite stock of Ibex Hills (DVD-007) on An (mol.%) vs. $^{87}Sr/^{86}Sr$ diagram.

The variation in $^{87}Sr/^{86}Sr$ ratios and An content across representative plagioclase crystals in trachyte stock are shown in Figures 40 and 41. All measured plagioclase crystals show variation in $^{87}Sr/^{86}Sr$ ratio from core to rim and the $^{87}Sr/^{86}Sr$ ratios generally decrease towards the phenocryst rims from the core and mid-crystal values. Five phenocrysts (DVD-007 PLG 1, DVD-007 PLG 2, DVD-007 PLG 3, DVD-007 PLG 5 and DVD-007 PLG 10) were analyzed with multiple laser ablation measurements across the length of the crystal. Four phenocrysts (DVD-007 PLG 6, DVD-007 PLG 7, DVD-007 PLG 8 and DVD-007 PLG 13) were analyzed from core and rim only. Further three phenocrysts (DVD-007 PLG 1, DVD-007 PLG 10, DVD-007 PLG 17) were measured with line

traverse across the width of the phenocryst (Figure 42) to show more detailed analysis of the $^{87}Sr/^{86}Sr$ ratios on a crystal scale.

Both the $^{87}Sr/^{86}Sr$ ratio and the anorthite content oscillate in phenocryst DVD-007 PLG 1. The phenocryst mid-section (Figure 40 A) has the most radiogenic $^{87}Sr/^{86}Sr$ ratio (0.70983) of the measured spot mode values while the lowest $^{87}Sr/^{86}Sr$ ratio (0.70727) in this phenocryst is measured in the rim. The An content varies from 30 to 43 mol percent, the lowest value is measured in the mid-section, the highest in the rim. Although both the $^{87}Sr/^{86}Sr$ ratio and An content shift across the crystal, they do not manifest an obvious relationship. DVD-007 PLG 3 (Figure 40 B) has oscillatory $^{87}Sr/^{86}Sr$ and An mol percent zoning. The *in situ* Sr isotopic ratios vary between 0.70724 and 0.70783 and are measured in the phenocryst rim and mid-section respectively. Overall the An content changes between 31 and 42 mol.%. The lowest An content is measured in the phenocryst mid-section where the $^{87}Sr/^{86}Sr$ ratio is generally high while the An content increases towards the phenocryst edge where the $^{87}Sr/^{86}Sr$ ratio decreases. However, as in DVD-007 PLG 1, the anorthite content and $^{87}Sr/^{86}Sr$ ratio do not have a clear relationship. The $^{87}Sr/^{86}Sr$ ratio in plagioclase crystal DVD-007 PLG 5 (Figure 40 C) oscillates from rim to core to rim between 0.70726 and 0.70740. The anorthite content ranges from 30 to 42 mol.% and correlates with the *in situ* Sr isotopic ratios by increasing with decreasing Sr ratios and decreasing with increasing Sr ratios. DVD-007 PLG 10 (Figure 40 D) has oscillating $^{87}Sr/^{86}Sr$ ratio ranging from 0.70732 to 0.70754 while the An content mostly remains at ~33 mol.% except briefly increasing to 42 mol.% in the crystal mid-section where the $^{87}Sr/^{86}Sr$ ratio is lower than in the adjacent analysis spots. Phenocryst DVD-007 PLG 2 shows a small but steady decrease in $^{87}Sr/^{86}Sr$ ratios from core to rim. The two innermost ablation spots have similar $^{87}Sr/^{86}Sr$ ratios at ~0.7074, the ratio decreasing to ~0.7073 at the both ablation spots towards the phenocryst rims. The change in An content is minor (31 to 36 mol.%) with the slightly less evolved values measured in the crystal rims.

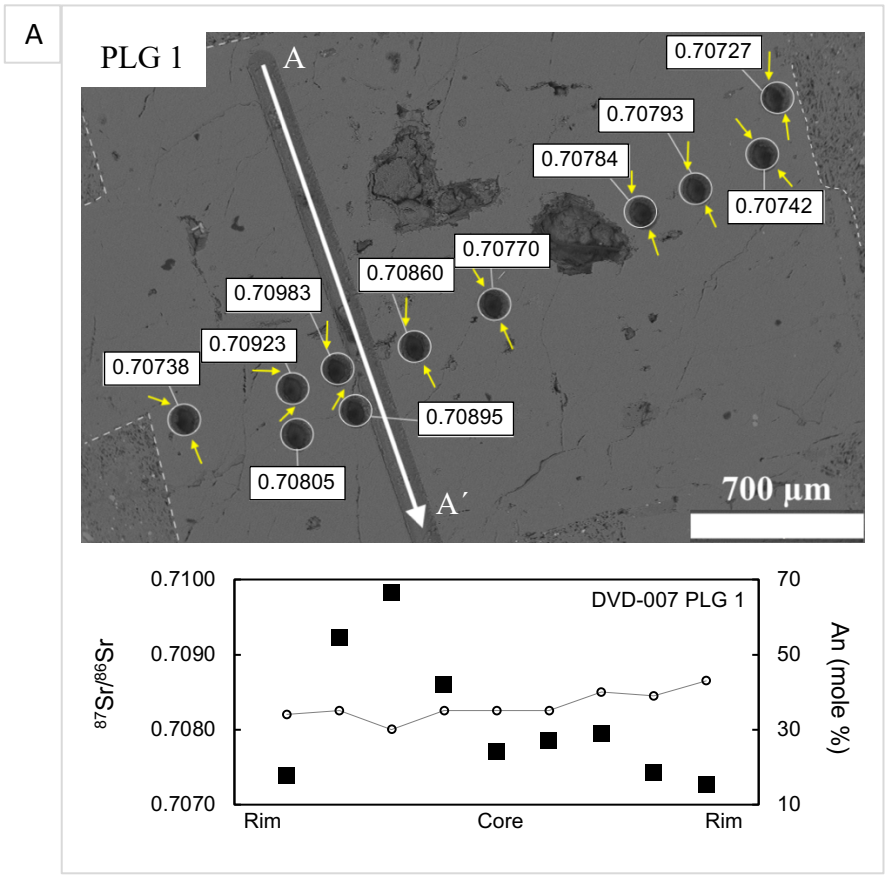

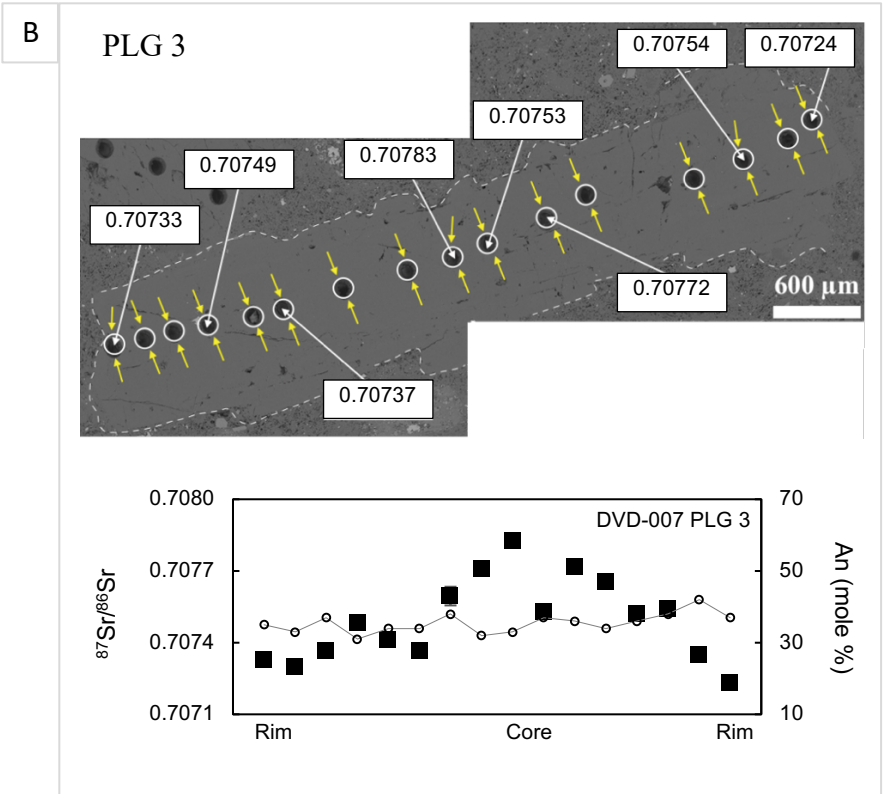

Figure 40 continues…

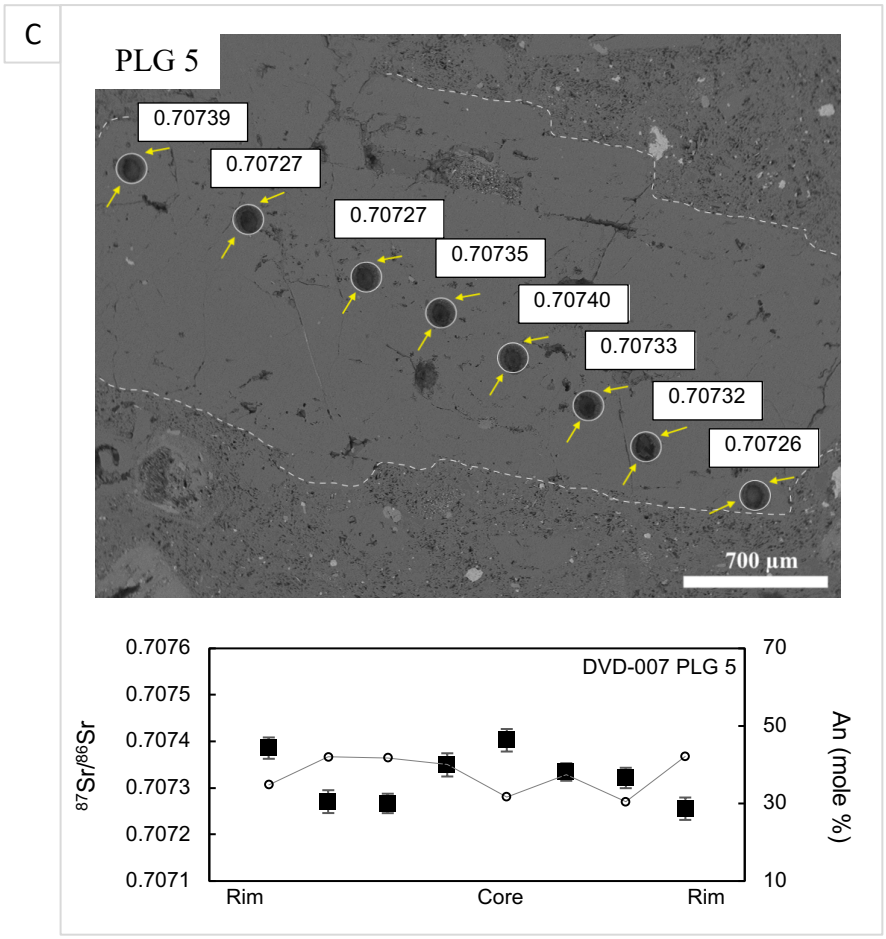

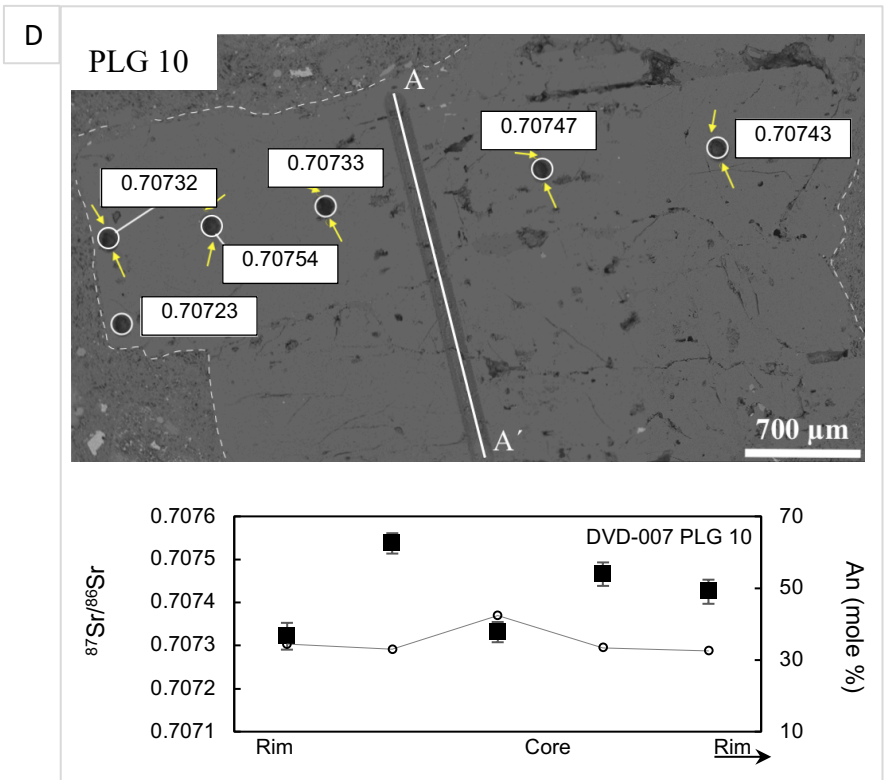

Figure 40 continues…

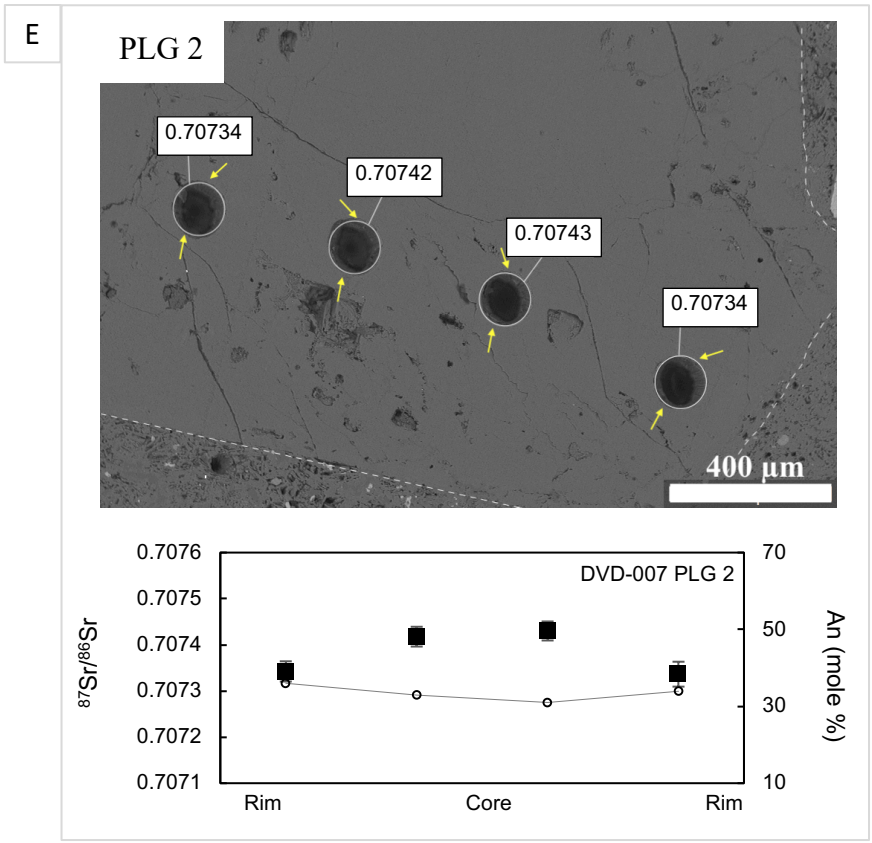

Figure 40. Plagioclase phenocryst BSE images showing LA-MC-ICP-MS analysis spots with $^{87}Sr/^{86}Sr$ ratios and LA-MC-ICP-MS and EPMA results diagrams for A) DVD-007 PLG 1, B) DVD-007 PLG 3, C) DVD-007 PLG 5, D) DVD-007 PLG 10 and E) DVD-007 PLG 2. Yellow arrows in BSE images indicate approximate locations of EPMA analysis spots. Black square = $^{87}Sr/^{86}Sr$ (error bar not shown if magnitude of 2σ within the symbol parameter); circle = An mol.%.

Four phenocrysts (DVD-007 PLG 6, DVD-007 PLG 7, DVD-007 PLG 8 and DVD-007 PLG 13) were measured with analysis spots in core and rim only and the results attest to the trend of decreasing $^{87}Sr/^{86}Sr$ ratio from core to rim (Figure 41 A-D). All, except phenocryst DVD-007 PLG 7 which has slightly increasing An content from core to rim, have slightly decreasing An content from core to rim.

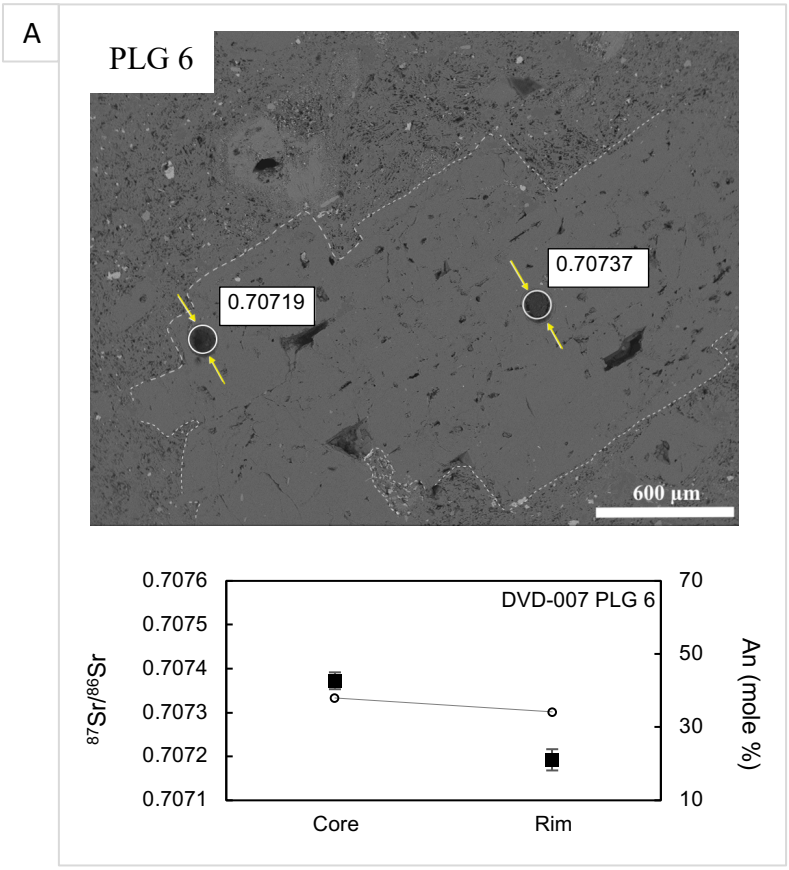

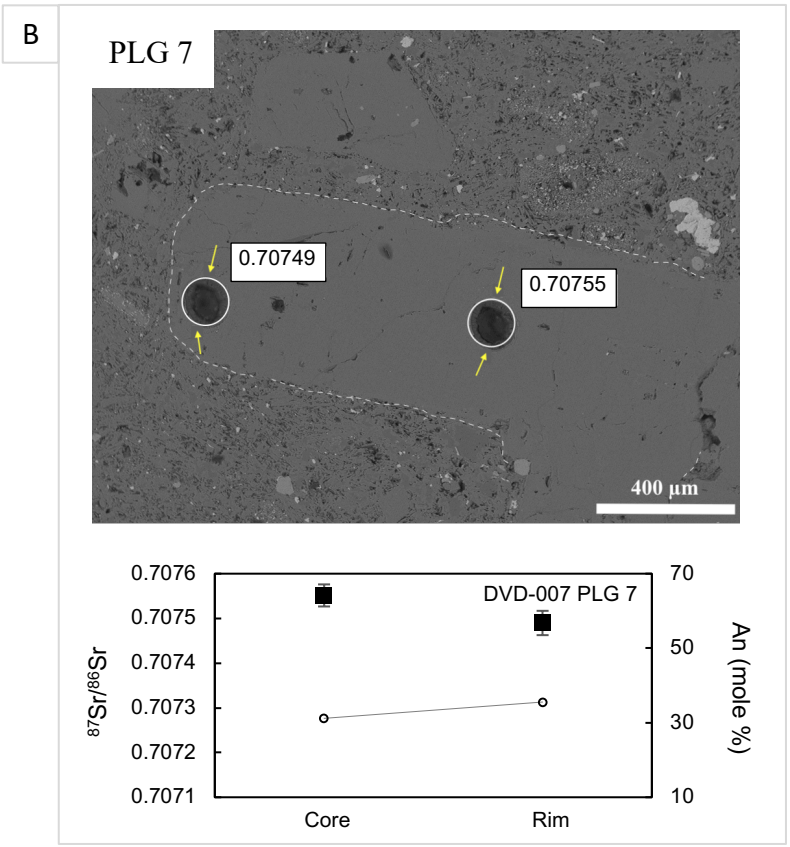

Figure 41 continues…

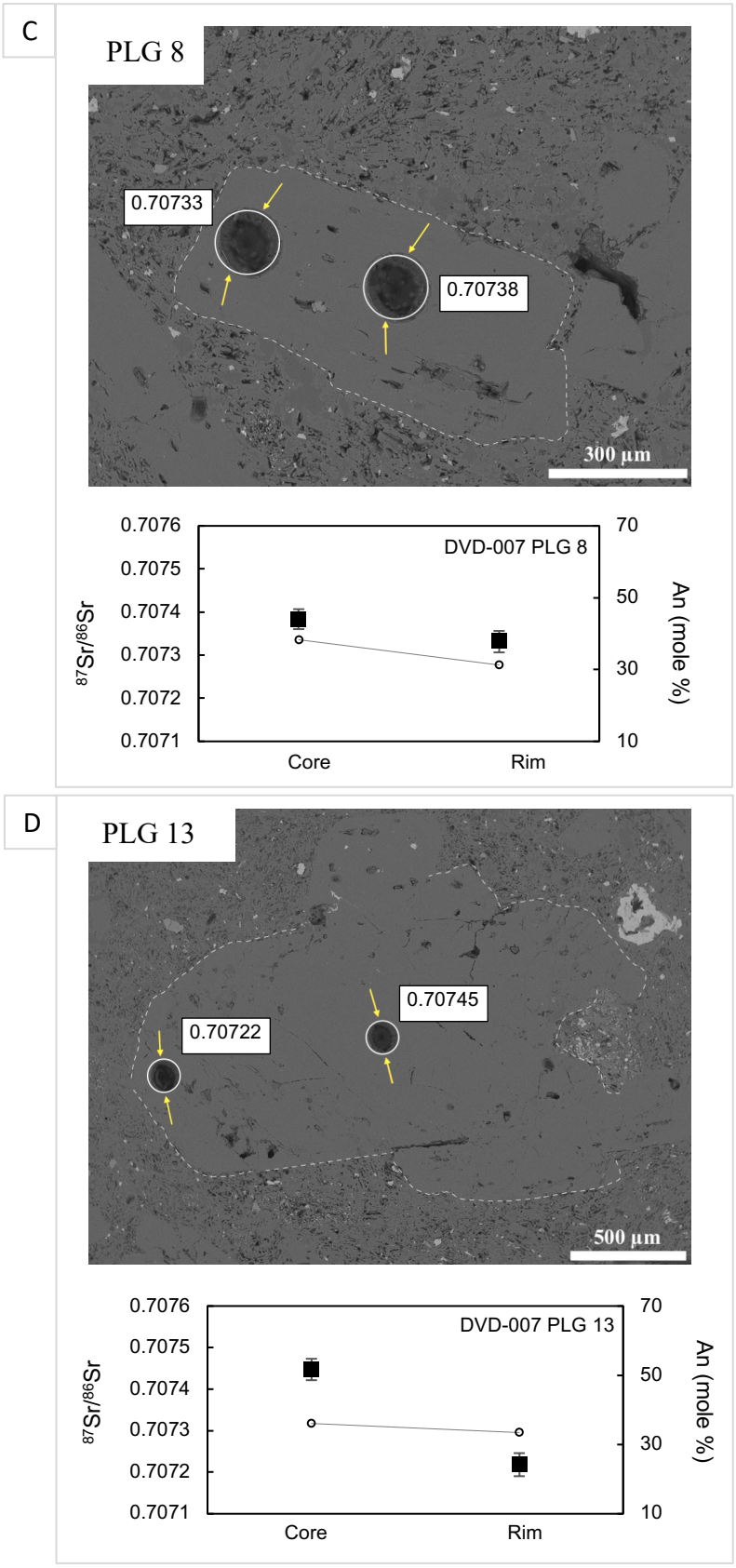

Figure 41. Plagioclase phenocryst BSE images showing LA-MC-ICP-MS analysis spots with $^{87}Sr/^{86}Sr$ ratios and LA-MC-ICP-MS and EPMA results diagrams for A) DVD-007 PLG 6, B) DVD-007 PLG 7, C) DVD-007 PLG 8 and D) DVD-007 PLG 13. Yellow arrows in BSE images indicate approximate locations of EPMA analysis spots. Black square = $^{87}Sr/^{86}Sr$ (error bar not shown if magnitude of 2σ within the symbol parameter); circle = An mol.%.

Line traverse across the width of the phenocryst (Figure 42) were measured for three phenocrysts (DVD-007 PLG 1, DVD-007 PLG 10 and DVD-007 PLG 17) and exhibit a more detailed analysis of variation in the $^{87}Sr/^{86}Sr$ ratios on a phenocryst scale. (See image 37 for phenocryst locations on thick section). All line traverse analyses show oscillating changes in the Sr-isotope values, forming roughly symmetrical $^{87}Sr/^{86}Sr$ peaks on both sides of the phenocryst cores. The line traverse analyses yield more substantial variety in the $^{87}Sr/^{86}Sr$ ratios across the phenocryst than was recorded in the spot mode analyses, and various high $^{87}Sr/^{86}Sr$ peaks were measured in all three phenocrysts. In DVD-007 PLG 1 the $^{87}Sr/^{86}Sr$ ratio varies between 0.7075 and 0.7150 with various high Sr isotope ratio peaks across the grain. The $^{87}Sr/^{86}Sr$ ratio in phenocryst DVD-007 PLG 10 ranges from 0.7075 to 0.7189 and the measurements form several high Sr isotope peaks along the analysis line. Similarly, DVD-007 PLG 17 shows high Sr peaks across the phenocryst, although the variation in $^{87}Sr/^{86}Sr$ ratio is not as significant as in phenocrysts DVD-007 PLG 1 and PLG 10, ranging from 0.7076 to 0.7100.

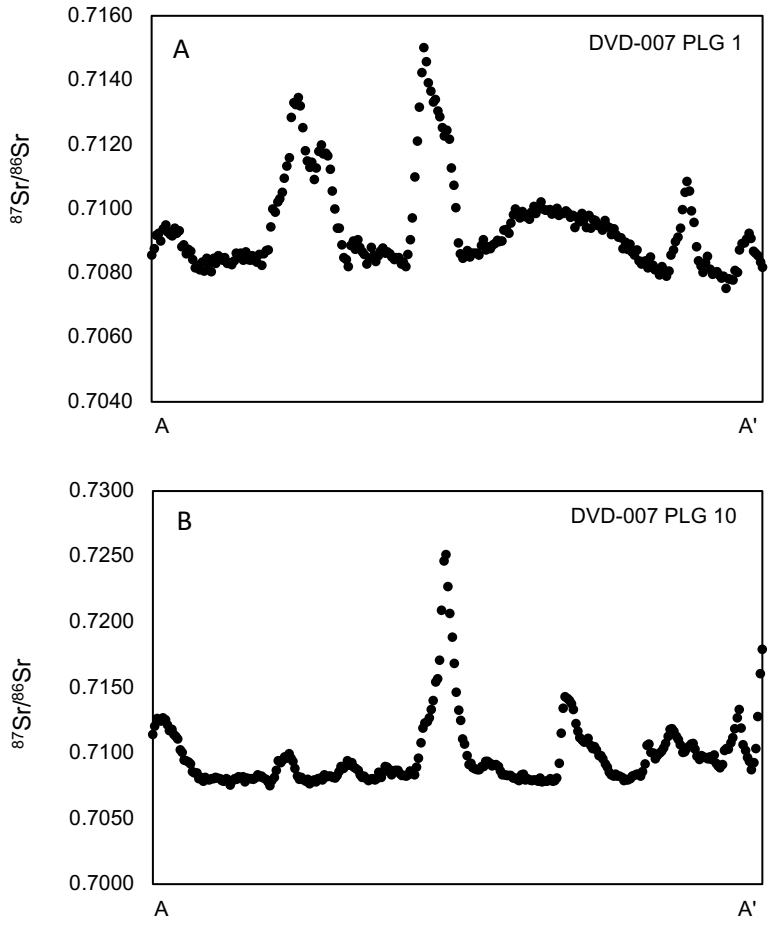

Figure 42 continues…

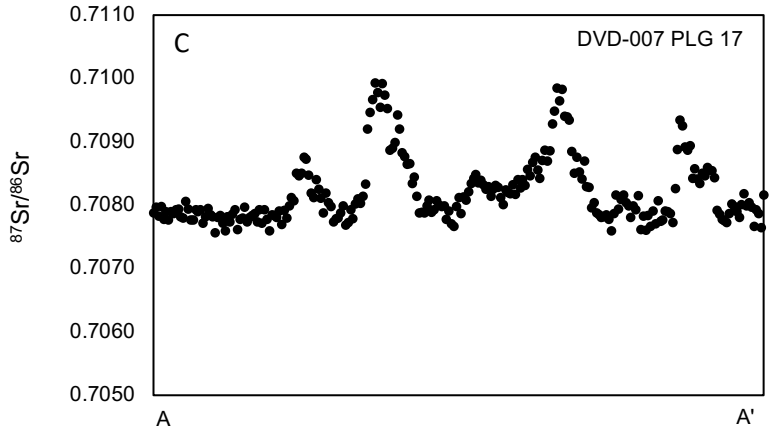

Figure 42. $^{87}Sr/^{86}Sr$ isotopic LA-MC-ICP-MS line traverse rim-to-core-to-rim (A-A') profile of A) DVD-007 PLG 1, B) DVD-007 PLG 10 and C) DVD-007 PLG 17. All line traverse profiles show oscillating $^{87}Sr/^{86}Sr$ ratios.

9.2 Trachyandesite dike of Ibex Hills (DVD-009)

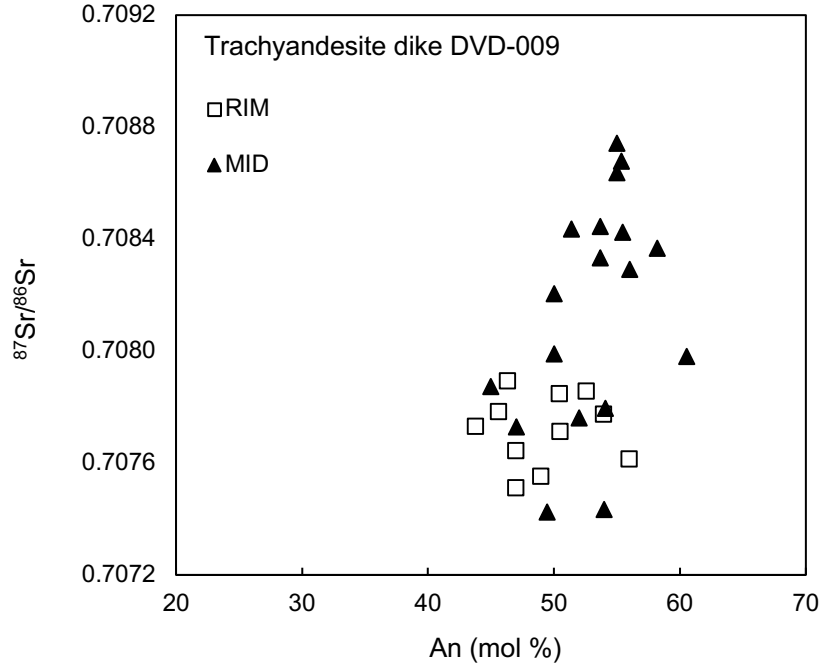

Figure 43. Comparison of rim and mid-crystal *in situ* laser ablation measurement versus An mol.% for representative plagioclase phenocrysts in the trachyandesite dike of Ibex Hills (DVD-009).

Figure 43 outlines the representative phenocryst rim and mid-section *in situ* $^{87}Sr/^{86}Sr$ laser ablation results with plagioclase anorthite content for the trachyandesite dike of Ibex Hills

(DVD-009). Like the trachyte stock, the less radiogenic Sr isotope values are typically measured in the phenocryst rims. The plagioclase rim compositions are slightly more evolved, although the An mol.% values largely overlap.

The $^{87}Sr/^{86}Sr$ ratios and plagioclase anorthite content on a single phenocryst scale for sample DVD-009 are shown in Figure 44 to 46. The decrease in $^{87}Sr/^{86}Sr$ ratios is mostly smooth across the length of the phenocryst and the characteristic feature of oscillating $^{87}Sr/^{86}Sr$ ratio commonly observed in the trachyte stock is recorded only in one of the trachyandesite dike phenocrysts, DVD-009 PLG 16 (Figure 44). The highest $^{87}Sr/^{86}Sr$ ratio in this phenocryst, ~0.7084, is measured in the mid-sections while the Sr isotopic values in the rim decrease to ~0.7077. The An content forms an oscillating pattern in the phenocryst mid-section increasing with decreasing $^{87}Sr/^{86}Sr$ ratio and decreasing with increasing $^{87}Sr/^{86}Sr$ ratio, but decreases slightly towards the rim. The total variation of An is 7 mol.% units.

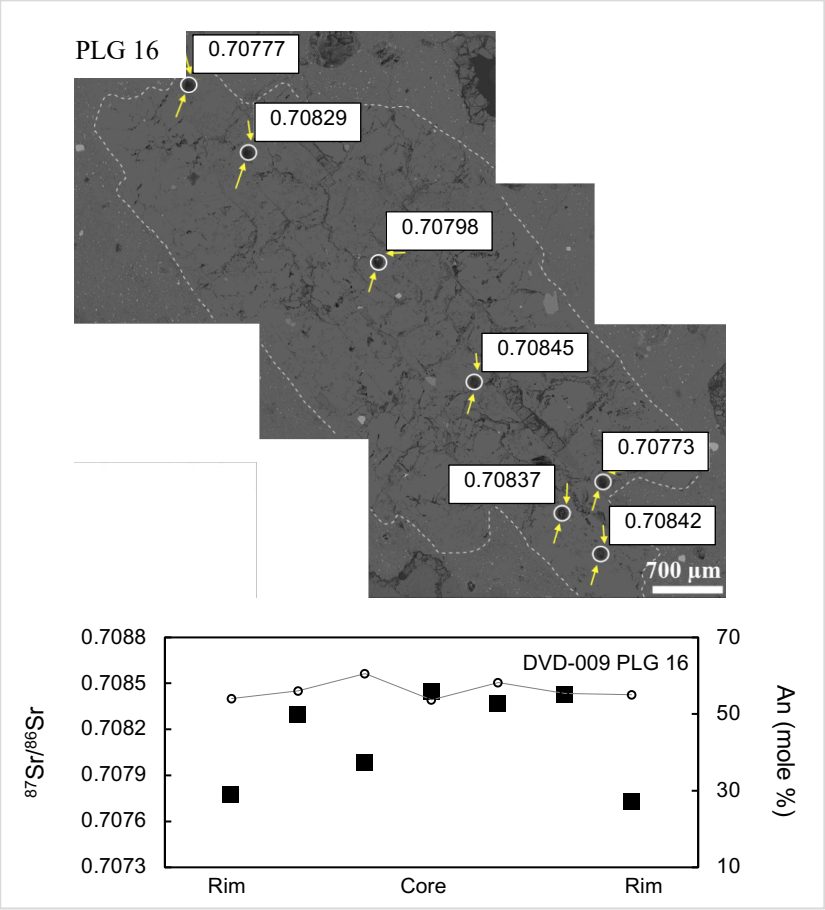

Figure 44. Plagioclase phenocryst BSE images showing LA-MC-ICP-MS analysis spots with $^{87}Sr/^{86}Sr$ ratios and LA-MC-ICP-MS and EPMA results diagrams for DVD-009 PLG 16. Yellow arrows in BSE images indicate approximate locations of EPMA analysis spots. Black square = $^{87}Sr/^{86}Sr$ (error bar not shown if magnitude of 2σ within the symbol parameter); circle = An mol.%.

The Sr isotopes profiles in phenocrysts DVD-009 PLG 11, PLG 14 and PLG 18 are similar (Figure 45). The $^{87}Sr/^{86}Sr$ ratios measured in the mid sections of these phenocrysts are typically >0.7080 and the value decreases to 0.7075-0.7076 in the rims. The anorthite mol.% content mostly follows the $^{87}Sr/^{86}Sr$ value across the phenocryst, i.e. the An content decreases from core to rim in line with the decreasing $^{87}Sr/^{86}Sr$ ratio. The maximum Δ_{An} in the DVD-009 PLG 11, PLG 14 and PLG 18 are 6, 5 and 8 mol.% units respectively. The smallest of the analyzed phenocrysts DVD-009 PLG 17 has least variety between core and rim $^{87}Sr/^{86}Sr$ ratios (~0.7078 and ~0.7076). The anorthite content increases from core 52 to rim 56 mol.%.

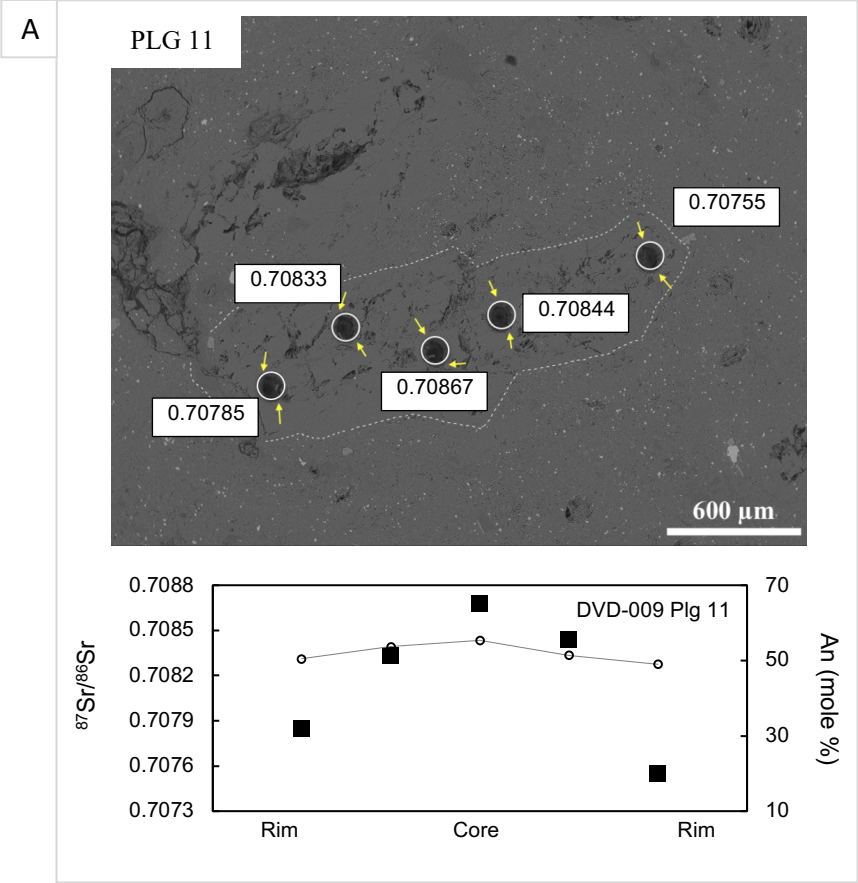

Figure 45 continues…

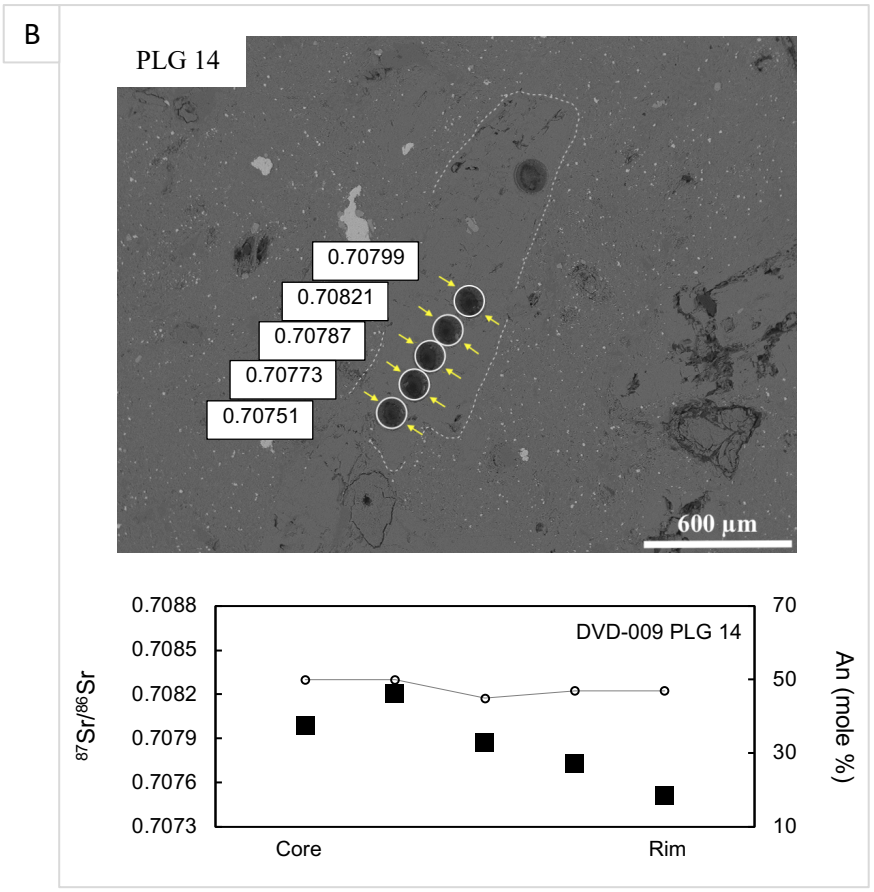

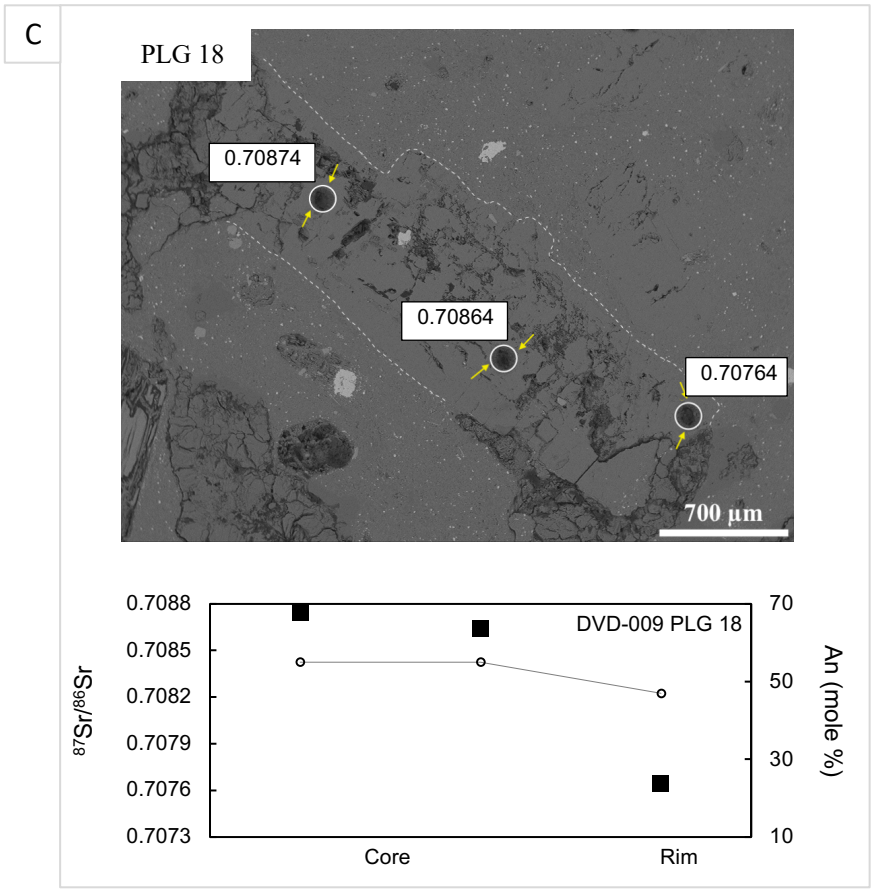

Figure 45 continues…

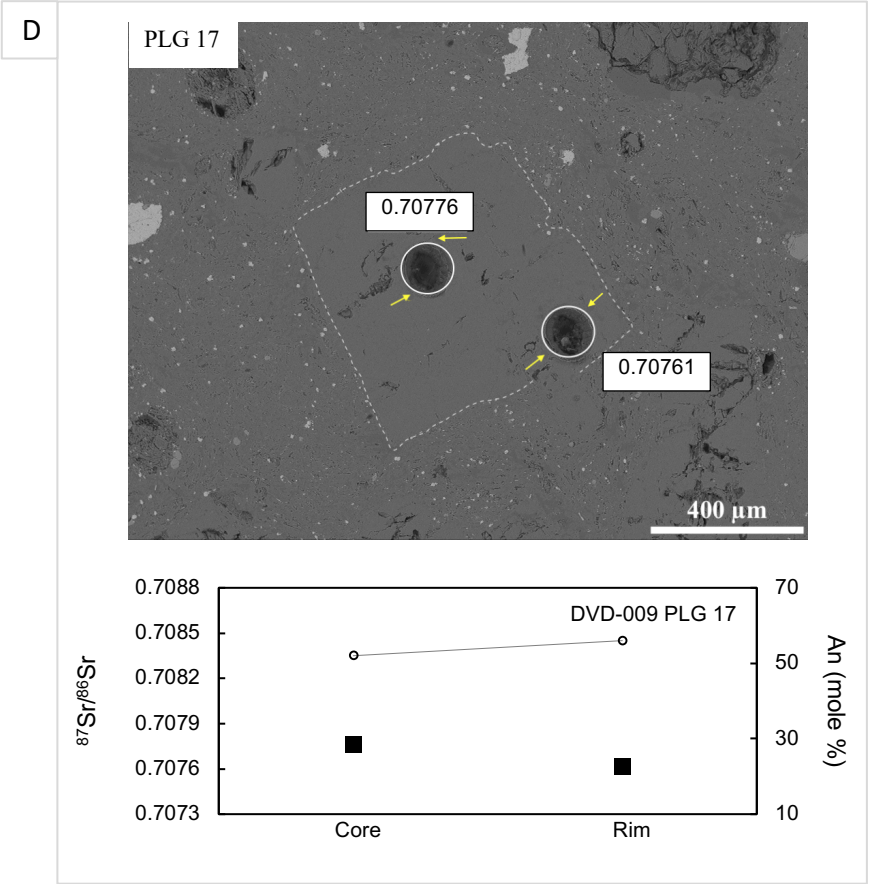

Figure 45. Plagioclase phenocryst BSE images showing LA-MC-ICP-MS analysis spots with $^{87}Sr/^{86}Sr$ ratios and LA-MC-ICP-MS and EPMA results diagrams for A) DVD-009 PLG 11, B) DVD-009 PLG 14, C) DVD-009 PLG 18 and D) DVD-009 PLG 17. Yellow arrows in BSE images indicate approximate locations of EPMA analysis spots. Black square = $^{87}Sr/^{86}Sr$ (error bar not shown if magnitude of 2σ within the symbol parameter); circle = An mol.%.

Contrary to the common overall trend of decreasing Sr isotopic composition from core to rim, one phenocryst, DVD-009 PLG 1, shows increasing $^{87}Sr/^{86}Sr$ ratios from core (~0.7074) to rim (~0.7079) (Figure 46). The An content varies between 46 and 54 mol.% and seems not to form any obvious relationship with the $^{87}Sr/^{86}Sr$ ratios. Because of the large number of cracks and inclusions in phenocryst DVD-009 PLG 9, a large section of the crystal could not be measured for $^{87}Sr/^{86}Sr$ ratios (Figure 46). The three measurements obtained from this phenocryst fall within the 2σ standard deviation values. Whether the mid-section of this phenocryst has varying $^{87}Sr/^{86}Sr$ ratios is unknown.

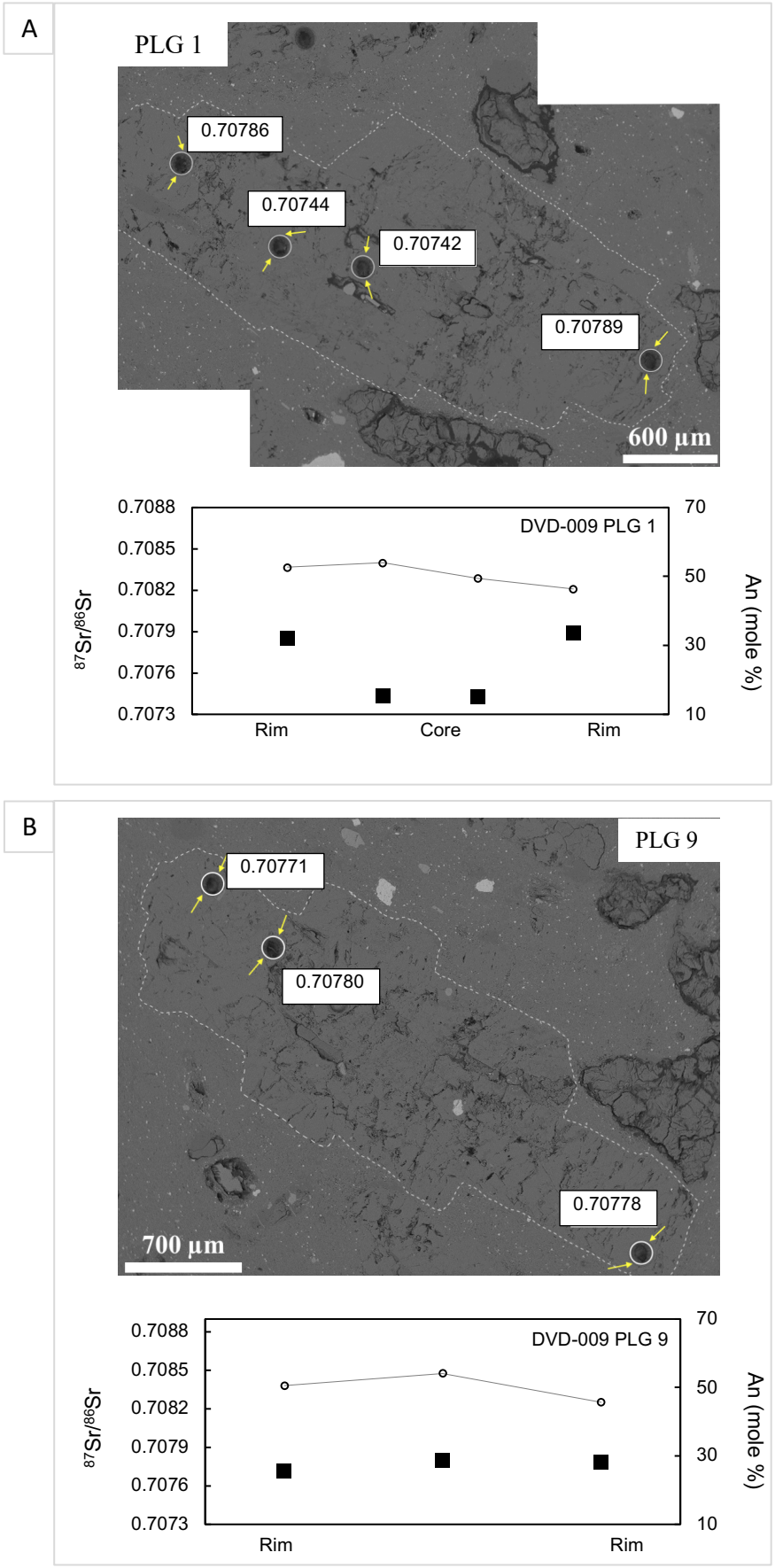

Figure 46. Plagioclase phenocryst BSE images showing LA-MC-ICP-MS analysis spots with $^{87}Sr/^{86}Sr$ ratios and LA-MC-ICP-MS and EPMA results diagrams for A) DVD-009 PLG 1 and B) DVD-007 PLG 9. Yellow

arrows in BSE images indicate approximate locations of EPMA analysis spots. Black square = $^{87}Sr/^{86}Sr$ (error bar not shown if magnitude of 2σ within the symbol parameter); circle = An mol.%.

10. DISCUSSION

The division to the four dike categories – Miocene, metamorphic, altered and Cretaceous – follows throughout the following chapter. The discussion will evaluate petrographic and geochemical similarities as well as differences between the sample groups. The secondary mineral overprint of the metamorphic and altered sample groups are addressed in detail by assessing the subsolidus processes and metamorphic conditions that have affected these samples. Miocene magma chamber dynamics during the Basin and Range crustal extension in the Southern Death Valley and magma source characteristics are evaluated with plagioclase major element and Sr-isotopic composition on phenocryst profiles from the two Miocene samples (trachyte stock and trachyandesite dike).

10.1 Petrographic constraints on the sample categories

The petrographic review of the studied samples uncovered substantial differences regarding secondary minerals. The Miocene samples of Ibex Hills (DVD-007, DVD-009 and DVD-010) and Saddlepeak Hills (DVD-001ALT and DVD-001ALT_2) are relatively unaltered. Minor (non-pervasive) sericite alteration is common in feldspars as is alteration of mafic minerals and secondary filling of amygdules, when present. Contrary to the Miocene samples, the metamorphic and altered samples of Saddlepeak Hills (DVD-001, DVD-002 and DVD-003) and Salt Spring Hills (DVD-005 and DVD-006) are dominated by secondary minerals with only minor, if any, magmatic minerals present. The feldspar in the Cretaceous dike of Mojave Desert (365) is pervasively altered but the hornblende is magmatic.

The difference in degrees of alteration and presence of secondary minerals, from minor sericitization of plagioclase and alteration of mafic minerals in the Miocene samples to the pervasive fabrication of the metamorphic and altered samples with secondary minerals, suggest that the dikes of Saddlepeak Hills and Salt Spring Hills are unlikely to

represent similar emplacement history with the fresh Miocene samples. The Miocene lava samples DVD-001ALT and DVD-001ALT_2, collected from the eastern side of Saddlepeak Hills adjacent to the location of the altered dike DVD-001, show only minor alteration. It is therefore unlikely that these Miocene samples would have retained their largely magmatic mineralogy had they been subject to similar metamorphic conditions with sample DVD-001. The altered and metamorphic dikes thus must represent an older period of dike emplacement in the Death Valley region.

10.1.1 DVD-003 – 1.1 Ga Diabase

The metamorphic sample DVD-003 shows similar geochemical composition with the Proterozoic 1.1 Ga Crystal Spring Diabase as is evident in the TAS-diagram (Figure 28 and Table 1). Pervasive greenschist facies alteration has been reported in the Crystal Spring Diabase by Hammond (1983) and similarities in the secondary mineral assemblages and textures between sample DVD-003 and a 1.1 Ga diabase sample from Jupiter Hill, California are shown in Figure 47. The grain size in sample DVD-003 is smaller and the fabrication by chlorite and epidote is more extensive, but the sub-ophiolitic texture and abundance of Fe-Ti-oxides are similar. It is therefore likely that sample DVD-003 represents a Proterozoic magmatic event and is either a dike or a sill emplaced in already cooled diabase sill, or is itself a chilled margin of a diabase sill (dike margins in the field were, however, difficult to constrain, see Chapter 5).

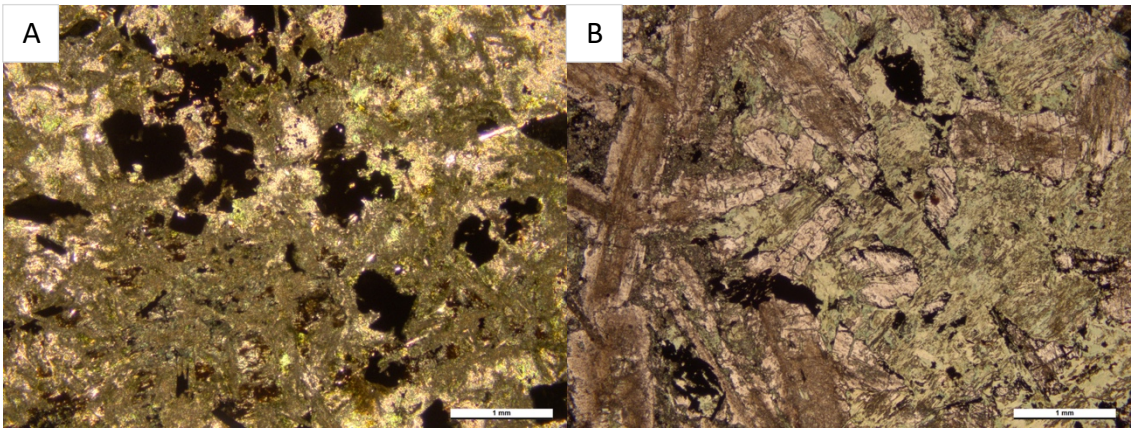

Figure 47. PPL image of A) sample DVD-003 and B) 1.1 Ga diabase, Jupiter Hill, Kingston Range, California. Thin section courtesy of J. Calzia and T. Rämö. Both images show typical sub-ophiolitic texture of diabase, although feldspar in image A is masqueraded in green secondary minerals. Fe-Ti-oxides are abundant in both images. The width of the scale bar is 1 mm.

10.2 Sub-solidus processes in the metamorphic and altered sample groups

The metamorphic samples DVD-002, DVD-003 and DVD-005 are characterized with typical low-grade greenschist facies metamorphic minerals chlorite, epidote and albite, whereas the altered samples DVD-001 and DVD-006 lack both chlorite and epidote but have pervasive sericite, secondary quartz and feldspar with abundant oxides. The varying mineral assemblages also show on hand specimen scale. The green color of samples DVD-002, DVD-003 and DVD-005 reflects epidote and chlorite. Samples DVD-001 and DVD-006 are red, and the color is especially intense in the abundant hematite containing sample DVD-006.

Secondary mineral assemblages reflect a complex summary of variables in a metamorphic environment such as pressure and temperature conditions, rock permeability, co-forming mineral assemblage, composition of protolith, composition of circulating fluids as well as fO_2 (Aguirre and Atherton 1987, Schmidt 1993, Bastias et al. 2016). The differences in the secondary mineral assemblages between the metamorphic and altered sample groups suggest that the samples have been subject to different post-magmatic conditions.

10.2.1 Metamorphic samples

Samples DVD-002, DVD-003 (Saddlepeak Hills) and DVD-005 (Salt Spring Hills) contain chlorite, epidote, sericite, albite, carbonate and ±actinolite. A comprehensive study of the metamorphic conditions that culminated in the secondary minerals observed in the studied samples is beyond the scope of this thesis. However, mineral geothermometers based on experimental studies of mineral stability in different physiochemical conditions have been established and can be applied to estimate the temperature-pressure conditions of the studies samples. The secondary minerals chlorite, epidote and albite are typical Barrovian low-grade greenschist metamorphic facies minerals (e.g. Schmidt 1993, Mathieu 2018, Starr and Pattison 2019) and commonly represent regional metamorphism and crystallization at ~300–500°C and 1-4 kbar (Kristmannsdottir 1979, Apted and Liou 1983, Bird et al. 1984). However, the typical greenschist facies mineral actinolite is not observed in the studied samples except in the metadiabase DVD-003. Actinolite commonly forms in temperatures close to 300°C

(Kristmannsdottir 1979, Aguirre and Atherton 1987) and it is therefore suggested that the metamorphic temperature in the study area did not substantially exceed 300°C. Neither field observations nor petrographic examination show evidence of ductile deformation (e.g. foliation, folding) in any of the metamorphic samples. However, veins filled with secondary minerals or oxidized veinlets showing brittle deformation are common and could indicate an effect of retrograde metamorphism, cooling or hydrothermal alteration and circulation of fluids (Bastias et al 2016).

10.2.2 Altered samples

The secondary mineral assemblage of samples DVD-001 and DVD-006 is different from that of the samples DVD-002, DVD-003 and DVD-005. Unique to these samples is their abundance in white mica, secondary K-feldspar and quartz, and oxides with minor carbonate. Epidote and chlorite, minerals observed in the metamorphic samples, are absent in DVD-001 and DVD-006. This suggests that the original rock composition, post-magmatic conditions or fluid composition affecting the samples were different.

Table 2. Summary of secondary minerals, LOI % and selected geochemical characters highlighting main differences between the metamorphic samples and altered samples. Ep = epidote, Chl = chlorite, Ab = albite, Kfsp = potassium feldspar, Amb = amphibole, Bt = biotite, Ser = sericite, Q = quartz, Ox = oxides.

Sample ID	Secondary minerals[a]	Sample group	LOI %	K_2O	Na_2O	CaO	MgO
DVD-002	Ep+Chl+Ab+Kfsp+Ser	Metamorphic	2.18	1.33	5.01	5.13	2.38
DVD-003	Ep+Ch+Amb+Bt	Metamorphic	2.73	1.27	2.37	6.55	5.34
DVD-005	Ep+Chl+Ser+Kfsp	Metamorphic	3.26	2.00	2.78	5.09	3.01
DVD-001	Ser+Q+Kfsp+Ox	Altered	7.01	4.07	<0.01	1.96	1.75
DVD-006	Ser+Q+Kfsp+Ox	Altered	8.89	3.33	0.35	2.57	1.92

[a] All samples contain carbonate minerals.

These differences are reflected in the major element composition of these dikes (Table 2). Perhaps the most striking difference is that the altered samples are marked by larger loss on ignition (LOI = 7.01-8.89%), which reflects a relatively large volatile content in these samples compared to the metamorphic samples (LOI = 2.18-3.26%). This difference in LOI reflects how these samples were modified by post-solidus processes with the altered samples having been more intensively percolated by hydrothermal fluids capable of mobilizing the major rock-forming elements. Fluid circulation mobilizes some

of the major elements including K, Na, Ca, Fe and Mg (see Chapter 10.4.1) during regional metamorphism as well as hydrothermal alteration (Christidis 1998, Neuhoff et al. 1999, Kousehlar et al. 2012) and Fe can be oxidized by metamorphic processes (Massey 1983).

The differences in the element compositions between the metamorphic and altered samples indicate element mobility and resultant precipitation of different secondary minerals. The epidote- and chlorite-bearing metamorphic samples have higher CaO and MgO, these oxides are less abundant in the altered samples. Of the alkali oxides, Na_2O has been almost completely removed from the altered samples whereas K_2O appears to have been added. The sericitization of feldspar suggests mildly acidic alteration with effective removal of Na and Ca and adding of K (Nogami and Yoshida 1995, Mathieu 2018). Also, precipitation of quartz, which is especially abundant in sample DVD-006, indicates acidic fluid circulation (Kousehlar et al. 2012). Leaching of usually immobile Al can be triggered by acidic solutions (Nogami and Yoshida 1995). However, no major differences are apparent in the Al_2O_3 content between the samples, although the altered samples have slightly higher aluminum. As decrease of pH increases the rate of Al leaching (Nogami and Yoshida 1995), the fluid affecting these samples were probably only mildly acidic.

The petrography of the altered samples does not show evidence for these samples having contained chlorite or epidote prior to hydrothermal alteration, although later fluid interaction might have altered the original secondary mineral assemblage. For example, epidote effectively dissolves in acidic conditions, such as in CO_2-rich fluid systems, by releasing Ca that can further contributed to the formation of carbonate (Marieni et al. 2021). All in all, the hydrated and oxidized profile of these samples combined with K enrichment and Na loss could imply low temperature (<100°C) hydrothermal metamorphism, typically discovered in oceanic metabasalts or retrograde metamorphic conditions (Schiffman 1995, Ague 2017).

10.3 Conditions of metamorphism

The secondary mineral assemblages of the studied metamorphic samples are typical of burial metamorphism processes (e.g. Schmidt 1993, Schiffman 1995, Bastias et al. 2016). Non-deformational low-grade metamorphosis has been recorded in a number of different geologic settings. These include the Precambrian Jotnian and sub-Jotnian lava sequences of central Sweden (Nyström 1983), the Proterozoic Zig-Zag Dal basalts of Greenland (Bevins et al. 1991) and the Proterozoic North Shore Volcanic Group in Minnesota (Schmidt 1993). The Mesozoic to Cenozoic arc related volcanic rocks of the Andean Cordillera are overprinted by zeolite to greenschist facies hydrothermal-burial metamorphism (Aquirre and Offler 1985, Aquirre and Atherton 1987).

Low- to medium-grade metamorphism related to the Mesozoic-Paleogene Sevier-Laramide orogeny has been widely reported in the southwestern USA (e.g. Lima et al. 2018, Long and Soignard 2016, Hoisch et al. 2014), although Cenozoic magmatism and crustal extension structures have made identification of them challenging (DeCelles 2004, Long and Soignard 2016). Examples of metamorphism recorded in the southwestern USA include thrust burial related to Mesozoic Barrovian metamorphism and crustal thickening in the Proterozoic sedimentary strata in the Funeral Mountains, northeastern Death Valley (Hoisch et al. 2014, Mattison et al. 2007); indications of similar burial metamorphism are absent from Tertiary sedimentary strata (Mattison et al. 2007). Elevated temperatures affected the Proterozoic basement gneiss of Black Mountains (adjacent to Ibex Hills) during the Sevier-Laramide orogenesis (Lima et al. 2018). Also, late Cretaceous shallow-crustal greenschist facies metamorphism of Cambrian to Pennsylvanian sedimentary rocks is recorded in eastern Nevada (Long and Soignard 2016). The Mesozoic-Paleogene orogenesis of western USA comprises a complex history of crustal shortening, Barrovian metamorphism and local extension in the retroarc hinterland and Sevier thrust belt east of the Sierra Nevada magmatic arc (DeCelles and Graham 2015). The compression tectonics of the Sevier-Laramide orogenesis might have caused the low-grade metamorphic sub-solidus processes and secondary mineral formation in the samples of this study, located in the Sevier hinterland and at the margins of the Sevier fold-thrust belt (Figure 1).

It is not clear why the altered samples are different in mineralogy from the metamorphic samples. Geographically, the altered samples are located in the middle of the metamorphic samples and thus the decreasing effect of burial metamorphic stratigraphy seems implausible (Figures 4 and 5). The distance between the altered sample DVD-006 and metamorphic sample DVD-005 is ca. 1200 meters. The altered and metamorphic samples do not necessarily represent same age and the rock composition and primary mineralogy could have been different. Also, rock permeability affects the rate and style of metamorphism and the degree of alteration is not necessarily linked to the depth of burial (Schmidt 1993). The physical character of a basalt flow, such as flow thickness and presence of vesicles affects the rock permeability and consequent fluid/rock ratios controlling the level of metamorphism (Bevins et al. 1991). The altered sample DVD-001 is located in a fault zone and thus in an ideal place for passing fluids. Similarly, sample DVD-006 contains vesicles, now filled with secondary products. These physical features could have enhanced the retrograde hydration and oxidation of these two samples.

Contact metamorphism is another possibility for the cause of recrystallisation of secondary minerals of the metamorphic and altered dikes of this study. The dike swarm of White-Inyo Range includes mafic and intermediate dikes that are metamorphosed up to upper-greenschist facies, generated by contact-metamorphism during injection of Jurassic-Cretaceous granitoids (Ernst 1997). Having metamorphosed to greenschist facies, the metamorphosed dikes of the present study bear similarities with the metamorphosed White-Inyo Range mafic dikes. A Cretaceous pluton is exhumated in the southern section of Salt Spring Hills and thus could have provided heat source for contact metamorphism as well as hydrothermal alteration. Miocene volcanic rocks in the Saddlepeak Hills can contribute as further heat source.

10.4 Whole-rock geochemical constraints on sample categories

10.4.1 Evaluation of post-magmatic element mobility

The chemical composition of igneous rocks is a combination of source composition modified by partial melting, fractional crystallization, assimilation and sub-solidus processes. As discussed above, the metamorphosed and altered dikes of Death Valley have been affected by alteration processes evident in the abundance of secondary minerals

and the possibility thus exists that the major element geochemistry of these samples is unlikely to represent magmatic composition. Major elements and the large ion lithophile elements (LILEs) Ba, Sr, Rb, K and Cs are prone to be mobilized by post-magmatic processes such as metamorphism and hydrothermal alteration (El Korh et al. 2009, Jenner et al. 2009) whereas the REEs and HFSE (Nb, Ta, Zr, Hf) and transition metals Cr, Ni are immobile (Pearce and Norry 1979), although the latter should not be considered completely immune to metamorphic or hydrothermal processes (Ague 2017). The major element oxide versus SiO_2 diagrams (Figure 30) show inconsistences between the metamorphic and altered samples, suggesting different source composition or sub-solidus element mobility. Based on differences in LOI percentage and some major element oxides (e.g. K_2O, Na_2O), it was established in Chapter 10.2 that the metamorphic and altered samples have been differently affected by fluid-induced element mobility.

MORB normalized multielement diagrams show consistent behavior for LIL-elements for the Miocene samples but irregular patterns for the metamorphic and altered samples (Figure 32). The scatter of the LILEs in the metamorphic and altered samples is interpreted here to have been caused by post-magmatic alteration, although the overall enrichment of LILEs over HFSEs in the metamorphic and altered samples is considered magmatic. The behavior of the generally immobile HFSEs is more coherent also in the metamorphic and altered samples implying that these elements have remained mostly immobile. There are, however, few HFSE anomalies between the samples, such as high Ti relative to Y in samples DVD-002 and DVD-003 as well as in the Cretaceous sample 356 ($Ti/Y_N > 1$ vs. $Ti/Y_N < 1$ for rest of the samples) (Figure 32). The positive Ti anomaly relative to Y reflects abundant Fe-Ti-oxides in samples DVD-003 and DVD-002 and in the Cretaceous dike possibly the incorporation of Ti into hornblende.

Altered samples DVD-001 and DVD-006 and the Miocene sample DVD-010 have relatively high volatile contents, LOI = 7.01, 8.89 and 6.35% respectively, compared to the rest of the samples (LOI ≤ 4.06%). To test whether the LILE mobility in these samples was affected by LOI, Sr, K, Rb and Ba vs. LOI are shown in Figure 48. The elevated K attests to the earlier analysis of K-metasomatism as it correlates with the LOI. Similarly, Rb appears to be added by fluids to the metamorphic and altered samples whereas Sr is removed. The trend is opposite in the Miocene samples: Rb and K have negative correlation, Sr is increased with LOI, although changes in the Miocene samples are minor.

Ba seems to be unaffected by the changing LOI. For comparison, generally immobile HFSE Nb and Zr (not shown) are not correlated with LOI. Similarly, sometimes mobile HFSEs La and Th appear to be unaffected by the changing LOI and are thus considered here to represent magmatic values (Figure 48). To constrain the primary geochemical features of these samples, the discussion hereafter will place emphasis on the immobile trace elements.

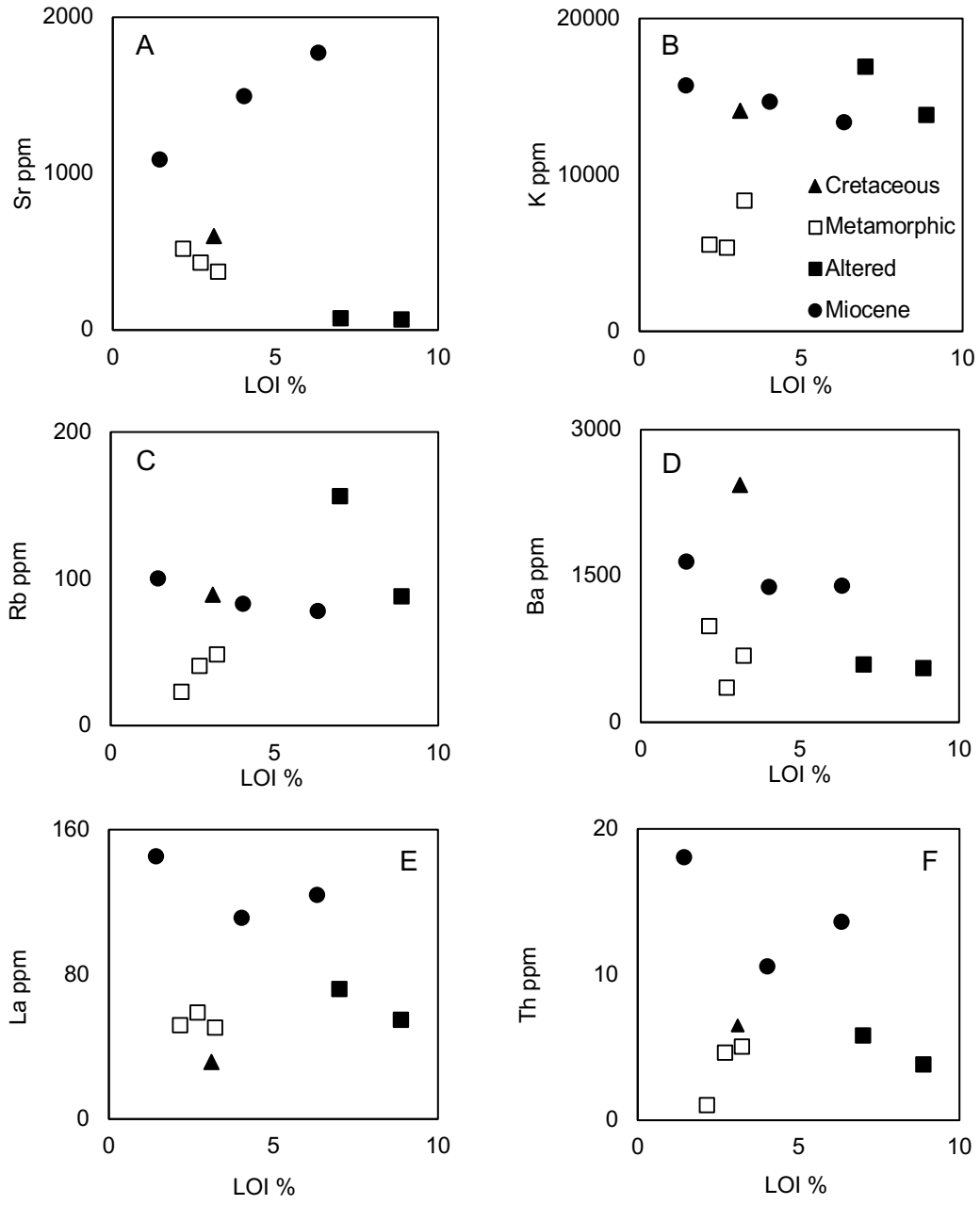

Figure 48. LILEs Sr, K, Rb and Ba and less mobile La and Th versus LOI % to reveal fluid induced element mobility in the metamorphic samples. A) Sr is removed, B) K is added, C) Rb is added, D) Ba, E) La and F) Th are unaffected by increasing LOI %.

10.4.2 Compositional trends between the sample groups

The different K_2O content of the Miocene and metamorphic samples at roughly similar SiO_2 questions the genetic affinity of these samples and origin from a single source (Figure 49). Alternatively, the K_2O content of the metamorphic samples could have been affected by metamorphic processes. As noted above, the potassium content of samples DVD-001 and DVD-006 does not represent magmatic values and these two dikes could have represented medium-K composition prior to alteration. Apart from signifying different source composition from the metamorphic samples, the high K_2O in the Miocene samples could be a response to an extensional strain producing a smaller degree of partial melts and coinciding enrichment in incompatible elements. Putirka and Platt (2012) documented such decrease in partial melts fractions and increase in the abundances of incompatible element in the Basin and Range magmas towards the east of the Cordillera and proposed this to indicate a thickening lithospheric mantle.

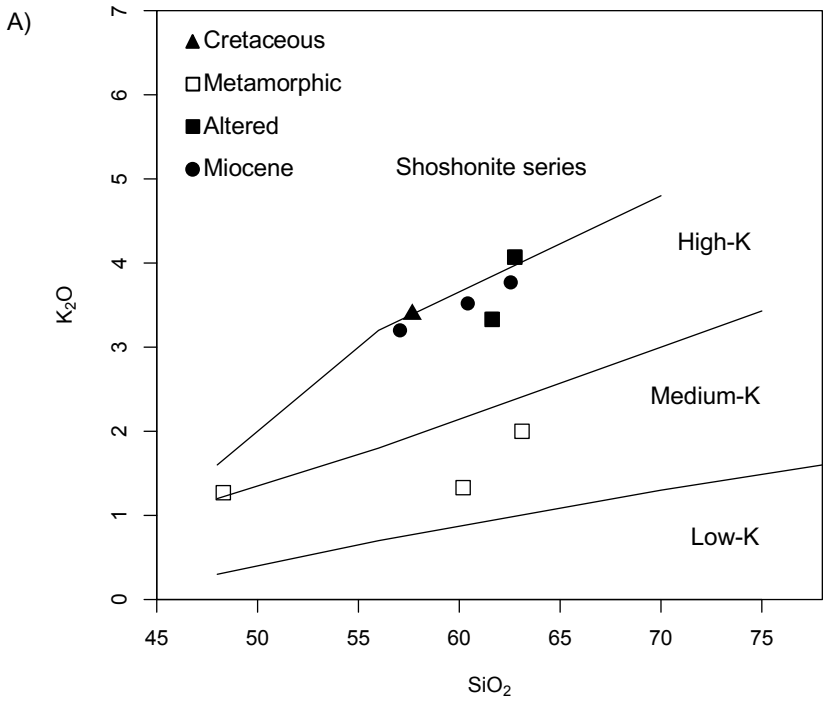

Figure 49 continues…

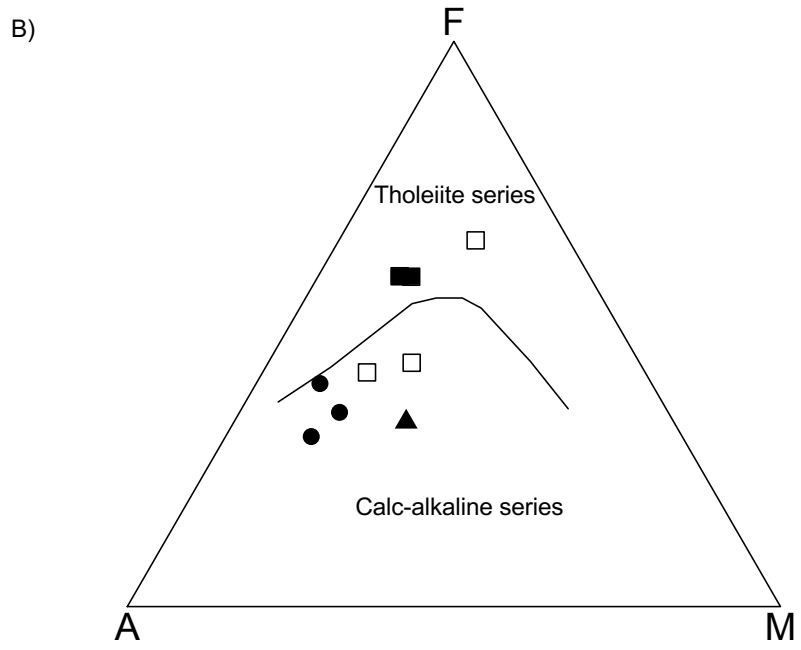

Figure 49. A) K_2O vs. SiO_2 diagram. The Miocene and Cretaceous samples plot on the high-K field, metamorphic as medium-K. Samples DVD-001 and DVD-006 plotting as high-K are likely to have elevated K_2O content by subsolidus processes. B) AFM diagram (Irvine and Baragar 1971). The Miocene, Cretaceous and two metamorphic samples plot as calc-alkaline, metadiabase DVD-003 and two metamorphic samples (DVD-001 and DVD-006) as tholeiites. Samples DVD-001 and DVD-006 are unlikely representing magmatic values.

The Miocene, the Cretaceous and metamorphic samples DVD-005 and DVD-002 are defined as calc-alkaline on the K_2O+Na_2O – FeO* – MgO diagram of Irvine and Baragar (1971) whereas the metadiabase DVD-003 and altered DVD-001 and DVD-006 plot as tholeiitic (Figure 49). However, post-solidus processes (K-metasomatism) indicated by samples DVD-001 and DVD-006 are likely to have mobilized Mg (MgO is lower in these two samples compared to samples DVD-002 and DVD-005). The metamorphic and altered samples DVD-001, DVD-002, DVD-005 and DVD-006 are thus medium-K calc-alkaline rocks whereas the metadiabase sample DVD-003, however, could be a “true” tholeiite.

Further constrains on the source composition can be drawn from the chondrite normalized REE patterns (Figure 31). The four ICP-MS/OES-analyzed samples (Table 1) can be grouped into three categories based on their REE pattern. The Cretaceous dike sample 365 has relatively high $(La/Sm)_N$ (=4.07) and $(Gd/Yb)_N$ (=2.42), the meta-andesite

samples DVD-001 (altered) and DVD-005 (metamorphic) have similar $(La/Sm)_N$ (=4.06) but lower $(Gd/Yb)_N$ (=1.40-1.66). The Miocene sample DVD-007 is the most enriched in LREE with $(La/Sm)_N$ =6.24 but is more depleted in HREE than the metamorphic and altered samples and has $(Gd/Yb)_N$ similar with the Cretaceous dike (=2.83). The overall $(La/Yb)_N$ ratios for the Cretaceous, metamorphic and altered, and Miocene samples are 15.27, 9.30-10.58 and 31.45, respectively. The higher LREE of the Miocene samples with a similar small Eu anomaly further suggests that it is unlikely that the Miocene samples are subsequent derivatives from the source of the metamorphic and altered samples or that these sample groups are co-genetic. The geochemical features support the petrographic evidence that the metamorphic and altered samples represent an older period of dike emplacement than the Miocene samples coeval with Basin and Range extension.

10.4.4 Subduction signature

All the studied samples show overall enrichment in MORB-normalized large ion lithophile elements (LILE) over high field strength elements (HFSE) and a notable depletion in Nb and Ta relative to LILEs and LREEs. These geochemical features are characteristic of arc magmas related to subduction of an oceanic crust (Gill 1981, Pearce and Peate 1995, Münker et al. 2004). The enrichment of the generally mobile LILEs are derived from the subducting slab component of wet sediments and basaltic oceanic crust by aqueous fluids that are mobilized by the heat in the mantle. Magmas generated from these components are enriched in LILEs Sr, K, Rb, Ba and depleted in immobile HFSEs Nb, Ta, Zr and Hf (Pearce and Peate 1995, Pearce and Stern 2006).

The enrichment of LILEs in subduction related magmas can be employed to distinguish lithospheric mantle derived magmas from enriched asthenospheric magmas as well as depleted MORB magmas with LILE over HFSE ratios such as La/Nb or Ba/Nb. The Ba/Nb vs. Nb/Y diagram (Figure 50) presents the effect of slab derived subduction element with Ba and the effect of mantle enrichment with Nb. The denominators minimize the effects of fractional crystallization. The horizontal line represents the minimum Ba/Nb ratio (=28) for magmas with subduction character as suggested by Fitton et al. (1988). The plot shows that the Cretaceous sample 365 has the highest subduction component. The metamorphic and altered samples show varying subduction component, the metadiabase DVD-003 has the lowest value and falls beneath the proposed minimum Ba/Nb ratio for subduction component. All the Miocene samples have moderate and

almost constant Ba/Nb. The Miocene samples show most enriched mantle component relative to the rest of the studied samples and have higher Nb/Y ratio. However, as Nb is more incompatible than Y, the degree of partial melting may affect the Nb/Y ratio, although Pearce and Stern (2006) argue that the effect of mantel enrichment in the value of Nb is superior to the effect of partial melting. The Cretaceous dike with metamorphic and altered samples show similar Nb/Y ratios. All samples show La enrichment relative to average N-MORB, E-MORB and OIB. The Ba/Nb and La/Nb show positive correlation in the Miocene, metamorphic and altered samples.

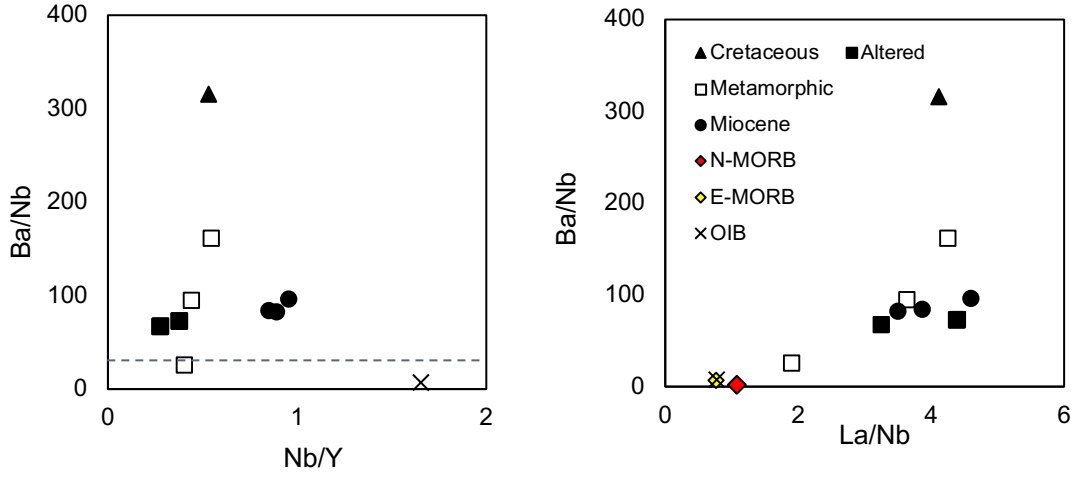

Figure 50. Ba/Nb vs. Nb/Y and Ba/Nb vs. La/Nb diagrams. The subduction character represented by high Ba/Nb (LILE/HFSE) is highest in the Cretaceous dike. Ba/Nb values are similar for the Miocene, metamorphic (except DVD-003) and altered samples. The metadiabase DVD-003 falls below the minimum subduction Ba/Nb value 28 (Fitton et al. 1988). The Miocene samples are the most enriched in mantle component (Nb/Y). La/Nb showing LILE enrichment and implying subduction character is similar in all of the samples except DVD-003, which has the lowest La/Nb. Average N-MORB, E-MORB, OIB for comparison (values are from Sun and McDonough 1989).

10.4.5 Miocene samples: typical Basin and Range extension magmas in the Death Valley region

Typical for the Basin and Range crustal extension magmatism in the southwestern USA is a temporal shift from lithospheric mantle source magmas to asthenorpheric mantle source magmas. This signifies the change from compression tectonic setting to an extensional one, evident in thinning of the crust and upwelling of the asthenosphere. Such temporal shifts have been recorded across the Basin and Range province, including the Colorado River Through (Bradshaw et al. 1993), Lunar Crater Volcanic Field (Valentine and Perry 2007) and central Nevada (Farmer et al. 1989). The shift in magma composition from subduction character to a within plate character that implies asthenospheric source

is commonly linked to the arrival of the Mendocino Triple Junction (Putirka and Platt 2012). However, no clear change into asthenospheric source has been documented in the Basin and Range magmatism in the Death Valley region.

Lithospheric mantle character is demonstrated in the Ce/Y vs. Zr/Nb diagram (Figure 51) where the Ce/Y emphasizes the level of LILE enrichment and Zr/Nb the magnitude of the Nb anomaly. All samples of this study plot outside the typical OIB composition. The Miocene samples are most LILE enriched and the samples DVD-002 and DVD-006 have the largest Nb anomaly. As Ce is more incompatible in typical mantle phases relative to Y, the higher Ce/Y ratio also reflects smaller degree of melting. The arc-like character in the extension related magmas reflects a relatively thick and old lithospheric mantle beneath eastern California and southwestern Nevada that has preserved the composition of an undisturbed ancient subduction event and creating local heterogeneities enriched in incompatible elements in the lithospheric mantle (Fitton 1988, Farmer et al. 1989). The dated Miocene dike has a K-Ar age of 12.7 Ma and therefore represents early extension magmas in Death Valley where extension initiated 13 Ma ago (Fowler and Calzia 1999). The subduction character of the Miocene samples demonstrated on the Ce/Y vs. Zr/Nb diagram thus implies that these early Basin and Range magmas of Death Valley originated in lithospheric mantle rather than asthenospheric mantle.

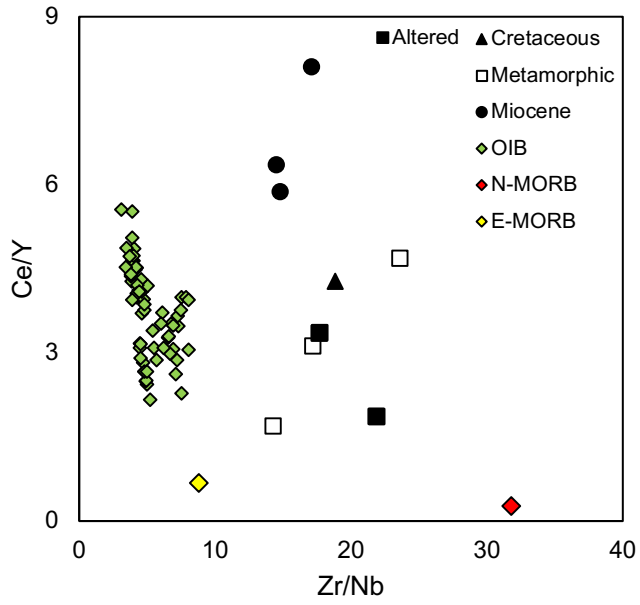

Figure 51. Samples plotted on Ce/Y vs. Zr/Nb diagram. The Miocene samples have highest Ce/Y (LILE enrichment). The magnitude of Nb anomaly (Zr/Nb) is largest for two metamorphic samples although the

values overlap through all samples. The average N-MORB, E-MORB and data from HIMU and EM1 type ocean island basalt are plotted for comparison. Data for average MORBs from Sun and McDonough 1989 and for OIBs from Willbold and Stracke 2006.

The negative Nb anomaly can also represent contamination of the dike margins by a crustal component. However, the possibility of crustal contamination modifying the geochemical character of Basin and Range magmatism has been evaluated in a number of studies by mainly Nd- and Sr-isotopic analysis with the conclusion that no major contamination of crustal component has been detected to affect their geochemical character (Fitton et al. 1988, Farmer et al. 1989).

10.5 Miocene magma chamber dynamics

The Miocene samples of this study represent the latest period of active magmatism and dike emplacement in southern Death Valley. Detailed petrogenetic information recorded in plagioclase growth zones can provide insight into magma chamber processes. By employing plagioclase phenocryst profiles major element and Sr isotopic composition, the following section provides insight into magma chamber dynamics during the Basin and Range crustal extension and coeval magmatism.

10.5.1 Origin of An mol.% zoning in plagioclase

The plagioclase An component partitions between the mineral and liquid relative to the Ab component, controlled by melt composition (X), magma temperature–pressure parameters (T, P), magma water pressure and oxygen fugacity (P_{H2O}, fO_2) and syn- to post-crystallization cation diffusion kinetics (Ginibre et al. 2002, Ustunisik et al. 2014).

The melt composition modifies the crystallizing plagioclase composition where the mineral An content is controlled by the available amount of Ca relative to Na as well as the amount of Al relative to Si. Higher Ca and Al content in melt increases the plagioclase An component (Panjasawatwong et al. 1995). Higher temperature melts crystallize more calcic plagioclase. Decrease of temperature in isobaric conditions will produce more sodic plagioclase and normal zoning, i.e. decrease in plagioclase anorthite content. Additionally, the increase of An content in isothermal conditions can be achieved by

decrease in total pressure or increase in water pressure (Ustunisik et al. 2014). However, the role of total pressure change in modifying the plagioclase anorthite content is small relative to the effect of P_{H2O}, T and melt composition (Ginibre et al. 2002, Lange et al. 2009). P_{H2O} affects the liquidus temperature in the isomorphic An-Ab system. Addition of water into melt decreases the melt liquidus temperature, resulting in more calcium-rich plagioclase (Ustunisk et al. 2014). Also, water dissolves in silicate melt as both molecular H_2O and hydroxyl groups (OH). The dissolved OH reacts more preferably with Na than Ca, thus ultimately reducing the activity of the plagioclase albite component $NaAlSi_3O_8$ in the melt and thereby the melt anorthite component $CaAl_2Si_2O_8$ is more available for the crystallizing minerals, ultimately producing more anorthite-rich plagioclase (Lange et al. 2009). Figure 52 shows the effect of temperature, pressure and water content on the plagioclase liquidus and solidus.

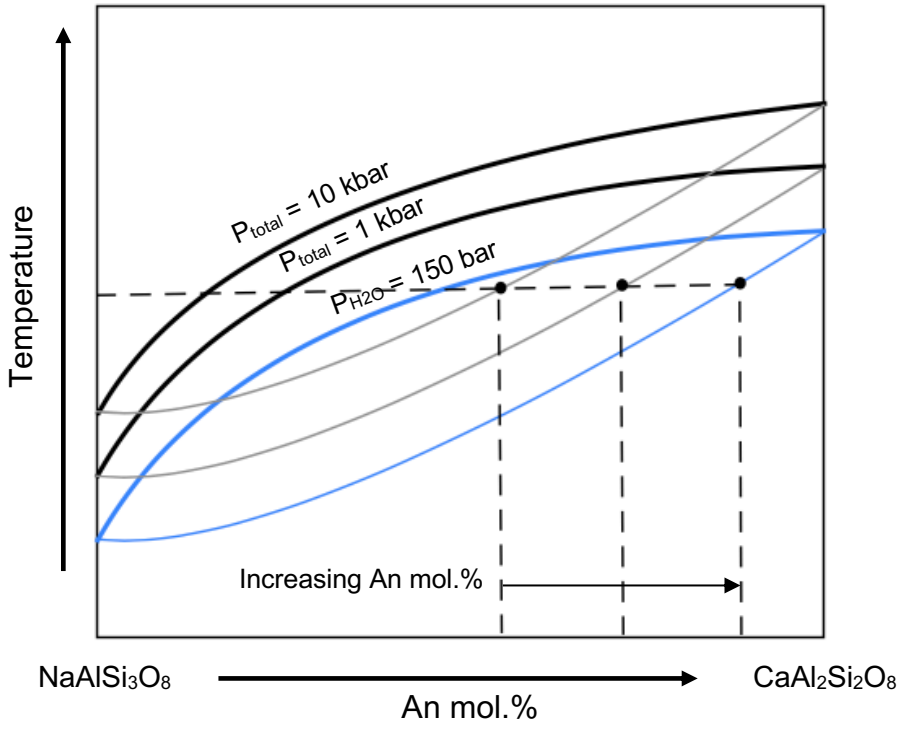

Figure 52. The effect of total pressure and water pressure on plagioclase anorthite content. Decrease in total pressure and increase in water pressure lowers the liquidus and solidus and results in higher An mol.%.

Oscillatory zoning in plagioclase can be generated by density-driven convection in magma chamber (closed-system) or magma recharge and mixing (open-system). Magma ascent by density-driven convection in isothermal conditions decreases pressure and the

melt dissolved water content, which in turn increases the calcic component in the crystallizing plagioclase. Magma descent in the convecting chamber generates pressure and melt dissolved water content increase, increasing the sodic component in the crystallizing plagioclase. Adiabatic decompression and increase in melt water content occur hand in hand, producing calcic plagioclase (Ustunisik et al. 2014). The pressure-directed compositional change in the crystallizing plagioclase generates small scale changes in An mol percent. Larger, >10 mol.% change in An is more likely to be caused by change in composition, temperature or water content of magma (Grove et al. 1984, Ginibre et al. 2002). Recharge by hotter and more primitive magma would increase the plagioclase An content by increasing temperature gradient as well as affecting the melt composition. Mixing of old (cooler and more evolved) and recharge (hotter and more primitive) magmas would decrease the temperature gradient and hybridize the magma bulk composition generating compositional variability in plagioclase.

All the analyzed plagioclase phenocrysts in the Miocene Ibex Hills samples show variation, albeit small, in the anorthite content across the crystal profiles reflecting changing magma chamber conditions. Distinguishing these small changes in An content in plagioclase zones created by pressure gradients from zones generated by open-system magma chamber with magma recharge and mixing requires analysis of trace element or FeO composition of plagioclase zones. The overall more anorthite rich plagioclase composition in the trachyandesite dike (An_{42-63}) DVD-009 (Figure 35) compared to the plagioclase of the trachyte stock DVD-007 (An_{27-48}) (Figure 34) indicates that these two samples were generated in compositionally different magmas.

10.5.2 Origin of Sr isotopic zoning in plagioclase

Chapter 10.4.5 concluded that the Miocene samples represent Basin and Range source magmas (i.e. lithospheric mantle) typically found in Death Valley. Whereas the anorthite content can be modified by a number of variables, $^{87}Sr/^{86}Sr$ ratios recorded in the plagioclase growth zones reflect the source $^{87}Sr/^{86}Sr$ ratios. Isotopes are thus powerful for analyzing source compositions. Lithospheric mantle magmas have more enriched Sr-isotopic composition (higher radiogenic $^{87}Sr/^{86}Sr$ ratio) compared to asthenospheric mantle magmas (Faure 2001). *In situ* laser ablation analysis from plagioclase core to rim profiles records changes in the crystallizing magma Sr-isotopic composition and can thus reveal changes in source magmas during the crystallization of plagioclase.

The Sr isotope composition of plagioclase is controlled by Sr isotopic composition of the crystallizing magma and by open-system processes that affect the Sr isotopic composition, such as assimilation of country-rock, magma chamber recharge or hybridization of two or more magmas of different isotopic composition. The changes are reflected in the crystallizing plagioclase through zones of varying $^{87}Sr/^{86}Sr$ ratios. As basement (cratonic) rocks typically have more radiogenic Sr isotopic composition than invading primitive magmas, zones with elevated $^{87}Sr/^{86}Sr$ ratios are usually a consequence of assimilation of country-rock whereas zones with low $^{87}Sr/^{86}Sr$ ratios originate from incorporation of new hotter and more primitive (less radiogenic) magma (Tepley et al. 2000, Davidson et al. 2001, Davidson et al. 2007, Andrews et al. 2008).

Diffusion re-equilibration can also modify the Sr isotope composition of phenocryst. At magmatic temperatures, diffusion will equilibrate the isotopic composition of the different mineral phases within the magma to some extent. However, as the mineral growth rate is usually larger than the diffusion rate, equilibrium will influence only few micron thick crystal rims. Studies on equilibration between mineral crystal and surrounding magma in volcanic rocks indicate that the effect of diffusion in equilibrating the isotope composition in minerals is minor (Davidson et al. 2007).

10.5.3 Decrease in $^{87}Sr/^{86}Sr$: magma replenishment

Both Miocene samples examined in this study for Sr isotopes (DVD-007 and DVD-009) show variation in $^{87}Sr/^{86}Sr$ ratios across the phenocryst profiles (Figures 40-42 and 44-46). The overall decrease in $^{87}Sr/^{86}Sr$ ratios from core to rim recorded in the plagioclase phenocryst profiles in the trachyte stock DVD-007 (mid-section average: 0.7076; rim average: 0.7073) (Figure 39) expresses a change in the melt composition and that the crystallizing magma encountered a less radiogenic contaminant during the crystallization of plagioclase. However, many of the analyzed phenocrysts with multiple analysis spots and all three phenocrysts analyzed with traverse mode analysis have oscillating Sr isotope profile across the phenocryst with oscillating $^{87}Sr/^{86}Sr$ ratios (Figures 40 and 42). This variation is best explained as a result of the crystallizing magma being in contact with contaminants with varying Sr isotopic composition – the repeatedly peaking Sr isotopic profiles of these phenocrysts cannot be accounted for by diffusion (Davidson et al. 2001). It is therefore proposed that the overall decreasing $^{87}Sr/^{86}Sr$ ratios

across the DVD-007 phenocrysts are the result of injection of new less radiogenic magma into the crystallizing chamber.

Similarly, the trachyandesite dike DVD-009 shows an overall decrease in $^{87}Sr/^{86}Sr$ ratios from the center to the margins of the examined plagioclase phenocrysts. These phenocrysts mostly lack the oscillatory zoning typical for sample DVD-007 phenocrysts – only one phenocryst, PLG 16 in DVD-009, shows more radiogenic Sr peaks on the phenocryst profile (Figure 44). The Sr isotopic profile for the non-oscillating phenocrysts is smooth and shows generally consistent $^{87}Sr/^{86}Sr$ ratios between the core and rim where the core $^{87}Sr/^{86}Sr$ ratios are typically >0.7080 and those in the phenocryst rims <0.7080 (Figure 45). This steady drop in Sr-isotopic composition towards the crustal edges suggests that the magma chamber was replenished by magma with less radiogenic composition prior to final ascent and emplacement of the magma.

10.5.4 Increase in $^{87}Sr/^{86}Sr$: assimilation of country rock

Potential for crustal assimilation is most prominently evident in phenocrysts PLG 1, PLG 3, PLG 10 and PLG 17 of the trachyte sample DVD-007 (Figures 40 and 42). These samples have radiogenic Sr peaks and intermittent lows, the latter reflecting periods of crystallization in less radiogenic magma. The $^{87}Sr/^{86}Sr$ ratios measured at the centermost analysis spots of the phenocrysts PLG 1 and PLG 3 are relatively low with $^{87}Sr/^{86}Sr$ increasing symmetrically from the center towards margins (Figure 40). This indicates that contamination of country rock occurred shortly after nucleation of the phenocryst from magma with lower $^{87}Sr/^{86}Sr$ ratios. Figure 53 shows division of isotope zones (I, II) identified by changing $^{87}Sr/^{86}Sr$ ratios across phenocrysts PLG 3 and PLG 17 in the trachyte sample DVD-007. Zone I represent decrease of $^{87}Sr/^{86}Sr$ ratios initiated by possible magma recharge and zone II represents a period of contamination of country rock. Red arrow points to a proposed nucleation composition. Alternatively, phenocrysts PLG 3 and PLG 17 in DVD-007 could be examples of plagioclase that nucleated in less radiogenic magma that was brought into the main magma chamber by a magma replenish and the phenocrysts continued to grow in a hybridized, more radiogenic magma.

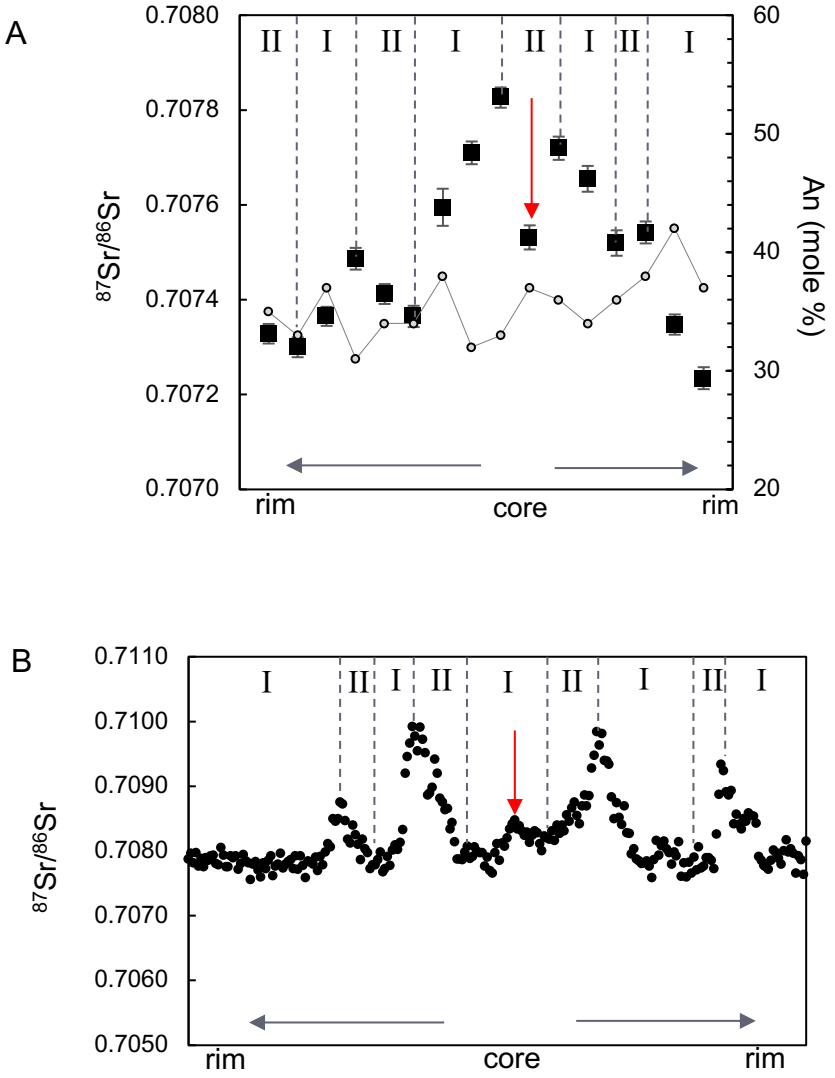

Figure 53. An example of representative zones recorded in the plagioclase $^{87}Sr/^{86}Sr$ profile on the phenocryst A) DVD-007 PLG 3 and B) DVD-007 PLG 17. Red arrow = nucleation; zone I = injection of less radiogenic magma and hybridization; zone II = assimilation of more radiogenic country rock. Both samples show oscillatory zoning and repeated episodes of magma replenish and assimilation.

The abnormally high peak in $^{87}Sr/^{86}Sr$ ratios recorded in one side of phenocryst PLG 1 in DVD-007, apparent in both spot mode and line traverse analysis (Figures 40 and 42), could result from a close contact with country-rock contaminant or magma with higher Sr isotopic composition, while the other side of the phenocryst crystallized in magma with slightly lower $^{87}Sr/^{86}Sr$ ratios.

Assimilation of more radiogenic contaminant is only suggested in phenocryst DVD-009 PLG 16 and possibly PLG 1 of sample DVD-009 (Figures 44 and 46). Phenocryst PLG 16 in DVD-009 has similar symmetrical Sr peaks towards the phenocryst rims as recorded in the trachyte stock, suggesting assimilation after nucleation in less radiogenic composition. The more radiogenic rims in phenocryst DVD-009 PLG 1 could be generated by assimilation.

10.5.5 Open-system magma chamber processes

The plagioclase phenocryst Sr isotopic profiles of both LA-MC-ICP-MS analyzed samples suggest that their magma chamber conditions have been unstable. The oscillatory zoning, as recorded in some of the phenocrysts especially in sample DVD-007, indicates repeated episodes of magma recharge and hybridization of old and new magmas typical of open-system magma chamber dynamics (Tepley et al. 2000, Davidson et al. 2001, Davidson et al. 2007, Andrews et al. 2008). It is suggested that the Sr isotopic zoning observed in the phenocrysts of sample DVD-007 show that the Ibex Hills magma chamber system was open and dynamic. Phenocryst textures support plagioclase having crystallized in an open-system magma chamber (Figure 54). Dissolution surfaces are typically created by change in composition or temperature of the crystallizing magma and indicate recharge of new hotter and/or compositionally different recharge into the magma chamber (Tepley et al. 2000, Andrews et al. 2008). Sieve texture or dissolution surfaces are visible in some of the plagioclase phenocrysts, especially in the trachyte stock DVD-007 (Figure 54). Although the phenocryst An component does not clearly correlate with the changing Sr-isotopic composition, the plagioclase anorthite composition does intermittently decrease with increasing $^{87}Sr/^{86}Sr$ ratios and vice versa. This is evident for example in phenocrysts PLG 3 and PLG 5 of DVD-007 (Figure 40).

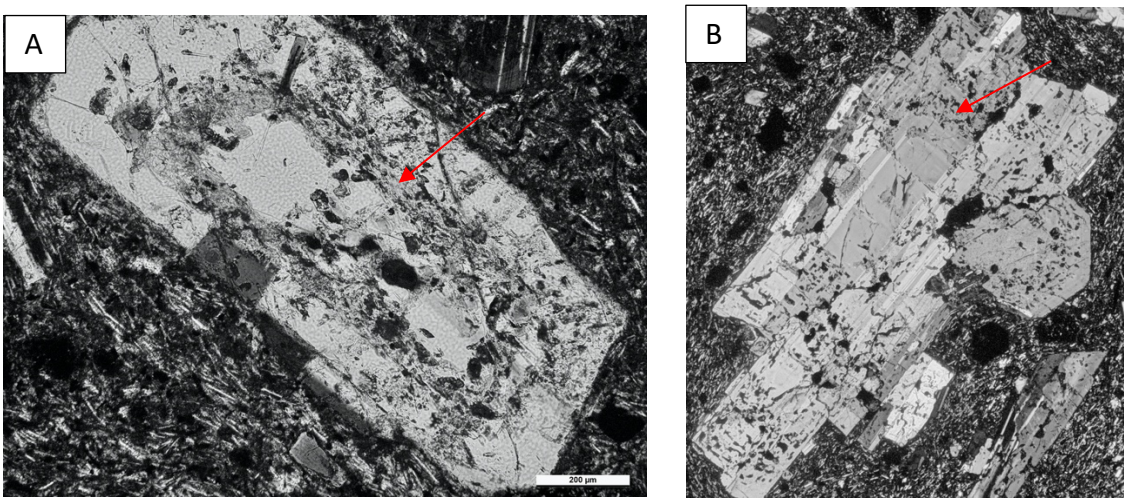

Figure 54. Photomicrographs (A, B) of plagioclase phenocrysts from trachyte stock DVD-007 showing dissolution patches with sieved or dissolved zones. Both phenocrysts have relatively clear core and rim. Red arrows point to the dissolution textures.

The decreasing anorthite content and increasing $^{87}Sr/^{86}Sr$ ratio imply incorporation of more radiogenic and compositionally evolved contaminant (such as another silicic magma or country-rock) followed by increasing anorthite content and decreasing $^{87}Sr/^{86}Sr$ ratios. The latter implies assimilation of less radiogenic and compositionally more mafic contaminant (such as injection of more primitive magma). However, as the magnitude of change in anorthite composition from one EPMA spot to the next is typically only a few mol.%, the change could be generated by pressure change in convecting magma or local temperature changes, i.e. new, hotter magma with less radiogenic Sr composition would also be able to generate more anorthite rich zones due to the higher temperature alone. As the change in anorthite composition coincides with the changing isotope composition (that cannot be modified by pressure or temperature alone), the first explanation is favored. The biggest change between the highest and lowest $^{87}Sr/^{86}Sr$ ratio within a single phenocryst was measured in the largest phenocrysts (Figure 40, Appendix 3). For example, in the ~5200 µm long phenocryst PLG 3 of DVD-007 the $^{87}Sr/^{86}Sr$ ratio in the core is 0.70783 and decreases to 0.70724 at the rim whereas the corresponding change between core and rim in the smaller ~800 µm long phenocryst PLG 8 of DVD-007 is from 0.70738 to 0.70733 (Figure 41). A longer magma residence time for the larger crystal allowed more time for interaction with the evolving magma than for the smaller, later nucleated phenocryst (Tepley et al. 2000).

The lack of oscillatory zoning in the majority of the plagioclase phenocrysts of the trachyandesite sample DVD-009 suggests more stable magma chamber conditions compared to sample DVD-007. However, the difference between core and rim Sr isotopic composition in all of the analyzed phenocrysts implies that sample DVD-009 also originates from an open-system magma chamber and that the phenocrysts analyzed reflect initial nucleation in a more radiogenic magma and subsequent growth in hybridized, less radiogenic magma. The anorthite content in the analyzed phenocrysts show very little, if any, change from one analysis spot to another. This implies (1) that the replenishing magma had similar anorthite content with the original magma or (2) that the difference in composition was small and the phenocryst growth took place in well-mixed magma. As with the trachyte sample DVD-007, the small-magnitude changes could also reflect local T-P-P_{H2O} changes in the magma chamber. Considering that the plagioclase in the trachyandesite sample DVD-009 is more radiogenic but more anorthite rich compared to the sample DVD-007, the more mafic composition could reflect magma with larger water content. Two phenocrysts, PLG 16 and PLG 1 of DVD-009, enclose further evidence for disruption to the crystallizing conditions: PLG 16 shows oscillatory zoning and PLG 1 is the only phenocryst with higher rim $^{87}Sr/^{86}Sr$ ratios relative to the core ratios (Figures 44 and 46). The mid-section $^{87}Sr/^{86}Sr$ ratios in phenocryst PLG 1 of DVD-009 are lower than any of the $^{87}Sr/^{86}Sr$ ratios measured in the rims of the rest of the phenocrysts of this sample. This suggests that it was brought into contact with the main magma at a later stage of the magma evolution, for example during the final ascent prior to emplacement in the crust.

A common feature for both the trachyte stock and trachyandesite dike is that, almost without exception, the rims of the plagioclase phenocrysts have lower $^{87}Sr/^{86}Sr$ ratios relative to the particular phenocryst mid-section. It is not atypical for an injection of hot magma into a magma chamber to trigger magma ascent and eruption (Tepley et al. 2000). Based on the plagioclase Sr isotopic profiles, the final ascent of these magmas could have taken place shortly after injection of new hotter and less radiogenic magma.

10.5.6 Magma sources

Figure 55 shows an illustrative representation of the dynamics of open-system magma chambers and possible source magmas for the Miocene trachyte and trachyandesite. The oscillating $^{87}Sr/^{86}Sr$ ratios across the phenocryst profiles in trachyte DVD-007 are

generated by repeated cycles of recharge of less radiogenic magma into main magma chamber with more radiogenic magma and hybridization of two magmas before the final ascent and emplacement in the shallow crust. The lack of oscillating $^{87}Sr/^{86}Sr$ ratios across the profiles but lower $^{87}Sr/^{86}Sr$ ratios at the rim in trachyandesite DVD-009 suggest a single recharge of magma with a larger mantle component, hybridization of initial more radiogenic and less radiogenic recharge, and rim crystallization in the hybridized magma prior to final magma ascent. Phenocryst PLG 1 in DVD-009 implies different evolution from the rest of the DVD-009 phenocrysts. It nucleated in less radiogenic magma, came into contact with more radiogenic magma during the growth of the crystal and ultimately joined the main magma body, possibly during ascent.

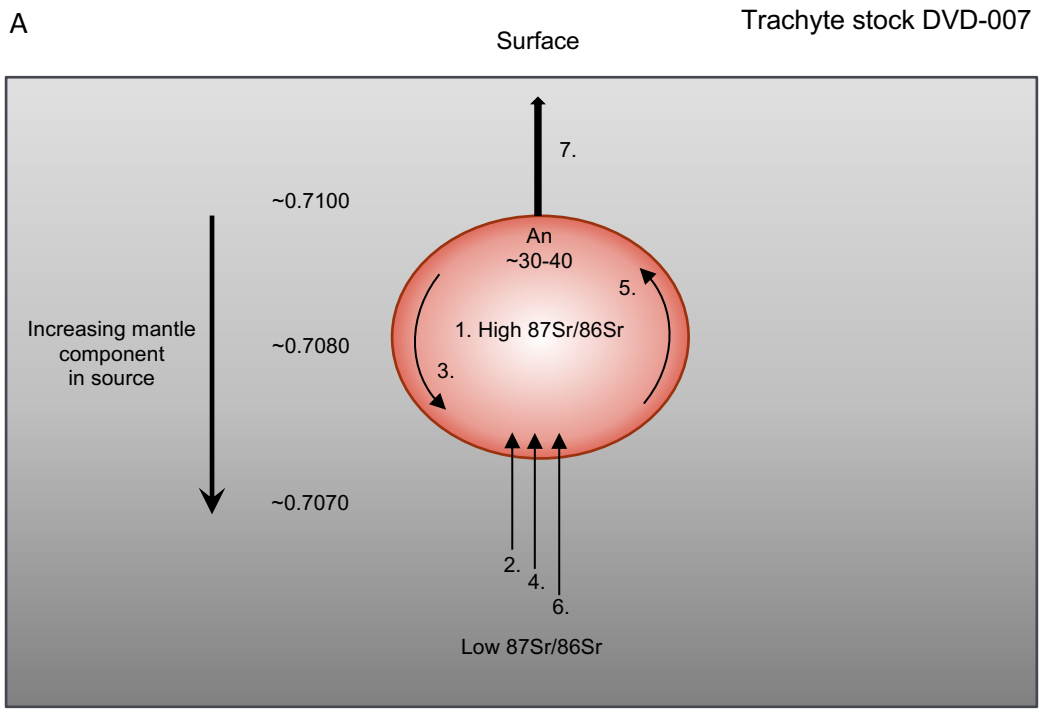

Figure 55 continues…

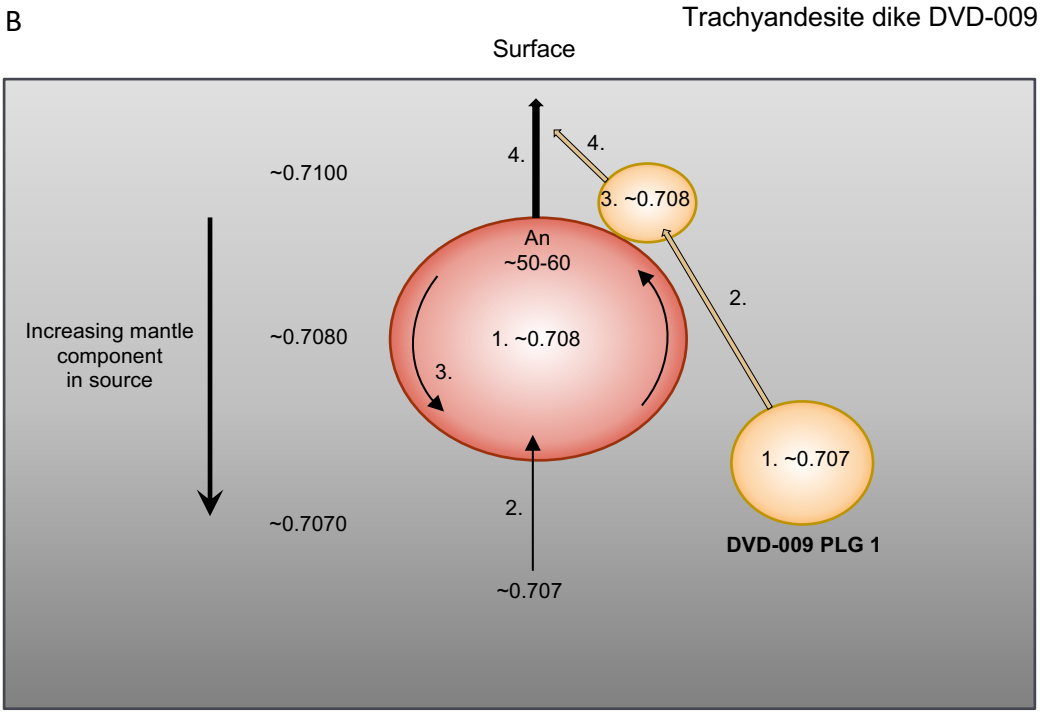

Figure 55. A schematic illustration of open-system magma chamber dynamics for typical plagioclase $^{87}Sr/^{86}Sr$ profiles of this study. A) DVD-007. 1: initial nucleation in higher $^{87}Sr/^{86}Sr$ magma; 2: replenish with less radiogenic magma; 3: hybridization of magmas, assimilation of country-rock; 4-6: repeat of 2 and 3; 7: final magma ascent shortly after 6. B) DVD-009. 1: nucleation in ~0.708 magma; 2: replenish with ~0.707 magma; 3: crystallization in hybridized magma; 4: magma ascent. DVD-009 PLG 1 with different evolution. 1: nucleation in ~0.707 magma; 2: contact with more radiogenic magma; 3: crystal growth in ~0.708 magma; 4: final ascent, possibly joining the ascent of the main magma.

10.5.7 Comparison with whole-rock Sr isotopic composition of Miocene felsic rocks of southern Death Valley

The *in situ* $^{87}Sr/^{86}Sr$ ratios of plagioclase phenocrysts of the studies samples compare with the whole-rock Sr isotopic composition of Miocene felsic rocks of similar age from southern Death Valley (Figure 56). The whole-rock $(^{87}Sr/^{86}Sr)_i$ of the Miocene felsic rocks is generally >0.7080, with few samples reaching just over 0.7100 and few straddle in the region of 0.7070 (Calzia and Rämö 2005). These ~0.7080 ratios are similar to the core *in situ* ratios measured in sample DVD-009. The lower end (~0.7070) and higher ratios (~0.7100) compare with the *in situ* ratios typical for sample DVD-007. Combining the Sr with Nd and Pb isotopic methods, Calzia and Rämö (2005) suggested lower crustal melts with a mantle component as the source for the Miocene felsic rocks of southern Death Valley. Following this analysis, it is suggested here that typical sample DVD-007 phenocrysts nucleated in melt with more mantle component in its composition compared

to initial nucleating magma of sample DVD-009. Phenocrysts of sample DVD-009 developed their rim Sr isotopic composition in magma with similar isotopic value to the average mid-section of the phenocrysts in sample DVD-007.

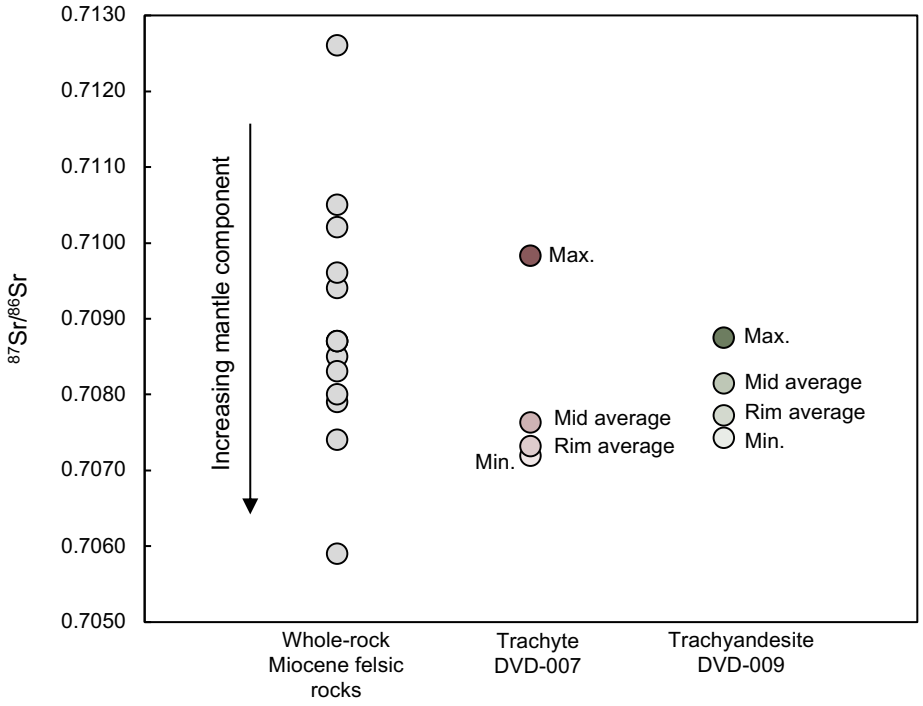

Figure 56. Comparison of whole-rock $(^{87}Sr/^{86}Sr)_i$ of Miocene felsic rocks of southern Death Valley region with maximum, minimum, average rim and average mid-section $^{87}Sr/^{86}Sr$ ratios measured with *in situ* LA-MC-ICP-MS spot-mode from trachyte DVD-007 and trachyandesite DVD-009 of this study. The maximum $^{87}Sr/^{86}Sr$ ratios were measured in the phenocryst mid-section in both samples. The minimum $^{87}Sr/^{86}Sr$ ratio in trachyte DVD-007 was measured in the phenocryst rim; the minimum $^{87}Sr/^{86}Sr$ ratio in trachyandesite DVD-009 was measured in the mid-section of phenocryst PLG 1. The whole-rock Miocene felsic $(^{87}Sr/^{86}Sr)_i$ ratios are from Calzia and Rämö (2005).

10.6 Multiple generations of dike emplacement in the southern Death Valley region

Based on the above discussion, it can be concluded (1) that the metadiabase sample DVD-003 is likely cogenetic with the 1.1 Ga Diabase and (2) that there has been at least two episodes of Phanerozoic dike emplacements in the southern Death Valley region. The Miocene samples represent typical Basin and Range magmatism coeval with crustal extension. The Cretaceous dike of Mojave Desert was emplaced during the Sevier orogeny and cuts the similarly aged Late Cretaceous Teutonia batholith that represents late Mesozoic arc magmatism. Compared to the Miocene samples the metamorphic and altered dikes are too altered to be of similar age and are thus inferred to represent one or

more episodes of pre-Miocene dike emplacement. The metamorphic samples DVD-002 and DVD-005 show some petrographic and geochemical similarities with the Cretaceous dike. Samples DVD-001 and DVD-006 show different style of alteration but bear some similarities in the trace element composition with the metamorphic dikes and the Cretaceous dike. Considering that the last period of metamorphism in Death Valley region was during the Sevier orogeny, the metamorphic overprint of these samples suggests that they are pre-Cenozoic. However, without appropriate geochronological analysis (e.g. U- Pb) the exact age of the metamorphic and altered samples, and whether they represent one or more magmatic events, remains unknown.

All the dikes considered in this study have a common NW-SE trend. Regional geology and the NW-SE strike of the Miocene dikes support the argument that the early Basin and Range extension in the Death Valley region was directed southwest, as suggested by the direction of Kingston Peak detachment fault. The Cretaceous dike of Mojave Desert is on trend with other Mesozoic dikes of southwestern USA, such as the Independence dike swarm and the dikes of White-Inyo Range (Coleman et al. 2000). According to Coleman et al. the temporal variety of dike injection from Jurassic to Cretaceous is unlikely to reflect regional stress imposed by the changing orientation of the subducting plate. Instead, the orientation of pre-existing fractures or continental margin might have directed the uniform trend of the dike emplacement spanning from Jurassic to Cretaceous. All in all, this uniform trend of dike emplacement from Jurassic to Miocene implies that the orientation of the maximum compressional stress (1σ) was NW-SE during generations of dike emplacement in the southern California. Jurassic to Cretaceous intrusions, roughly trending NW-SE from the southern Panamint Mountains through Avawatz Mountains to the northeastern Mojave Desert with a flank of the Cretaceous Teutonia batholith exhumated at the southern tip of Salt Spring Hills, are common in the southern Death Valley region (Figure 1). The metamorphic and altered dikes of Saddlepeak Hills and Salt Spring Hills, on trend with other Mesozoic dike emplacements of southwestern USA, are likely to represent dike injection coeval with Mesozoic arc magmatism.

11. CONCLUSIONS

1. The dikes of Saddlepeak Hills and Salt Spring Hills of southern Death Valley are pervasively altered. The secondary mineral assemblage can be divided into two groups. The secondary mineral overprint with chlorite, epidote and albite represents low-grade regional or contact metamorphism. White mica, quartz, K-feldspar and oxides of two Saddlepeak Hills and Salt Spring Hills dike samples DVD-001 and DVD-006 are typical for hydrothermally alteration or very low-grade or retrograde metamorphism.

2. The major elements in two southern Death Valley altered samples (DVD-001 and DVD-006) have been mobilized and these samples have large LOI. Similar trend was not detected in samples DVD-003, DVD-002 or DVD-005.

3. One mapped sample (DVD-003), that cuts the coarse-grained presumably 1.1 Ga diabase, shows geochemical and mineralogical similarities with the diabase and represents a sill, dike or chilled margin of a mafic body belonging to the 1.1 Ga diabase suite of southwestern USA.

4. All studied samples are LILE enriched and have negative Ta-Nb anomaly typical of magmas with a subduction source component signature.

5. The Miocene samples have enriched lithospheric mantle source character and are typical Basin and Range magmas of the Death Valley region.

6. The *in situ* $^{87}Sr/^{86}Sr$ ratios of the plagioclase phenocryst profiles in the Miocene samples compare with the bulk-rock $^{87}Sr/^{86}Sr$ composition of felsic Miocene intrusions of southern Death Valley. The magma chamber dynamics in the southern Death Valley during the Basin and Range extension were open-system processes with repeated cycles of recharge of less radiogenic magma and hybridization. The overall difference in the strontium isotopic compositions recorded in the two samples of this study reveal local heterogeneities in the source magmas.

7. The studied dikes represent at least two generations of NW-SE trending dike emplacement in the southern Death Valley region during the Phanerozoic, Miocene and

possibly Mesozoic. The metamorphic and altered dikes are on trend with the Jurassic Independence dike swarm and Cretaceous dikes of California that are coeval with magmatic intrusions of Mesozoic North American Cordilleran orogeny. The trend of the Miocene dikes indicates southwest directed extension during early Basin and Range extension in the southern Death Valley.

8. A thorough sampling of the dikes in the Saddlepeak Hills and Salt Spring Hills would probably reveal whether they represent the older generation of dikes or whether there are Miocene dikes present. A study of metamorphic conditions in the southern Death Valley would further benefit from X-Ray diffraction (XRD) and EPMA analysis of the metamorphic samples and their minerals.

12. ACKNOWLEDGEMENTS

I would like to thank my supervisors Dr. James Calzia (USGS) and Dr. Tapani Rämö (University of Helsinki) for providing me with the opportunity to work on this subject. Special thanks to James Calzia for guidance during the April 2019 field campaign, crash course in Death Valley geology and date shakes, and for Tapani Rämö for tireless help and comments throughout the whole process. I am grateful for Dr. Yann Lahaye for instructions and help with LA-MC-ICP-MS analysis at the GTK, Dr. Radoslaw Michallik for sample preparation and microprobe guidance at the University of Helsinki, and Pasi Heikkilä (GTK) for comments on the EPMA data.

13. REFERENCES

Anderson, J.L., Wooden, J.L. and Bender, E.E. 1993. Mojave Province of southern California and vicinity in Van Schmus, W.R. and Bickford, M.E. (eds.) Transcontinental Proterozoic Provinces. Geological Society of America, 176-188.

Ague, J.J. 2017. Element mobility during regional metamorphism in crustal and subduction zone environments with a focus on the rare earth elements (REE). American Mineralogist 102, 1796-1821.

Aguirre, L. and Atherton, M.P. 1987. Low-grade metamorphism and geotectonic setting of the Macuchi Formation, Western Cordillera of Ecuador. Journal of Metamorphic Geology 5, 473-494.

Aguirre, L. & Offler, R. 1985. Burial metamorphism in the Western Peruvian Trough: its relation to Andean magmatism and tectonics. In: Pitcher, W.S., Atherton, M.P., Cobbing, E.J. and

Beckinsale, R.D. (eds.) Magmatism at a Plate Edge, The Peruvian Andes. Blackie & Son, Glasgow, pp. 59-71.

Andrews, B.J., Gardner, J.E. and Housh, T.B. 2008. Repeated recharge, assimilation, and hybridization in magmas erupted from El Chichón as recorded by plagioclase and amphibole phenocrysts. Journal of Volcanology and Geothermal Research 175, 415-426.

Apted, M.J. and Liou, J.G. 1983. Phase relations among greenschist, epidote-amphibolite, and amphibolite in a basaltic system. American Journal of Science 283-A, 328-354.

Barth, A.P., Wooden, J.L., Coleman, D.S. and Vogel, M.B. 2009. Assembling and disassembling California: A zircon and monazite geochronologic framework for Proterozoic crustal evolution in southern California. Journal of Geology 117, 221-239.

Bastias, J., Fuentes, F., Aguirre, L., Hervé, F., Demant, A., Deckart, K. and Torres, T. 2016. Very low-grade secondary minerals as indicators of palaeo-hydrothermal systems in the Upper Cretaceous volcanic succession of Hannah Point, Livingston Island, Antarctica. Applied Clay Science 134, 246-256.

Beckerman, G.M., Robinson, J.P. and Anderson, J.L. 1982. The Teutonia batholith: A large intrusive complex of Jurassic and Cretaceous age in the eastern Mojave Desert, California in Frost E.G. and Martin D.L. eds., Mesozoic-Cenozoic Tectonic Evolution of the Colorado River Region, California, Arizona, and Nevada. San Diego, California, Cordilleran Publishers, 205-221.

Bennet, V.C. and DePaolo, D.J. 1987. Proterozoic crustal history of the western United States as determined by neodymium isotopic mapping. Geological Society of America Bulletin 99, 674-685.

Bevins, R.E., Rowbotham, G. and Robinson, D. 1991. Zeolite to prehnite-pumpellyite facies metamorphism of the late Proterozoic Zig-Zag Dal Basalt Formation, eastern North Greenland. Lithos 27, 155-165.

Bidgoli, T.S., Amir, E., Walker, J.D., Stockli, D.F., Andrew, J.E., & Caskey, S.J. 2015. Low-temperature thermochronology of the black and Panamint Mountains, Death Valley, California: Implications for geodynamic controls on Cenozoic intraplate strain. Lithosphere 7, 473-480.

Bird, D.K., Schiffman, P., Elders, W.A., Williams, A.E. and McDowell, S.D. 1984. Calc-silicate mineralization in active geothermal systems. Economic Geology 79, 671-695.

Boynton, W.V. 1984 Geochemistry of rare earth elements: Meteorite studies. In: Henderson, P., (ed.) Rare Earth Element Geochemistry, Elsevier, New York, 63-114.

Bradshaw, T.K., Hawkesworth, C.J. and Gallagher, K. 1993. Basaltic volcanism in the Southern Basin and Range: no role for a mantle plume. Earth and Planetary Science Letters 116, 45-62.

Calzia, J.P. and Rämö, O.T. 2000. Late Cenozoic crustal extension and magmatism, southern Death Valley region, California. In: Lageron, D.R., Peters, S.G. and Lahren, M.M. (eds.) Great Basin and Sierra Nevada: Boulder, Colorado. Geological Society of America Field Guide 2, 135-164.

Calzia, J.P. and Rämö, O.T. 2005. Miocene rapakivi granites in the southern Death Valley region, California, USA. Earth-Science Reviews 73, 221-243.

Carl, B.S. and Glazner, A.F. 2002. Extent and significance of the Independence dike swarm, eastern California. In: Glazner, A.F., Walker, J.D. and Bartley, J.M. (eds.) Geologic Evolution of the Mojave Desert and Southwestern Basin and Range: Boulder, Colorado, Geological Society of America Memoir 195, 117-130.

Chen, J.H. and Moore, J.G. 1979. Late Jurassic Independence dike swarm in eastern California. Geology 7, 129-133.

Christidis, G. 1998. Comparative study of the mobility of major and trace elements during alteration of an andesite and a rhyolite to bentonite, in the islands of Milos and Kimolos, Aegean, Greece. Clays and Clay Minerals 46, 379–99.

Coleman, D.S., Carl, B.S., Glazner, A.F. and Bartley, J.M. 2000. Cretaceous dikes within the Jurassic Independence dike swarm in eastern California. Geological Society of America Bulletin 112, 504-511.

Condie, K.C. 1992. Proterozoic terranes and continental accretion in southwestern North America in Condie, K.C., ed., Proterozoic Crustal Evolution. Elsevier, Amsterdam, 447-480.

Corsetti, F.A. and Kaufman, A.J. 2005. The relationship between the Neoproterozoic Noonday Dolomite and the Ibex Formation: New observations and their bearing on 'snowball Earth'. Earth-Science Reviews 73, 63-78.

Davidson, J.P., Morgan, D.J., Charlier, B.L.A., Harlou, R. and Hora, J.M. 2007. Microsampling and isotopic analysis of igneous rocks: Implications for the study of magmatic systems. Annual Review of Earth and Planetary Sciences 35, 273-311.

Davidson, J., Tepley, F.J., Palacz, Z. and Meffan-Main, S., 2001. Magma recharge, contamination and residence times revealed by in situ laser ablation isotopic analysis of feldspar in volcanic rocks. Earth and Planetary Science Letters 184, 427-442.

DeCelles, P.G. 2004. Late Jurassic to Eocene evolution of the Cordilleran thrust belt and foreland basin system, western U.S.A. American Journal of Science 304, 105-168.

DeCelles, P.G. and Graham, S.A. 2015. Cyclical processes in the North American Cordilleran orogenic system. Geology 43, 499-502.

DeWitt, E., Armstrong, R.L., Sutter, J.F. and Zartman, R.E. 1984. U-Th-Pb, Rb-Sr, and Ar-Ar mineral and whole-rock isotopic systematics in a metamorphosed granitic terrane, southeastern California. Geological Society of America Bulletin 95, 723-739.

Dickinson, W.R. 2004. Evolution of the North American Cordillera. Annual Review of Earth and Planetary Sciences 32, 13-45.

Dokka, R.K. and Travis, C.J. 1990. Role of the Eastern California Shear Zone in accommodating Pacific-North American plate motion. Geophysical Research Letters 17, 1323-1326.

El Korh, A., Schmidt, S., Ulianov, A. and Potel, S. 2009. Trace element partitioning in HP-LT metamorphic assemblages during subduction-related metamorphism, Ile de Groix, France: A detailed LA-ICPMS study. Journal of Petrology 50, 1107-1148.

Ernst, R. E., Grosfils, E. B. and Mége, D. 2001. Giant dike swarms: earth, Venus, and Mars. Annual Review of Earth and Planetary Sciences 29, 489-534.

Ernst, W. G. 1997. Metamorphism of mafic dikes from the central White-Inyo Range, eastern California. Contributions to Mineral Petrology 128, 30-44.

Farmer, G.L., Perry, F.V., Semken, S., Crowe, B., Curtis, D. and DePaolo, D.J. 1989. Isotopic evidence on the structure and origin of subcontinental lithospheric mantle in Southern Nevada. Journal of Geophysical Research 94, 7885-7898.

Faure, G. 2001. Origin of igneous rocks: the isotopic evidence. Springer, Berlin, 494 p.

Fitton, J.G., James, D., Kempton, P.D., Ormerod, D.S. and Leeman, W.P. 1988. The role of lithospheric mantle in the generation of the late Cenozoic basic magmas in the Western United States. Journal of Petrology, Special Litosphere Issue, 331-349.

Fleming, Z.D. 2018. Geometry, timing, and kinematics of Neogene extensional and transtensional structures of southern Death Valley: Implications for regional reconstruction and a corrective method for rigid body rotations. PhD Dissertation. University of Texas at El Paso.

Fowler, T.K. and Calzia, J.P. 1999. Kingston Range detachment fault, southwestern Death Valley region, California: Relation to Tertiary deposits and reconstruction of initial dip. Geological Society of America Special Paper 333, 245-257.

Gans, P. B. and Gentry, B. J. 2016. Dike emplacement, footwall rotation, and the transition from magmatic to tectonic extension in the Whipple Mountains metamorphic core complex, southeastern California. Tectonics 35, 2564-2608.

Giletti, B.J. and Casserly, J.E.D. 1994. Strontium diffusion kinetics in plagioclase feldspar. Geochimica et Cosmochimica Acta 58, 3785-3793.

Gill, J.B. 1981. Orogenic Andesites and Plate Tectonics. Springer-Verlag, Heidelberg, 390p.

Ginibre, C., Wörner, G. and Kronz A. 2002. Minor- and trace-element zoning in plagioclase: implications for magma chamber processes at Parinacota volcano, northern Chile. Contributions to Mineral Petrology 143, 300-315.

Glazner, A.F., Walker, J.D., Bartley, J.M. and Fletcher, J.M. 2002. Cenozoic evolution of the Mojave block of southern California. in Glazner, A.F., Walker, J.D., and Bartley, J.M., eds., Geologic Evolution of the Mojave Desert and Southwestern Basin and Range: Boulder, Colorado, Geological Society of America Memoir 195, 19-41.

Grove, T.L., Baker, M.B. and Kinzler R.L. 1984. Coupled CaAl-NaSi diffusion in plagioclase feldspar: experiments and applications to cooling rate speedometry. Geochimica et Cosmochimica Acta 48, 2113-2121.

Guest, B., Pavlis, T.L., Golding, H. and Serpa, L. 2003. Chasing the Garlock: A study of tectonic response to vertical axis rotation. Geology 31, 553-556.

Hammond, J. 1983. Late Precambrian diabase intrusions in the southern Death Valley region, California: Their petrology, geochemistry, and tectonic significance. PhD Dissertation. University of southern California.

Heaman, L.M and Grotzinger. J.P. 1992. 1.08 diabase sills in the Pahrump Group, California: Implications for development of the Cordilleran miogeocline. Geology 20, 637-640.

Hodges, K. V. and Walker, J. D. 1992. Extension in the Cretaceous Sevier orogen, North American Cordillera. Geological Society of America Bulletin 104, 560-569.

Hoisch, T., Wells, M., Beyene, M., Styger, S. and Vervoort, J. 2014. Jurassic Barrovian metamorphism in a western U.S. Cordilleran metamorphic core complex, Funeral Mountains, California. Geology 42, 399-402.

Hopson, R. F., Hillhouse, J. W. and Howard, K. A. 2008. Dike orientation in the vertical Late Jurassic Independence dike swarm and implications for vertical-axis tectonic rotations in eastern California. The Geological Society of America Special Paper 438, 481-498.

Hou, G. 2012. Mechanism for three types of mafic dyke swarms. Geoscience Frontiers 3, 217-223.

Hou, G., Kusky, T. M., Wang, C. and Wang, Y. 2010. Mechanics of the giant radiating Mackenzie dyke swarm: A paleostress field modeling. Journal of Geophysical Research 115.

Irvine, T.N. and Baragar, W.R.A. 1971. A Guide to the Chemical Classification of the Common Volcanic Rocks. Canadian Journal of Earth Science 8, 523-548.

Jenner, F.E., Bennett, V.C., Nutman, A.p., Friend, C.R., Norman, M.D. and Yaxley, G. 2009. Evidence for subduction at 3.8 Ga: Geochemistry of arc-like metabasalts from the southern edge of the Isua Supracrustal Belt. Chemical Geology 261, 83-98.

Knott, J.R., Sarna-Wojcicki, A.M., Mechette, M.N. and Kilnger, R.E. 2005. Upper Neogene stratigraphy and tectonics of Death Valley – a review. Earth-Science Reviews 73, 245-270.

Kousehlar, M., Weisenberger, T.B., Tutti, F. and Mirnejad, H. 2012. Fluid control on low-temperature mineral formation in volcanic rocks of Kahrizak, Iran. Geofluids 12, 295-311.

Kristmannsdottir, H. 1979. Alteration of basaltic rocks by hydrothermal activity at 100-300 °C. Developments in Sedimentology 27, 359-367.

Lange R.A., Frey, H.M. and Hector, J. 2009 A thermodynamic model for the plagioclase-liquid hygrometer/thermometer. American Mineralogist 94, 494-506.

Le Bas, M.J., Le Maitre, R.W., Streckeisen, A. and Zanettin, B. 1986. A chemical classification of volcanic rocks based on the total alkali-silica diagram. Journal of Petrology 27, 745-750.

Lee, C., Yin, Q., Rudnick, R. and Jacobsen. S. 2001. Preservation of ancient and fertile lithospheric mantle beneath the southwestern United States. Nature 144, 69-73.

Lima, R.D., Prior, M.G., Stockli, D.F. and Hayman, N.W. 2018. Protracted heating of the orogenic crust in Death Valley, California, USA. Geology 46, 315-318.

Long, S.P. and Soignard, E. 2016. Shallow-crustal metamorphism during Late Cretaceous anatexis in the Sevier hinterland plateau: Peak temperature conditions from the Grant Range, eastern Nevada, U.S.A. Lithosphere 8, 150-164.

Luffi, P., Saleeby, J.B., Lee, C.A. and Ducea, M.N. 2009. Lithospheric mantle duplex beneath the central Mojave Desert revealed by xenoliths from Dish Hill, California. Journal of Geophysical Research 114, B03202.

Marieni, Chiara, Voigt, M. J and Oelkers, E.H. 2021. Experimental study of epidote dissolution rates from pH 2 to 11 and temperatures from 25 to 200 °C. Geochimica et Cosmochimica Acta 294, 70-88.

Martin, M.W. and Walker, J.D. 1992. Extending the western North American Proterozoic and Paleozoic continental crust through the Mojave Desert. Geology 20, 753-756.

Massey, N. W. D. 1983. Magma genesis in a late Proterozoic proto-oceanic rift: REE and other trace-element data from the Keweenawan Mamainse Point Formation, Ontario, Canada. Precambrian Research 21, 81-100.

Mathieu, L. 2018. Quantifying hydrothermal alteration: A review of methods. Geosciences 8.

Mattinson, C., Colgan, J., Metcalf, J., Miller, E. and Wooden, J. 2007. Late Cretaceous to Paleocene metamorphism and magmatism in the Funeral Mountains metamorphic core complex, Death Valley, California. GSA Special paper 419, 205-223.

Miller, J.S. and Miller, C.F. 1991. Tertiary extension-related volcanism, Old Woman Mountains area, eastern Mojave Desert, California. Journal of Geophysical Research 96, 13 629-13 643.

Miller, J.S., Glazner, A.F., Farmer, G.L., Suayah, I.B. and Keith, L.A. 2000. A Sr, Nd, and Pb isotopic study of mantle domains and crustal structure from Miocene volcanic in the Mojave Desert, California. Geological Society of America Bulletin 112, 1264-1279.

Miller, M.B. and Pavlis, T.L. 2005. The Black Mountains turtlebacks: Rosetta stones of Death Valley tectonics. Earth Science Reviews 73, 115-138.

Miller, M.G. and Prave, A.R. 2002. Rolling hinge or fixed basin?: A test of continental extensional models in Death Valley, California, United States: Geology 30, 847-850.

Müller, W., Shelley, M., Miller, P. and Broude, S. 2009. Initial performance metrics of a new custom-designed ArF excimer LA-ICPMS system coupled to a two-volume laser-ablation cell. Journal of Analytical Atomic Spectrometry 24, 209-214.

Münker, C., Wörner, G., Yogodzinski, G. and Churikova, T. 2004. Behaviour of high field strength elements in subduction zones: Constraints from Kamchatka-Auletia arc lavas. Earth and Planetary Science Letters 224, 275-293.

Neuhoff, P.S., Fridriksson, T., Arnórsson, S. and Bird. D.K. 1999. Porosity evolution and mineral paragenesis during low-grade metamorphism of basaltic lavas at Teigarhorn, eastern Iceland. American Journal of Science 299, 467-501.

Nielson, J.E. and Beratan, K.K. 1995. Stratigraphic and structural synthesis of a Miocene extensional terrane, southeast California and west-central Arizona. Geological Society of America Bulletin 107, 241-252.

Nogami, K. and Yoshida, M. 1995. Leaching rates of rock-forming components through acidic alteration. Journal of Volcanology and Geothermal Research 65, 41-49.

Nyström, J.O. 1983. Pumpellyite-bearing rocks in central Sweden and extent of host rock alteration as a control of pumpellyite composition. Contributions to Mineralogy and Petrology 83, 159-168.

Panjasawatwong, Y., Danyushevsky, L.V., Crawford, A.J. and Harris, K.L. 1995. An experimental study of the effects of melt composition on plagioclase – melt equilibria at 5 and 10 kbar: implications for the origin of magmatic high-An plagioclase. Contributions to Mineral Petrology 118, 420-432.

Pavlis, T.L., Rutkofske, J., Guerrero, F. and Serpa, L.F. 2014. Structural overprinting of Mesozoic thrust systems in eastern California and its importance to reconstruction of Neogene extension in the southern Basin and Range. Geosphere 10, 732-756.

Pearce, J.A. 1983. Role of the sub-continental lithosphere in magma genesis at active continental margins. In: Hawkesworth, C.J. and Norry, M.J. (eds.) Conlinenta1 Basalts and Mantle Xenoliths, Nantwich, 230-249.

Pearce, J.A. 1996. A user's guide to basalt discrimination diagrams. In Wyman, D.A. (ed.) Trace Element Geochemistry of Volcanic Rocks: Applications for Massive Sulphide Exploration. Geological Association of Canada, Short Course Notes 12, 79-113.

Pearce, J.A. and Norry, M.J. 1979. Petrogenetic implications of Ti, Zr, Y, and Nb variations in volcanic rocks. Contributions to Mineral Petrology 69, 33-47.

Pearce, J.A. and Peate, D.W. 1995. Tectonic implications of the composition of volcanic arc magmas. Annual Review of earth and Planetary Sciences 23, 251-285.

Pearce, J.A., Stern, R.J. 2006. The origin of back-arc basin magmas: trace element and isotope perspectives. In: Christie, D.M., Fisher, C.R., Lee, S.-M., Givens, S. (eds.), Back-arc Spreading Systems: Geological, Biological, Chemical and Physical Interactions: American Geophysical Union Geophysical Monograph, 166, pp. 63–86.

Peter Hooper GeoAnalytical Lab Technical notes. Site visited 03.08.2020. https://environment.wsu.edu/facilities/geoanalytical-lab/technical-notes/.

Pouchou, J.L. and Pichoir, F. 1984. A new model for quantitative X-ray microanalysis. Recherce Aerospatiale 3, 167-192.

Putirka, K. and Platt, B. 2012. Basin and Range volcanism as a passive response to extensional tectonics. Geosphere 8, 1274-1285.

Rämö, O.T. and Calzia, J.P. 1998. Nd isotopic composition of cratonic rocks in the southern Death Valley region: Evidence for a substantial Archean source component in Mojavia. Geology 26, 891-894.

Rämö, O.T., Calzia J.P. and Kosunen, P.J. 2002. Geochemistry of Mesozoic plutons, southern Death Valley region, California: Insight into the origin of Cordilleran interior magmatism. Contributions to Mineral Petrology 143, 416-437.

Ramos, F.C., Wolff, J.A. and Tollstrup, D.L. 2004 Measuring $^{87}Sr/^{86}Sr$ variations in minerals and groundmass from basalts using LA-MC-ICPMS. Chemical Geology 211, 135-158.

Rankenburg, K., Lassiter, J.C. and Brey, G. 2004. Origin of megacrysts in volcanic rocks of the Cameroon volcanic chain - constraints on magma genesis and crustal contamination. Contribution to Mineralogy and Petrology 147, 129-144.

Schiffman, P. 1995. Low grade metamorphism of mafic rocks. Reviews of Geophysics 33, 81-86.

Schmidt, S. 1993. Regional and local patterns of low-grade metamorphism in the North Shore Volcanic Group, Minnesota, USA. Journal of Metamorphic Geology 11, 401-414.

Serpa, L. and Pavlis, T. 1996. Three-dimensional model of the late Cenozoic history of the Death Valley region, southeastern Califonia. Tectonics 15, 1113-1128.

Snow, J.K. and Wernicke, B.P. 2000. Cenozoic tectonism in the central Basin and Range: magnitude, rate, and distribution of upper crustal strain. American Journal of Science 300, 659- 719.

Starr, P. and Pattison, D. 2019. Metamorphic devolatization of basalts acrossthe greenschist-amphibole facies transition zone: Insights from isograd mapping, petrography and thermodynamic modelling. Lithos 342-343, 295-314.

Stewart, J.H. 1970. Upper Precambrian and lower Cambrian strata in the southern Great Basin California and Nevada. Geological Survey Special Paper 620, 1-206.

Sun, W. and McDonough W.F. 1989. Chemical and isotopic systematics of oceanic basalts: Implications for mantle composition and processes. Geological Society, London, Special Publications 42, 313-345.

Tepley, F.J., Davidson, J., Tilling, R.I. and Arth, J.G., 2000. Magma mixing, recharge and eruptive histories recorded in plagioclase phenocrysts from El Chichón Volcano, Mexico. Journal of Petrology 41, 1397-1411.

Thirlwall, M.F. 1991. Long-term reproducibility of multicollector Sr and Nd isotope ratio analysis. Chemical Geology 94, 85-104.

Topping, D.J. 1993. Paleogeographic reconstruction of the Death Valley extended region: Evidence from Miocene large rock-avalanche deposits in the Amargosa Chaos Basin, California. Geological Society of America Bulletin 105, 1190-1213.

Troxel, B.W. and Calzia, J.P. 1994. Geology of the middle Miocene Ibex Pass volcanic field, southern Death Valley, California. Geological Society of America Abstracts with Program 26, 99.

Troxel, B.W., Calzia, J.P. and Pavlis, T.L. 1992. Southwest directed extensional features and related magmatism, southern Death Valley region and Kingston Range. Geological Society of America Abstracts with Program 24, 87.

USGS Contract Chemistry Method Summaries. Site visited 01.06.2020. https://www.usgs.gov/media/files/contract-chemistry-method-summaries.

Ustunisik, G., Kilinc, A. and Nielsen, R.L. 2014. New insights into the processes controlling compositional zoning in plagioclase. Lithos 200-201, 80-93.

Valentine, G.A. and Perry, F.V. 2007. Tectonically controlled, time-predictable basaltic volcanism from a lithospheric mantle source (central Basin and Range Province, USA). Earth and Planetary Science Letters 261, 201-216.

Vandyk, T., Le Heron, D., Chew, D., Amato, J., Thirlwall, M., Dehler, C., Hennig, J., Castonguay, S., Knott, T., Tofaif, S., Ali, D., Manning, C., Busfield, M., Doepke, D. and Grassineau, N. 2018. Precambrian olistoliths masquerading as sills from Death Valley, California. Journal of the Geological Society.

Walker, J.D., Martin, M.W. and Glazner, A.F. 2002. Late Paleozoic to Mesozoic development of the Mojave Desert and environs, California in Glazner, A.F., Walker, J.D., and Bartley, J.M., eds., Geologic Evolution of the Mojave Desert and Southwestern Basin and Range: Boulder, Colorado, Geological Society of America Memoir 195, 1-18.

Wells, M. L. and Hoisch, T. D. 2008. The role of mantle delamination in widespread Late Cretaceous extension and magmatism in the Cordilleran orogen, western United States. Geological Society of America Bulletin 120, 515-530.

Willbold, M. and Stracke, A. 2006. Trace element composition of mantle end-members: Implications for recycling of oceanic and upper and lower continental crust. Geochemistry, Geophysics, Geosystems 7.

Wilshire, H.G., Bedford, D.R. and Coleman, T. 2002. Digital Version of Open-File Report 92-183: Geologic Map of the Granite Spring Quadrangle, San Bernardino county, California. U.S. geological Survey Open-File Report 02-273, 27 pp.

Winchester, J.A. and Floyd, P.A. 1977. Geochemical discrimination of different magma series and their differentiation products using immobile elements. Chemical Geology 20, 325-343.

Wolf, M.B. and Saleeby, J.B. 1992. Jurassic Cordilleran dike swarm-shear zones: Implications for the Nevadan orogeny and North American plate motion. Geology 20, 745-748.

Wooden, J.L. and Miller, D.M. 1990. Chronologic and isotopic framework for early Proterozoic crustal evolution in the eastern Mojave Desert region, SE California. Journal of Geophysical Research 95, 20133-20146.

Wooden, J.L., Barth, A.P. and Mueller, P.A. 2012. Crustal growth and tectonic evolution of the Mojave crustal province: Insights from hafnium isotope systematics in zircons. Lithosphere 5, 17-28.

Appendix 1. Whole-rock geochemical analysis data.

Sample ID	365[1]	DVD-001[1]	DVD-002[2]	DVD-003[2]	DVD-005[1]	DVD-006[2]	DVD-007[1]	DVD-009[2]	DVD-010[2]
Rock type	Trachyandesite	Meta-andesite	Meta-andesite	Metabasaltic	Meta-andesite	Meta-andesite	Trachyte	Trachyandesite	Trachyandesite
Latitude	35°19'11.8"	35°42'22.7"	35°43'37.0"	35°43'40.6"	35°40'16.6"	35°39'44.0"	35°46'11.0"	35°46'09.9"	35°46'10.3"
Longitude	115°51'29.9"	116°20'15.0"	116°22'17.7"	116°22'19.5"	116°16'18.6"	116°16'13.0"	116°24'49.8"	116°24'56.4"	116°25'03.3"
SiO_2 wt.%	55.30	57.60	58.52	46.72	60.3	55.86	60.7	57.70	53.03
TiO_2	0.90	0.76	1.020	3.929	0.61	0.70	0.67	0.83	0.84
Al_2O_3	16.40	18.20	17.87	14.39	16.4	19.09	16.9	16.25	15.65
FeO*	5.61	7.53	5.99	15.99	5.64	7.11	4.34	5.08	5.45
MnO	0.12	0.23	0.073	0.222	0.11	0.23	0.08	0.08	0.12
MgO	4.54	1.61	2.31	5.16	2.88	1.74	1.89	2.27	1.34
CaO	5.71	1.80	4.99	6.33	4.86	2.33	3.82	5.34	8.95
Na_2O	3.80	<0.01	4.87	2.30	2.66	0.32	4.53	4.08	4.04
K_2O	3.25	3.74	1.29	1.23	1.91	3.02	3.66	3.36	2.98
P_2O_5	0.26	0.32	0.287	0.462	0.17	0.25	0.46	0.51	0.55
Total	96	92	97.22	96.73	95.54	90.65	97.05	95.49	92.94
LOI	3.12	7.01	2.18	2.73	3.26	8.89	1.46	4.06	6.35
Mg#	63	31	45	40	52	34	48	48	34
Ag ppm	<1	<1			<1		<1		
As	<5	<5			5		<5		
B	21	78			35		23		
Ba	2430	592	979	350	677	550	1640	1383	1391
Be	<5	<5			<5		<5		
Bi	0.1	<0.1			<0.1		0.2		
Cd	<0.2	<0.2			<0.2		<0.2		
Ce	61.7	71.7	52	59	50.4	55	145	111	124
Co	19.2	23.1			14.2		13.1		
Cr	94	<10	10	9	26	1	25	23	78
Cs	1	8.7			3.8		1.3		
Cu	46	10	4	35	<5	2	20	29	22
Dy	2.96	3.89			2.99		3.58		

Appendix 1 continued.

Er	1.44	2.28			1.73		1.67		
Eu	1.39	1.5			1.05		2		
Ga	20.3	18.4	21	24	14.9	18	20.6	17	16
Gd	4.2	4.72			3.3		5.96		
Ge	1	2			2		2		
Hf	4	4			3		7		
Ho	0.52	0.8			0.59		0.62		
In	<0.2	<0.2			<0.2		<0.2		
La	31.7	36.1	26	27	26.2	27	79.3	60	65
Li	19	50			17		19		
Lu	0.2	0.37			0.28		0.25		
Mn	834	1690			836		592		
Mo	<2	<2			<2		<2		
Nb	7.7	8.2	6.1	14.2	7.2	8.3	17.2	17	16.7
Nd	27.3	30.7	24	34	20.4	26	55.1	45	52
Ni	30	12	9	65	13	0	24	26	31
Pb	7	<5	9	11	13	5	24	18	19
Pr	7.18	8.31			5.71		15.8		
Rb	89.1	156	22	40	47.8	88	99.8	82	77
Sb	<0.1	0.6			0.2		0.4		
Sc	18	14	8	23	16	13	6	8	12
Se	<5	<5			<5		<5		
Sm	4.9	5.6			3.6		8		
Sn	<1	<1			<1		1		
Sr	601	75.5	518	429	369	65	1090	1494	1772
Ta	<0.5	<0.5			<0.5		<0.5		
Tb	0.54	0.69			0.49		0.79		
Te	<0.5	<0.5			<0.5		<0.5		
Th	6.5	5.8	1	5	5	4	18	11	14
Tl	1.4	0.9			<0.5		<0.5		

Appendix 1 continued.

Tm	0.21	0.34			0.27		0.23		
U	1.72	1	1	3	1.02	2	3.62	4	5
V	178	108	114	341	102	39	40	103	133
W	<1	<1			<1		<1		
Y	14.4	21.4	11	35	16.2	29	17.9	19	20
Yb	1.4	2.3			1.9		1.7		
Zn	61	83	60	182	64	66	64	67	58
Zr	145	145	144	204	124	181	295	252	243

[1] Whole-rock geochemical analysis at Agat Laboratories.
[2] Whole-rock geochemical analysis at Peter Hooper GeoAnalytical Lab.
Mg# = $Mg^{2+}/(Mg^{2+}+Fe^{2+})*100$

Appendix 2. EMPA analysis data for sample DVD-007.

DVD-007										
Phenocryst	PLG 1	PLG 1	PLG 1	PLG 1	PLG 1	PLG 1	PLG 1	PLG 1	PLG 1	PLG 1
Spot	1a	1b	2a	2b	3a	3b	4a	4b	5a	5b
LA-ICP-MS spot	DVD-007 PLG 1 plg1-1		DVD-007 PLG 1 plg1-2		DVD-007 PLG 1 plg1-3		DVD-007 PLG 1 plg1-4		DVD-007 PLG 1 plg1-5	
SiO2	57.96	58.29	59.54	58.29	59.14	58.56	57.58	56.70	57.35	56.35
Al2O3	23.47	23.72	23.19	23.62	22.83	22.06	23.06	22.24	22.38	22.48
MgO	0.33	b.d.	b.d.	b.d.	b.d.	b.d.	b.d.	b.d.	b.d.	b.d.
CaO	6.64	6.65	6.43	7.20	6.30	5.84	7.04	6.64	6.81	7.28
BaO	b.d.	b.d.	0.41	b.d.	b.d.	b.d.	b.d.	b.d.	b.d.	b.d.
Na2O	6.31	6.49	6.86	6.27	7.02	7.09	6.42	6.58	6.46	6.45
K2O	0.91	1.12	0.90	0.79	0.99	1.02	0.87	0.94	0.92	0.96
Total	95.61	96.26	97.32	96.17	96.28	94.57	94.98	94.98	94.98	94.98
Na	0.57	0.58	0.61	0.56	0.63	0.65	0.58	0.61	0.60	0.60
K	0.05	0.07	0.05	0.05	0.06	0.06	0.05	0.06	0.06	0.06
Ca	0.33	0.33	0.32	0.36	0.31	0.29	0.35	0.34	0.35	0.37
Ba	0.00	0.00	0.01	0.00	0.00	0.00	0.00	0.00	0.00	0.00
Mg	0.02	0.00	0.00	0.00	0.00	0.00	0.00	0.00	0.00	0.00
Si	2.70	2.70	2.73	2.70	2.74	2.76	2.71	2.72	2.72	2.70
Al	1.29	1.30	1.25	1.29	1.25	1.22	1.28	1.26	1.25	1.27
Sum (cat)	4.97	4.98	4.97	4.96	4.98	4.98	4.97	4.99	4.97	5.00
Ab	59.66	59.55	62.34	58.24	62.95	64.54	58.97	60.55	59.66	58.08
An	34.68	33.72	32.30	36.92	31.22	29.37	35.75	33.78	34.73	36.23
Or	5.65	6.73	5.36	4.84	5.83	6.09	5.28	5.68	5.61	5.70

Appendix 2 continued.

PLG 1 6a DVD-007 PLG 1 plg1-6	PLG 1 6b DVD-007 PLG 1 plg1-6	PLG 1 7a DVD-007 PLG 1 plg1-7	PLG 1 7b DVD-007 PLG 1 plg1-7	PLG 1 8a DVD-007 PLG 1 plg1-8	PLG 1 8b DVD-007 PLG 1 plg1-8	PLG 1 9a DVD-007 PLG 1 plg1-9	PLG 1 9b DVD-007 PLG 1 plg1-9	PLG 2 1a DVD-007 PLG 2 plg2-1	PLG 2 1b DVD-007 PLG 2 plg2-1	PLG 2 2a DVD-007 PLG 2 plg2-2	PLG 2 2b DVD-007 PLG 2 plg2-2
57.23	56.45	56.24	56.74	54.43	54.59	53.15	53.29	53.12	54.99	55.50	54.83
22.00	22.09	22.20	22.15	22.62	21.76	22.72	21.90	21.87	20.41	20.72	21.08
b.d.	b.d.	b.d.	b.d.	b.d.	b.d.	b.d.	b.d.	b.d.	b.d.	b.d.	b.d.
6.39	7.11	6.99	7.24	7.88	6.75	8.42	7.68	7.68	6.01	5.97	6.21
0.00	b.d.	b.d.	b.d.	b.d.	b.d.	b.d.	b.d.	b.d.	b.d.	b.d.	b.d.
6.46	6.37	6.21	4.59	5.84	5.92	5.46	5.62	6.10	6.13	6.20	6.22
0.87	0.91	0.87	0.88	0.69	0.87	0.66	0.79	0.83	1.03	1.16	0.85
94.98	94.98	94.98	94.98	94.98	94.98	94.98	94.98	94.98	94.98	94.98	94.98
0.60	0.59	0.58	0.43	0.55	0.57	0.53	0.55	0.59	0.60	0.60	0.60
0.05	0.06	0.05	0.05	0.04	0.06	0.04	0.05	0.05	0.07	0.07	0.05
0.33	0.37	0.36	0.38	0.41	0.36	0.45	0.41	0.41	0.32	0.32	0.33
0.00	0.00	0.00	0.00	0.00	0.00	0.00	0.00	0.00	0.00	0.00	0.00
0.00	0.00	0.00	0.00	0.00	0.00	0.00	0.00	0.00	0.00	0.00	0.00
2.74	2.72	2.71	2.74	2.66	2.71	2.64	2.67	2.66	2.76	2.76	2.74
1.24	1.25	1.26	1.26	1.31	1.27	1.33	1.29	1.29	1.21	1.22	1.24
4.96	4.98	4.97	4.87	4.98	4.97	4.98	4.98	5.01	4.96	4.97	4.97
61.14	58.45	58.30	50.06	54.85	57.93	51.79	54.13	56.03	60.52	60.39	60.94
33.42	36.05	36.29	43.62	40.88	36.47	44.10	40.89	38.95	32.81	32.15	33.60
5.45	5.50	5.40	6.32	4.27	5.60	4.11	4.98	5.02	6.67	7.46	5.46

Appendix 2 continued.

PLG 2 3a DVD-007 PLG 2 plg2-3	PLG 2 3b DVD-007 PLG 2 plg2-3	PLG 2 4a DVD-007 PLG 2 plg2-4	PLG 2 4b DVD-007 PLG 2 plg2-4	PLG 3 1a DVD-007 PLG 3 plg3-1	PLG 3 1b DVD-007 PLG 3 plg3-1	PLG 3 2a DVD-007 PLG 3 plg3-2	PLG 3 2b DVD-007 PLG 3 plg3-2	PLG 3 3a DVD-007 PLG 3 plg3-3	PLG 3 3b DVD-007 PLG 3 plg3-3	PLG 3 4a DVD-007 PLG 3 plg3-4	PLG 3 4b DVD-007 PLG 3 plg3-4
57.01	54.79	55.22	54.93	53.42	56.15	56.06	53.85	54.37	52.90	55.79	54.94
20.25	20.52	20.11	20.83	21.70	19.68	19.90	21.24	20.77	21.19	20.04	19.86
b.d.	b.d.	b.d.	b.d.	b.d.	b.d.	b.d.	b.d.	b.d.	b.d.	b.d.	b.d.
5.58	5.98	5.84	6.61	7.45	5.38	5.20	6.73	6.58	7.20	5.47	5.58
b.d.	b.d.	b.d.	b.d.	b.d.	b.d.	b.d.	b.d.	b.d.	b.d.	b.d.	b.d.
6.55	6.22	6.34	5.80	5.60	6.53	6.44	5.86	6.15	5.86	6.21	6.34
1.29	1.13	1.21	1.02	0.78	1.07	1.20	0.81	0.98	0.71	0.96	1.06
94.98	94.98	94.98	94.98	94.98	94.98	94.98	94.98	94.98	94.98	94.98	94.98
0.62	0.61	0.62	0.56	0.55	0.63	0.62	0.57	0.60	0.58	0.60	0.62
0.08	0.07	0.08	0.07	0.05	0.07	0.08	0.05	0.06	0.05	0.06	0.07
0.29	0.32	0.31	0.35	0.40	0.29	0.28	0.36	0.35	0.39	0.29	0.30
0.00	0.00	0.00	0.00	0.00	0.00	0.00	0.00	0.00	0.00	0.00	0.00
0.00	0.00	0.00	0.00	0.00	0.00	0.00	0.00	0.00	0.00	0.00	0.00
2.80	2.76	2.78	2.75	2.69	2.81	2.80	2.72	2.73	2.69	2.80	2.79
1.17	1.22	1.19	1.23	1.29	1.16	1.17	1.26	1.23	1.27	1.18	1.19
4.97	4.97	4.98	4.95	4.97	4.96	4.96	4.97	4.98	4.98	4.94	4.97
62.49	60.58	61.15	57.26	54.74	63.96	63.74	57.94	58.94	56.88	62.97	62.61
29.43	32.17	31.16	36.09	40.26	29.14	28.46	36.81	34.85	38.61	30.62	30.47
8.08	7.24	7.69	6.65	5.01	6.91	7.80	5.25	6.21	4.51	6.41	6.92

Appendix 2 continued.

PLG 3 5a DVD-007	PLG 3 5b PLG 3 plg3-5	PLG 3* 6a DVD-007	PLG 3 6b PLG 3 plg3-6	PLG 3 7a DVD-007	PLG 3 7b PLG 3 plg3-7	PLG 3 8a DVD-007	PLG 3 8b PLG 3 plg3-8	PLG 3 9a DVD-007	PLG 3 9b PLG 3 plg3-9	PLG 3 10a DVD-007	PLG 3 10b PLG 3 plg3-10
54.72	54.11	57.80	53.67	53.75	53.23	54.47	55.19	54.16	55.83	53.82	53.10
20.23	20.52	17.10	20.14	20.80	21.15	20.59	20.20	20.59	20.16	21.10	21.22
b.d.	b.d.	b.d.	b.d.	b.d.	b.d.	b.d.	b.d.	b.d.	b.d.	b.d.	b.d.
5.90	7.00	2.32	6.25	6.94	7.13	6.08	5.76	6.44	5.91	6.91	7.34
b.d.	b.d.	b.d.	b.d.	b.d.	b.d.	b.d.	b.d.	b.d.	b.d.	b.d.	b.d.
6.31	6.10	4.96	6.04	5.73	5.90	6.43	6.17	6.02	6.73	6.02	6.02
0.96	0.81	6.58	0.91	0.78	0.83	0.87	1.03	0.87	1.03	0.96	0.81
94.98	94.98	94.98	94.98	94.98	94.98	94.98	94.98	94.98	94.98	94.98	94.98
0.62	0.60	0.49	0.60	0.56	0.58	0.63	0.60	0.59	0.65	0.59	0.59
0.06	0.05	0.43	0.06	0.05	0.05	0.06	0.07	0.06	0.07	0.06	0.05
0.32	0.38	0.13	0.34	0.38	0.39	0.33	0.31	0.35	0.32	0.37	0.40
0.00	0.00	0.00	0.00	0.00	0.00	0.00	0.00	0.00	0.00	0.00	0.00
0.00	0.00	0.00	0.00	0.00	0.00	0.00	0.00	0.00	0.00	0.00	0.00
2.77	2.73	2.94	2.75	2.73	2.70	2.75	2.78	2.74	2.78	2.71	2.69
1.21	1.22	1.02	1.22	1.24	1.26	1.22	1.20	1.23	1.18	1.25	1.27
4.97	4.98	5.01	4.97	4.96	4.99	4.98	4.96	4.97	4.99	4.99	5.00
61.83	58.07	46.93	59.85	56.83	56.84	62.09	61.49	59.31	63.06	57.48	56.73
31.97	36.85	12.13	34.21	38.07	37.91	32.41	31.74	35.03	30.62	36.49	38.26
6.20	5.08	40.95	5.94	5.11	5.26	5.50	6.77	5.66	6.33	6.03	5.02

Appendix 2 continued.

PLG 3 11a DVD-007	PLG 3 11b PLG 3 plg3-11	PLG 3 12a DVD-007	PLG 3 12b PLG 3 plg3-12	PLG 3 13a DVD-007	PLG 3 13b PLG 3 plg3-13	PLG 3 14a DVD-007	PLG 3 14b PLG 3 plg3-14	PLG 3 15a DVD-007	PLG 3 15b PLG 3 plg3-15	PLG 3 16a DVD-007	PLG 3 16b PLG 3 plg3-16
55.02	53.73	54.55	55.87	55.97	53.78	56.49	54.02	55.41	55.91	57.70	56.67
20.72	21.10	20.97	20.62	20.71	21.79	21.21	23.04	22.69	22.93	23.93	24.28
b.d.	b.d.	b.d.	b.d.	b.d.	b.d.	b.d.	b.d.	0.12	b.d.	b.d.	b.d.
6.69	7.51	6.73	5.91	6.07	7.35	6.25	8.51	7.58	7.23	7.01	7.24
b.d.	b.d.	b.d.	b.d.	b.d.	b.d.	b.d.	b.d.	b.d.	b.d.	b.d.	b.d.
6.36	6.28	5.76	6.43	6.40	5.82	6.45	5.73	4.41	6.07	6.36	6.06
0.92	0.91	0.84	1.11	0.96	0.75	1.02	0.67	0.78	0.89	0.97	0.95
94.98	94.98	94.98	94.98	94.98	94.98	94.98	94.98	94.98	94.98	94.98	94.98
0.61	0.61	0.56	0.62	0.61	0.56	0.61	0.54	0.42	0.57	0.57	0.55
0.06	0.06	0.05	0.07	0.06	0.05	0.06	0.04	0.05	0.05	0.06	0.06
0.36	0.40	0.36	0.31	0.32	0.39	0.33	0.45	0.40	0.37	0.35	0.36
0.00	0.00	0.00	0.00	0.00	0.00	0.00	0.00	0.00	0.00	0.00	0.00
0.00	0.00	0.00	0.00	0.00	0.00	0.00	0.00	0.01	0.00	0.00	0.00
2.74	2.70	2.74	2.77	2.77	2.69	2.75	2.64	2.70	2.69	2.68	2.66
1.22	1.25	1.24	1.20	1.21	1.28	1.22	1.33	1.30	1.30	1.31	1.34
4.99	5.02	4.95	4.97	4.97	4.98	4.97	4.99	4.88	4.98	4.98	4.97
59.67	56.92	57.39	61.67	61.61	56.08	60.99	52.69	48.38	57.00	58.50	56.69
34.65	37.63	37.07	31.32	32.29	39.13	32.69	43.27	45.97	37.52	35.63	37.45
5.68	5.45	5.54	7.01	6.10	4.79	6.33	4.04	5.64	5.49	5.86	5.86

Appendix 2 continued.

PLG 5 1a DVD-007 PLG 5 plg5-1	PLG 5 1b DVD-007 PLG 5 plg5-1	PLG 5 2a DVD-007 PLG 5 plg5-2	PLG 5 2b DVD-007 PLG 5 plg5-2	PLG 5 3a DVD-007 PLG 5 plg5-3	PLG 5 3b DVD-007 PLG 5 plg5-3	PLG 5 4a DVD-007 PLG 5 plg5-4	PLG 5 4b DVD-007 PLG 5 plg5-4	PLG 5 5a DVD-007 PLG 5 plg5-5	PLG 5 5b DVD-007 PLG 5 plg5-5	PLG 5 6a DVD-007 PLG 5 plg5-6	PLG 5 6b DVD-007 PLG 5 plg5-6
58.11	58.06	57.75	54.04	55.14	57.55	57.02	56.46	57.41	60.10	57.83	58.06
24.69	24.49	25.52	26.64	27.13	25.32	25.82	25.72	24.92	23.83	25.55	25.05
b.d.	b.d.	b.d.	b.d.	b.d.	b.d.	b.d.	b.d.	b.d.	b.d.	b.d.	b.d.
7.10	6.81	7.87	8.83	9.42	6.96	7.67	7.86	7.03	5.68	7.75	7.31
b.d.	b.d.	b.d.	b.d.	b.d.	b.d.	b.d.	b.d.	b.d.	b.d.	b.d.	b.d.
6.43	6.75	6.33	5.86	5.42	6.44	6.08	6.09	6.59	7.18	6.26	6.66
0.88	0.95	0.57	0.49	0.43	0.70	0.54	0.52	0.84	1.22	0.70	0.75
97.20	97.05	98.05	95.86	97.53	96.97	97.14	96.65	96.79	98.02	98.09	97.84
0.57	0.60	0.56	0.53	0.48	0.57	0.54	0.55	0.59	0.63	0.55	0.59
0.05	0.06	0.03	0.03	0.03	0.04	0.03	0.03	0.05	0.07	0.04	0.04
0.35	0.34	0.38	0.44	0.46	0.34	0.38	0.39	0.35	0.28	0.38	0.36
0.00	0.00	0.00	0.00	0.00	0.00	0.00	0.00	0.00	0.00	0.00	0.00
0.00	0.00	0.00	0.00	0.00	0.00	0.00	0.00	0.00	0.00	0.00	0.00
2.67	2.67	2.63	2.53	2.54	2.65	2.62	2.61	2.65	2.73	2.63	2.65
1.34	1.33	1.37	1.47	1.47	1.37	1.40	1.40	1.36	1.28	1.37	1.35
4.98	4.99	4.98	5.01	4.98	4.98	4.97	4.98	4.99	4.98	4.98	4.99
58.82	60.59	57.26	53.00	49.67	59.95	56.95	56.52	59.78	64.57	56.87	59.50
35.91	33.81	39.33	44.09	47.73	35.79	39.70	40.31	35.21	28.21	38.94	36.08
5.28	5.61	3.42	2.90	2.60	4.26	3.35	3.17	5.01	7.22	4.19	4.42

Appendix 2 continued.

PLG 5 7a DVD-007 PLG 5 plg5-7	PLG 5 7b DVD-007 PLG 5 plg5-7	PLG 5 8a DVD-007 PLG 5 plg5-8	PLG 5 8b DVD-007 PLG 5 plg5-8	PLG 6 1a DVD-007 PLG 6 plg6-2	PLG 6 1b DVD-007 PLG 6 plg6-2	PLG 6 2a DVD-007 PLG 6 plg6-1	PLG 6 2b DVD-007 PLG 6 plg6-1	PLG 7 1a DVD-007 PLG 7 plg7-2	PLG 7 1b DVD-007 PLG 7 plg7-2	PLG 7 2a DVD-007 PLG 7 plg7-1	PLG 7 2b DVD-007 PLG 7 plg7-1
62.20	58.25	57.47	56.98	58.07	58.69	58.52	58.14	58.85	58.62	60.63	60.72
23.68	24.84	25.78	26.00	23.71	24.97	25.26	25.76	25.28	25.15	24.20	24.12
b.d.	b.d.	b.d.	b.d.	b.d.	b.d.	b.d.	b.d.	b.d.	b.d.	b.d.	b.d.
5.47	6.61	8.19	8.77	6.62	7.29	7.30	8.07	7.35	7.23	6.44	6.03
b.d.	b.d.	b.d.	b.d.	b.d.	b.d.	b.d.	0.42	b.d.	b.d.	b.d.	0.38
7.44	6.48	5.98	5.91	7.01	6.43	6.34	6.43	6.79	6.56	6.72	7.03
1.18	0.93	0.72	0.73	1.20	0.90	0.84	0.80	0.92	1.00	1.18	1.05
99.97	97.11	98.14	98.39	96.61	98.27	98.25	99.62	99.19	98.56	99.18	99.34
0.64	0.58	0.53	0.52	0.63	0.57	0.56	0.56	0.59	0.58	0.59	0.61
0.07	0.05	0.04	0.04	0.07	0.05	0.05	0.05	0.05	0.06	0.07	0.06
0.26	0.33	0.40	0.43	0.33	0.35	0.36	0.39	0.36	0.35	0.31	0.29
0.00	0.00	0.00	0.00	0.00	0.00	0.00	0.01	0.00	0.00	0.00	0.01
0.00	0.00	0.00	0.00	0.00	0.00	0.00	0.00	0.00	0.00	0.00	0.00
2.76	2.67	2.62	2.60	2.69	2.67	2.66	2.62	2.65	2.66	2.72	2.73
1.24	1.34	1.38	1.40	1.29	1.34	1.35	1.37	1.34	1.34	1.28	1.28
4.97	4.97	4.97	4.99	5.01	4.98	4.97	5.00	5.00	4.99	4.96	4.97
66.19	60.27	54.48	52.61	61.19	58.20	58.01	56.34	59.26	58.48	60.79	63.57
26.91	34.02	41.19	43.10	31.92	36.47	36.93	39.05	35.47	35.64	32.20	30.15
6.90	5.71	4.33	4.29	6.88	5.33	5.06	4.61	5.27	5.87	7.01	6.28

Appendix 2 continued.

PLG 8 1a DVD-007 PLG 8 plg8-2	PLG 8 1b	PLG 8 2a DVD-007 PLG 8 plg8-1	PLG 8 2b	PLG 10 1a DVD-007 PLG 10 plg10-1	PLG 10 1b	PLG 10 2a DVD-007 PLG 10 plg10-3	PLG 10 2b	PLG 10 3a DVD-007 PLG 10 plg10-3	PLG 10 3b	PLG 10 4a DVD-007 PLG 10 plg10-4	PLG 10 4b
60.62	60.04	57.44	58.46	59.82	60.78	60.44	60.64	58.13	57.07	59.82	60.46
24.16	24.29	25.95	25.06	24.87	24.22	24.69	24.62	25.54	26.32	24.79	24.01
b.d.	b.d.	b.d.	b.d.	b.d.	b.d.	b.d.	b.d.	b.d.	b.d.	b.d.	b.d.
6.11	6.53	8.26	7.22	7.37	6.37	6.64	6.44	8.22	8.75	6.95	6.32
b.d.	b.d.	b.d.	b.d.	b.d.	b.d.	b.d.	b.d.	b.d.	b.d.	b.d.	b.d.
6.99	6.69	6.21	6.50	6.24	6.99	6.96	6.60	6.29	5.80	6.31	6.62
1.34	1.24	0.67	0.95	0.83	1.13	0.92	0.86	0.62	0.42	0.99	1.62
99.22	98.79	98.52	98.19	99.12	99.48	99.65	99.16	98.80	98.37	98.86	99.03
0.61	0.59	0.55	0.57	0.54	0.61	0.60	0.57	0.55	0.51	0.55	0.58
0.08	0.07	0.04	0.06	0.05	0.06	0.05	0.05	0.04	0.02	0.06	0.09
0.29	0.32	0.40	0.35	0.35	0.31	0.32	0.31	0.40	0.43	0.34	0.30
0.00	0.00	0.00	0.00	0.00	0.00	0.00	0.00	0.00	0.00	0.00	0.00
0.00	0.00	0.00	0.00	0.00	0.00	0.00	0.00	0.00	0.00	0.00	0.00
2.72	2.71	2.61	2.66	2.69	2.72	2.70	2.72	2.63	2.60	2.69	2.72
1.28	1.29	1.39	1.34	1.32	1.28	1.30	1.30	1.36	1.41	1.32	1.27
4.98	4.97	4.99	4.98	4.95	4.98	4.98	4.95	4.98	4.97	4.95	4.97
62.15	60.18	55.38	58.46	57.45	62.09	61.94	61.56	55.93	53.17	58.41	59.20
30.03	32.49	40.72	35.89	37.54	31.28	32.67	33.15	40.43	44.29	35.58	31.24
7.82	7.33	3.91	5.64	5.01	6.63	5.39	5.29	3.65	2.54	6.02	9.56

Appendix 2 continued.

PLG 10	PLG 10	PLG 13	PLG 13	PLG 13	PLG 13
5a	5b	1a	1b	2a	2b
DVD-007 PLG 10 plg10-5		DVD-007 PLG 13 plg13-2		DVD-007 PLG 13 plg13-1	
60.32	60.30	60.61	61.05	59.91	59.60
24.63	24.28	24.39	23.84	24.84	24.74
b.d.	b.d.	b.d.	b.d.	b.d.	b.d.
6.98	6.03	6.97	6.47	7.67	7.44
b.d.	b.d.	b.d.	b.d.	b.d.	b.d.
6.69	6.80	6.54	6.76	6.67	6.92
0.98	1.17	0.98	1.27	0.95	0.89
99.59	98.59	99.49	99.40	100.04	99.59
0.58	0.60	0.57	0.59	0.58	0.60
0.06	0.07	0.06	0.07	0.05	0.05
0.33	0.29	0.33	0.31	0.37	0.36
0.00	0.00	0.00	0.00	0.00	0.00
0.00	0.00	0.00	0.00	0.00	0.00
2.70	2.72	2.71	2.74	2.68	2.68
1.30	1.29	1.29	1.26	1.31	1.31
4.97	4.97	4.96	4.97	4.98	5.00
59.78	62.37	59.29	60.50	57.85	59.55
34.46	30.55	34.88	32.02	36.74	35.40
5.76	7.08	5.83	7.48	5.40	5.05

* Discarded from analysis.

Appendix 2 EMPA analysis data for sample DVD-009.

DVD-009										
Phenocryst	PLG 1	PLG 1	PLG 1	PLG 1*	PLG 1	PLG 1	PLG 1	PLG 1	PLG 9	PLG 9
Spot	1a	1b	2a	2b	3a	3b	4a	4b	1a	1b
LA-ICP-MS spot	DVD-009 PLG 1 plg1-1		DVD-009 PLG 1 plg1-2		DVD-009 PLG 1 plg1-3		DVD-009 PLG 1 plg1-4		DVD-009 PLG 9 plg9-1	
SiO2	55.55	55.86	55.41	61.63	55.37	57.35	58.16	55.84	56.40	55.92
Al2O3	27.81	27.41	27.84	23.27	27.59	26.92	25.96	27.51	26.81	27.30
MgO	b.d.	b.d.	b.d.	0.89	b.d.	b.d.	b.d.	b.d.	b.d.	b.d.
CaO	10.96	10.02	10.68	5.03	10.91	9.03	8.90	10.24	10.55	10.45
BaO	b.d.	b.d.	b.d.	b.d.	b.d.	b.d.	b.d.	b.d.	b.d.	b.d.
Na2O	4.78	5.07	4.76	6.21	5.10	5.48	6.28	5.17	5.55	5.17
K2O	0.42	0.45	0.41	0.41	0.46	0.53	0.71	0.54	0.49	0.51
Total	99.53	98.81	99.10	97.45	99.42	99.30	100.01	99.31	99.80	99.35
Na	0.42	0.45	0.42	0.54	0.45	0.48	0.55	0.45	0.49	0.45
K	0.02	0.03	0.02	0.02	0.03	0.03	0.04	0.03	0.03	0.03
Ca	0.53	0.49	0.52	0.24	0.53	0.44	0.43	0.50	0.51	0.51
Ba	0.00	0.00	0.00	0.00	0.00	0.00	0.00	0.00	0.00	0.00
Mg	0.00	0.00	0.00	0.06	0.00	0.00	0.00	0.00	0.00	0.00
Si	2.51	2.54	2.51	2.78	2.51	2.58	2.61	2.53	2.55	2.53
Al	1.48	1.47	1.49	1.24	1.47	1.43	1.37	1.47	1.43	1.46
Sum (cat)	4.97	4.96	4.96	4.89	4.99	4.96	5.00	4.98	5.00	4.98
Ab	43.01	46.48	43.55	67.07	44.60	50.64	53.85	46.18	47.39	45.84
An	54.48	50.79	54.00	30.00	52.78	46.13	42.13	50.61	49.84	51.20
Or	2.51	2.73	2.45	2.94	2.63	3.23	4.02	3.20	2.77	2.95

Appendix 2 continued.

PLG 9 2a DVD-009	PLG 9 2b PLG 9 plg9-2	PLG 9 3a DVD-009	PLG 9 3b PLG 9 plg9-3	PLG 11 1a DVD-009	PLG 11 1b PLG 11 plg11-1	PLG 11 2a DVD-009	PLG 11 2b PLG 11 plg11-2	PLG 11 3a DVD-009	PLG 11* 3b PLG 11 plg11-3	PLG 11 4a DVD-009	PLG 11 4b PLG 11 plg11-4
54.97	54.42	57.25	56.66	56.14	55.26	54.93	54.72	54.02	69.00	56.15	53.47
27.71	27.79	26.01	26.19	26.46	26.67	26.45	26.86	26.98	19.39	25.10	26.71
b.d.	b.d.	b.d.	b.d.	b.d.	b.d.	b.d.	0.08	b.d.	b.d.	b.d.	b.d.
10.97	11.22	8.92	9.34	9.98	10.87	11.17	11.61	11.19	0.23	9.39	11.32
b.d.	b.d.	b.d.	b.d.	b.d.	b.d.	b.d.	b.d.	b.d.	b.d.	b.d.	b.d.
4.85	5.01	5.72	5.54	5.50	5.10	5.27	4.88	4.58	9.93	5.43	4.55
0.45	0.40	0.65	0.49	0.53	0.51	0.58	0.52	0.61	0.10	0.79	0.48
98.95	98.84	98.54	98.23	98.61	98.41	98.41	98.66	97.38	98.64	96.86	96.52
0.43	0.44	0.50	0.49	0.49	0.45	0.47	0.43	0.41	0.85	0.49	0.41
0.03	0.02	0.04	0.03	0.03	0.03	0.03	0.03	0.04	0.01	0.05	0.03
0.54	0.55	0.43	0.46	0.49	0.53	0.55	0.57	0.56	0.01	0.47	0.57
0.00	0.00	0.00	0.00	0.00	0.00	0.00	0.00	0.00	0.00	0.00	0.00
0.00	0.00	0.00	0.00	0.00	0.00	0.00	0.01	0.00	0.00	0.00	0.00
2.50	2.49	2.60	2.59	2.56	2.53	2.52	2.51	2.50	3.03	2.60	2.50
1.49	1.50	1.39	1.41	1.42	1.44	1.43	1.45	1.47	1.00	1.37	1.47
4.98	5.00	4.97	4.97	4.99	4.99	5.01	5.00	4.98	4.89	4.98	4.98
43.26	43.65	51.62	50.25	48.41	44.59	44.56	41.94	41.02	98.13	48.75	40.94
54.09	54.05	44.52	46.81	48.51	52.48	52.20	55.13	55.37	1.24	46.60	56.24
2.65	2.30	3.86	2.94	3.08	2.93	3.23	2.93	3.61	0.63	4.65	2.83

Appendix 2 continued.

PLG 11* 5a DVD-009 PLG 11 plg11-5	PLG 11 5b	PLG 14 1a DVD-009 PLG 14 plg14-1	PLG 14 1b	PLG 14* 2a DVD-009 PLG 14 plg14-2	PLG 14 2b	PLG 14 3a DVD-009 PLG 14 plg14-3	PLG 14 3b	PLG 14 4a DVD-009 PLG 14 plg14-4	PLG 14 4b	PLG 14 5a DVD-009 PLG 14 plg14-5	PLG 14 5b
67.97	55.04	55.01	54.58	60.85	54.97	53.91	55.99	55.19	52.30	53.66	53.46
19.57	25.59	24.99	24.66	21.57	24.35	25.05	23.81	24.20	25.64	24.95	25.01
b.d.	b.d.	b.d.	b.d.	b.d.	b.d.	b.d.	b.d.	b.d.	b.d.	b.d.	b.d.
0.57	9.48	9.49	9.42	4.47	9.18	9.23	8.61	8.49	10.95	9.48	9.80
b.d.	b.d.	b.d.	b.d.	b.d.	b.d.	b.d.	b.d.	b.d.	b.d.	0.33	b.d.
10.12	5.10	5.48	5.37	6.87	5.35	5.48	5.70	5.42	4.58	4.86	5.02
0.13	0.56	0.56	0.62	0.33	0.58	0.54	0.72	0.64	0.36	0.62	0.51
98.35	95.77	95.54	94.65	94.09	94.42	94.21	94.84	93.94	93.84	93.90	93.80
0.87	0.46	0.50	0.49	0.62	0.49	0.51	0.52	0.50	0.43	0.45	0.47
0.01	0.03	0.03	0.04	0.02	0.04	0.03	0.04	0.04	0.02	0.04	0.03
0.03	0.48	0.48	0.48	0.22	0.47	0.47	0.44	0.43	0.56	0.49	0.50
0.00	0.00	0.00	0.00	0.00	0.00	0.00	0.00	0.00	0.00	0.01	0.00
0.00	0.00	0.00	0.00	0.00	0.00	0.00	0.00	0.00	0.00	0.00	0.00
3.00	2.58	2.59	2.59	2.84	2.61	2.57	2.65	2.63	2.52	2.57	2.56
1.02	1.41	1.39	1.38	1.19	1.36	1.41	1.33	1.36	1.45	1.41	1.41
4.92	4.96	4.99	4.98	4.89	4.97	4.99	4.97	4.96	4.98	4.97	4.98
96.22	47.66	49.41	48.87	71.87	49.50	50.12	52.14	51.43	42.11	46.21	46.60
2.99	48.90	47.27	47.39	25.87	46.97	46.64	43.53	44.54	55.68	49.88	50.29
0.79	3.44	3.31	3.73	2.26	3.53	3.24	4.33	4.03	2.20	3.91	3.11

Appendix 2 continued.

PLG 18 1a DVD-009 PLG 18 plg18-1	PLG 18 1b DVD-009 PLG 18 plg18-1	PLG 18 2a DVD-009 PLG 18 plg18-2	PLG 18 2b DVD-009 PLG 18 plg18-2	PLG 18 3a DVD-009 PLG 18 plg18-3	PLG 18 3b DVD-009 PLG 18 plg18-3	PLG 17 1a DVD-009 PLG 17 plg17-1	PLG 17 1b DVD-009 PLG 17 plg17-1	PLG 17 2a DVD-009 PLG 17 plg17-2	PLG 17 2b DVD-009 PLG 17 plg17-2	PLG 16 1a DVD-009 PLG 16 plg16-1	PLG 16 1b DVD-009 PLG 16 plg16-1
53.08	55.32	51.98	52.68	52.29	52.48	52.99	54.30	52.85	52.77	53.15	52.61
25.03	23.43	25.54	25.11	25.24	25.18	24.80	24.17	25.04	24.93	24.94	24.93
b.d.	b.d.	b.d.	b.d.	b.d.	b.d.	b.d.	b.d.	b.d.	b.d.	b.d.	b.d.
10.50	8.37	11.40	10.80	11.30	11.30	11.00	10.04	10.97	11.17	10.90	10.64
b.d.	b.d.	b.d.	b.d.	b.d.	b.d.	b.d.	b.d.	b.d.	b.d.	b.d.	b.d.
4.92	5.85	4.68	4.81	4.68	4.74	4.95	5.27	4.60	4.62	5.04	4.65
0.55	0.83	0.46	0.52	0.56	0.39	0.46	0.59	0.40	0.50	0.47	0.44
94.08	93.81	94.05	93.92	94.07	94.10	94.20	94.37	93.86	93.98	94.51	93.27
0.46	0.54	0.44	0.45	0.44	0.44	0.46	0.49	0.43	0.43	0.47	0.44
0.03	0.05	0.03	0.03	0.03	0.02	0.03	0.04	0.02	0.03	0.03	0.03
0.54	0.43	0.59	0.56	0.58	0.58	0.57	0.51	0.57	0.58	0.56	0.55
0.00	0.00	0.00	0.00	0.00	0.00	0.00	0.00	0.00	0.00	0.00	0.00
0.00	0.00	0.00	0.00	0.00	0.00	0.00	0.00	0.00	0.00	0.00	0.00
2.55	2.65	2.50	2.53	2.52	2.52	2.54	2.59	2.54	2.54	2.54	2.54
1.42	1.32	1.45	1.42	1.43	1.43	1.40	1.36	1.42	1.41	1.41	1.42
4.99	4.99	5.00	4.99	5.00	5.00	5.00	4.99	4.98	4.99	5.00	4.98
44.40	53.07	41.50	43.23	41.44	42.15	43.70	47.00	42.09	41.54	44.31	42.99
52.33	41.97	55.84	53.68	55.28	55.55	53.63	49.54	55.49	55.53	52.95	54.34
3.27	4.95	2.66	3.09	3.28	2.30	2.67	3.46	2.42	2.93	2.74	2.67

Appendix 2 continued.

PLG 16* 2a DVD-009	PLG 16 2b PLG 16 plg16-2	PLG 16 3a DVD-009	PLG 16 3b PLG 16 plg16-3	PLG 16 4a DVD-009	PLG 16 4b PLG 16 plg16-4	PLG 16 5a DVD-009	PLG 16 5b PLG 16 plg16-5	PLG 16 6a DVD-009	PLG 16 6b PLG 16 plg16-6	PLG 16 7a DVD-009	PLG 16* 7b PLG 16 plg16-7
60.02	53.48	52.29	53.48	55.28	55.43	53.61	55.58	55.35	54.42	55.26	60.64
22.00	25.78	27.14	27.47	27.34	27.46	29.03	27.87	28.08	28.59	27.89	24.57
b.d.	b.d.	b.d.	b.d.	b.d.	b.d.	b.d.	b.d.	b.d.	b.d.	b.d.	b.d.
5.08	11.30	12.43	12.35	11.21	10.60	12.65	11.34	10.46	12.22	11.00	6.63
b.d.	b.d.	b.d.	b.d.	b.d.	b.d.	b.d.	b.d.	b.d.	b.d.	b.d.	b.d.
7.18	4.66	3.89	4.56	4.54	5.28	4.13	4.80	4.86	4.59	4.76	6.71
0.30	0.32	0.33	0.43	0.41	0.49	0.40	0.50	0.41	0.49	0.47	1.05
94.59	95.54	96.09	98.30	98.79	99.26	99.83	100.10	99.17	100.31	99.38	99.59
0.65	0.43	0.36	0.41	0.40	0.46	0.36	0.42	0.43	0.40	0.42	0.58
0.02	0.02	0.02	0.03	0.02	0.03	0.02	0.03	0.02	0.03	0.03	0.06
0.25	0.57	0.63	0.61	0.55	0.52	0.61	0.55	0.51	0.59	0.53	0.32
0.00	0.00	0.00	0.00	0.00	0.00	0.00	0.00	0.00	0.00	0.00	0.00
0.00	0.00	0.00	0.00	0.00	0.00	0.00	0.00	0.00	0.00	0.00	0.00
2.80	2.53	2.46	2.47	2.52	2.52	2.43	2.50	2.51	2.46	2.50	2.71
1.21	1.44	1.51	1.49	1.47	1.47	1.55	1.48	1.50	1.52	1.49	1.29
4.93	4.98	4.97	5.00	4.96	5.00	4.99	4.98	4.97	5.00	4.97	4.96
70.49	41.95	35.44	39.09	41.28	46.06	36.29	42.09	44.53	39.36	42.69	60.64
27.57	56.17	62.61	58.50	56.28	51.13	61.40	55.01	52.99	57.90	54.55	33.13
1.94	1.88	1.96	2.41	2.44	2.82	2.32	2.91	2.48	2.74	2.75	6.22

* Discarded from analysis.

Appendix 3. *In situ* LA-MC-ICP-MS analysis results of plagioclase phenocrysts.

Sample ID	Phenocryst	Spot	Spot location	$^{87}Rb/^{86}Sr$	$^{87}Sr/^{86}Sr$	2σ
DVD-007	DVD-007 PLG 1	plg1-1	rim	0.0090	0.707378	0.000020
	DVD-007 PLG 1	plg1-2	mid	0.0024	0.709227	0.000021
	DVD-007 PLG 1	plg1-3	mid	0.0033	0.709826	0.000026
	DVD-007 PLG 1	plg1-4	mid	0.0037	0.708597	0.000022
	DVD-007 PLG 1	plg1-5	mid	0.0083	0.707703	0.000021
	DVD-007 PLG 1	plg1-6	mid	0.0125	0.707844	0.000029
	DVD-007 PLG 1	plg1-7	mid	0.0018	0.707934	0.000022
	DVD-007 PLG 1	plg1-8	mid	0.0015	0.707423	0.000019
	DVD-007 PLG 1	plg1-9	rim	0.0205	0.707267	0.000019
	DVD-007 PLG 1	plg1-2 dubl.	mid	0.0017	0.708049	0.000027
	DVD-007 PLG 1	plg1-3 dubl.	mid	0.0106	0.708946	0.000031
	DVD-007 PLG 2	plg2-1	mid	0.0243	0.707342	0.000022
	DVD-007 PLG 2	plg2-2	mid	0.0026	0.707418	0.000021
	DVD-007 PLG 2	plg2-3	mid	0.0019	0.707430	0.000021
	DVD-007 PLG 2	plg2-4	rim	0.0016	0.707336	0.000027
	DVD-007 PLG 3	plg3-1	rim	0.0031	0.707328	0.000021
	DVD-007 PLG 3	plg3-2	mid	0.0040	0.707300	0.000021
	DVD-007 PLG 3	plg3-3	mid	0.0016	0.707365	0.000020
	DVD-007 PLG 3	plg3-4	mid	0.0050	0.707486	0.000023
	DVD-007 PLG 3	plg3-5	mid	0.0051	0.707412	0.000021
	DVD-007 PLG 3	plg3-6	mid	0.0028	0.707365	0.000022
	DVD-007 PLG 3	plg3-7	mid	0.0158	0.707595	0.000039
	DVD-007 PLG 3	plg3-8	mid	0.0037	0.707710	0.000024
	DVD-007 PLG 3	plg3-9	mid	0.0024	0.707826	0.000021
	DVD-007 PLG 3	plg3-10	mid	0.0025	0.707531	0.000025
	DVD-007 PLG 3	plg3-11	mid	0.0067	0.707719	0.000024
	DVD-007 PLG 3	plg3-12	mid	0.0024	0.707655	0.000027
	DVD-007 PLG 3	plg3-13	mid	0.0044	0.707520	0.000027
	DVD-007 PLG 3	plg3-14	mid	0.0033	0.707542	0.000023
	DVD-007 PLG 3	plg3-15	mid	0.0020	0.707348	0.000021
	DVD-007 PLG 3	plg3-16	rim	0.0161	0.707235	0.000023
	DVD-007 PLG 4	plg4-1	mid	0.0019	0.707537	0.000022
	DVD-007 PLG 5	plg5-1	rim	0.0021	0.707386	0.000023
	DVD-007 PLG 5	plg5-2	mid	0.0036	0.707271	0.000025
	DVD-007 PLG 5	plg5-3	mid	0.0011	0.707267	0.000021
	DVD-007 PLG 5	plg5-4	mid	0.0095	0.707350	0.000025
	DVD-007 PLG 5	plg5-5	mid	0.0064	0.707403	0.000024
	DVD-007 PLG 5	plg5-6	mid	0.0038	0.707334	0.000019
	DVD-007 PLG 5	plg5-7	mid	0.0018	0.707322	0.000022
	DVD-007 PLG 5	plg5-8	rim	0.0028	0.707255	0.000024
	DVD-007 PLG 6	plg6-1	core	0.0045	0.707372	0.000019
	DVD-007 PLG 6	plg6-2	rim	0.0120	0.707192	0.000024
	DVD-007 PLG 7	plg7-1	core	0.0021	0.707551	0.000025
	DVD-007 PLG 7	plg7-2	rim	0.0034	0.707490	0.000027
	DVD-007 PLG 8	plg8-1	core	0.0028	0.707384	0.000023

Appendix 3 continued.

	DVD-007 PLG 8	plg8-2	rim	0.0019	0.707331	0.000025
	DVD-007 PLG 9	plg9-2	core	0.0027	0.707471	0.000024
	DVD-007 PLG 10	plg10-1	rim	0.0077	0.707322	0.000031
	DVD-007 PLG 10	plg10-2	rim	0.0050	0.707231	0.000020
	DVD-007 PLG 10	plg10-3	mid	0.0019	0.707537	0.000024
	DVD-007 PLG 10	plg10-4	mid	0.0018	0.707331	0.000024
	DVD-007 PLG 10	plg10-5	mid	0.0023	0.707466	0.000027
	DVD-007 PLG 10	plg10-6	mid	0.0028	0.707425	0.000028
	DVD-007 PLG 11	plg11-2	core	0.0029	0.707385	0.000024
	DVD-007 PLG 13	plg13-1	core	0.0014	0.707447	0.000026
	DVD-007 PLG 13	plg13-2	rim	0.0055	0.707218	0.000028
	DVD-007 PLG 14	plg14-1	core	0.0011	0.707314	0.000016
	DVD-007 PLG 15	plg15-1	core	0.0040	0.707185	0.000020
	DVD-007 PLG 16	plg16-1	core	0.0026	0.707327	0.000020
DVD-009	DVD-009 PLG 1	plg1-1	rim	0.0031	0.707854	0.000014
	DVD-009 PLG 1	plg1-2	mid	0.0133	0.707435	0.000022
	DVD-009 PLG 1	plg1-3	mid	0.0077	0.707424	0.000020
	DVD-009 PLG 1	plg1-4	rim	0.0042	0.707891	0.000021
	DVD-009 PLG 2	plg2-1	rim	0.0026	0.707684	0.000018
	DVD-009 PLG 2	plg2-2	core	0.0024	0.708110	0.000022
	DVD-009 PLG 3	plg3-1	core	0.0020	0.707368	0.000020
	DVD-009 PLG 4	plg4-1	rim	0.0056	0.707790	0.000027
	DVD-009 PLG 5	plg5-1	mid	0.0027	0.707808	0.000022
	DVD-009 PLG 6	plg6-1	mid	0.0010	0.707706	0.000021
	DVD-009 PLG 7	plg7-1	mid	0.0054	0.707719	0.000040
	DVD-009 PLG 8	plg8-1	rim	0.0213	0.707736	0.000044
	DVD-009 PLG 9	plg9-1	rim	0.0020	0.707711	0.000028
	DVD-009 PLG 9	plg9-2	mid	0.0029	0.707795	0.000028
	DVD-009 PLG 9	plg9-3	rim	0.0058	0.707782	0.000027
	DVD-009 PLG 10	plg10-1	mid	0.0008	0.707825	0.000028
	DVD-009 PLG 11	plg11-1	rim	0.0040	0.707846	0.000029
	DVD-009 PLG 11	plg11-2	mid	0.0095	0.708332	0.000032
	DVD-009 PLG 11	plg11-3	mid	0.0068	0.708677	0.000038
	DVD-009 PLG 11	plg11-4	mid	0.0076	0.708436	0.000030
	DVD-009 PLG 11	plg11-5	rim	0.0050	0.707550	0.000034
	DVD-009 PLG 12	plg12-1	mid	0.0037	0.707771	0.000034
	DVD-009 PLG 13	plg13-1	rim	0.0014	0.707705	0.000034
	DVD-009 PLG 13	plg13-2	core	0.0064	0.707822	0.000033
	DVD-009 PLG 14	plg14-1	rim	0.0115	0.707509	0.000039
	DVD-009 PLG 14	plg14-2	mid	0.0017	0.707730	0.000032
	DVD-009 PLG 14	plg14-3	mid	0.0028	0.707873	0.000031
	DVD-009 PLG 14	plg14-4	mid	0.0081	0.708205	0.000034
	DVD-009 PLG 14	plg14-5	mid	0.0077	0.707988	0.000034
	DVD-009 PLG 15	plg15-1	rim	0.0007	0.707708	0.000031
	DVD-009 PLG 15	plg15-2	mid	0.0019	0.707746	0.000035
	DVD-009 PLG 16	plg16-1	rim	0.0060	0.707773	0.000038

Appendix 3 continued.

DVD-009 PLG 16	plg16-2	mid	0.0041	0.708291	0.000040
DVD-009 PLG 16	plg16-3	mid	0.0186	0.707980	0.000041
DVD-009 PLG 16	plg16-4	mid	0.0186	0.708446	0.000035
DVD-009 PLG 16	plg16-5	mid	0.0025	0.708367	0.000033
DVD-009 PLG 16	plg16-6	mid	0.0204	0.708424	0.000035
DVD-009 PLG 16	plg16-7	rim	0.0010	0.707728	0.000031
DVD-009 PLG 17	plg17-1	core	0.0008	0.707762	0.000030
DVD-009 PLG 17	plg17-2	rim	0.0013	0.707613	0.000030
DVD-009 PLG 18	plg18-1	rim	0.0037	0.707641	0.000033
DVD-009 PLG 18	plg18-2	mid	0.0091	0.708638	0.000037
DVD-009 PLG 18	plg18-3	mid	0.0012	0.708742	0.000036
DVD-009 PLG 19	plg19-1	core	0.0010	0.707824	0.000036
DVD-009 PLG 20	plg20-1	mid	0.0018	0.707822	0.000025
DVD-009 PLG 21	plg21-1	rim	0.0053	0.707868	0.000032
DVD-009 PLG 21	plg21-2	mid	0.0206	0.707683	0.000037
DVD-009 PLG 21	plg21-3	mid	0.0010	0.708835	0.000036